NASA TECHNICAL NOTE

NASA TN D-4726

C.1

NASA TN D-4726

LOW SUBSONIC FLIGHT AND FORCE INVESTIGATION OF A SUPERSONIC TRANSPORT MODEL WITH A VARIABLE-SWEEP WING

by Delma C. Freeman, Jr.

Langley Research Center
Langley Station, Hampton, Va.

NATIONAL AERONAUTICS AND SPACE ADMINISTRATION • WASHINGTON, D. C. • NOVEMBER 1968

LOW SUBSONIC FLIGHT AND FORCE INVESTIGATION OF A SUPERSONIC TRANSPORT MODEL WITH A VARIABLE-SWEEP WING

By Delma C. Freeman, Jr.

Langley Research Center
Langley Station, Hampton, Va.

Technical Film Supplement L-1008 available on request.

NATIONAL AERONAUTICS AND SPACE ADMINISTRATION

For sale by the Clearinghouse for Federal Scientific and Technical Information
Springfield, Virginia 22151 – CFSTI price $3.00

LOW SUBSONIC FLIGHT AND FORCE INVESTIGATION OF A SUPERSONIC TRANSPORT MODEL WITH A VARIABLE-SWEEP WING

By Delma C. Freeman, Jr.
Langley Research Center

SUMMARY

An investigation has been conducted in the Langley full-scale tunnel to determine the low-speed static and dynamic longitudinal and lateral-directional stability characteristics of a 1/20-scale model of a variable-sweep-wing supersonic commercial air transport configuration.

The results of the investigation showed that the dynamic longitudinal stability and control characteristics of the model were generally satisfactory over the test angle-of-attack range except for the landing configuration at high angles of attack where the model was statically longitudinally unstable. The effects of power were found to be very large and stabilizing on the longitudinal stability of the model. In the wing-sweep range from 20° to 42°, the model generally had good lateral-directional characteristics except for flights at the highest lift coefficients where the model diverged in yaw. The angles of attack at which these divergences occurred, however, were in the range where there was extensive stalling of the movable wing panels, and the airplane would not ordinarily be operated. As the sweep was increased past 42°, there was a marked deterioration in both lateral control effectiveness and Dutch roll damping, and at maximum sweep ($\Lambda = 72^{\circ}$) an unstable Dutch roll oscillation together with very weak roll control made flight almost impossible.

INTRODUCTION

For the past few years, the National Aeronautics and Space Administration has been conducting extensive research in support of a supersonic transport program. As part of this general study, the Langley Research Center has conducted an investigation in the Langley full-scale tunnel to determine the low-speed static and dynamic stability characteristics of a 1/20-scale model of a proposed supersonic commercial air transport configuration utilizing the variable-sweep wing concept. The results of previous work with configurations employing the variable-sweep concept have indicated that its use offers a means of realizing efficient subsonic and supersonic flight characteristics in one airplane.

The investigation consisted of free-flight tests in the Langley full-scale tunnel to determine the low-speed dynamic stability and control characteristics of the configuration. In addition, static force tests were made to document the aerodynamic characteristics of the flight test model.

SYMBOLS

The longitudinal data are referred to the stability system of axes and the lateral-directional data are referred to the body system of axes. (See fig. 1.) The origin of the axes was located to correspond to the center of gravity shown in figure 2(a). The reference dimensions used in reducing the data are based on the maximum wing sweep condition ($\Lambda = 72^{\circ}$).

In order to facilitate international usage of data presented, dimensional quantities are presented in both U.S. Customary Units and in the International System of Units (SI). The equivalent dimensions were determined in each case by using the conversion factors given in reference 1.

b	reference wing span ($\Lambda = 72^{\circ}$), feet (centimeters)
$\bar{c}$	reference mean aerodynamic chord, feet (centimeters)
F_L	lift force, pounds (newtons)
F_D	drag force, pounds (newtons)
F_Y	lateral force, pounds (newtons)
I_X	moment of inertia about longitudinal body axis, slug-feet^2 (kilogram-meters^2)
I_Z	moment of inertia about normal body axis, slug-feet^2 (kilogram-meters^2)
L/D	lift-drag ratio
M_X	rolling moment, foot-pound (newton-meter)
M_Y	pitching moment, foot-pound (newton-meter)
M_Z	yawing moment, foot-pound (newton-meter)

q	dynamic pressure, pound/foot^2 (newton/meter^2)
S	reference wing area ($\Lambda = 72^{\circ}$), foot^2 (centimeter^2)
X, Y, Z	body reference axes unless otherwise noted
α	angle of attack, degrees
β	angle of sideslip, degrees
δ_a	total aileron deflection $\delta_{a,L} - \delta_{a,R}$, degrees
$\delta_{a,L}$	left aileron deflection (positive when trailing edge is down), degrees
$\delta_{a,R}$	right aileron deflection (positive when trailing edge is down), degrees
i_t	horizontal-tail incidence (positive when trailing edge is down), degrees
δ_r	rudder deflection (positive when trailing edge is deflected to left), degrees
ψ	angle of yaw, degrees
C_D	drag coefficient, F_D/qS
C_l	rolling-moment coefficient, M_X/qSb
C_T	thrust coefficient, T/qS
T	thrust, pounds (newtons)
ΔC_l	incremental rolling-moment coefficient
$C_{l_\beta} = \frac{\partial C_l}{\partial \beta}$, per degree	
C_L	lift coefficient, F_L/qS
C_m	pitching-moment coefficient, $M_Y/qS\bar{c}$

C_n yawing-moment coefficient, M_Z/qSb

ΔC_n incremental yawing-moment coefficient

$C_{n_\beta} = \frac{\partial C_n}{\partial \beta}$, per degree

$C_{n_{\beta,\text{dynamic}}} = C_{n_\beta} - \frac{I_Z}{I_X} C_{l_\beta} \sin \alpha$

C_Y side-force coefficient, F_Y/qS

ΔC_Y incremental side-force coefficient

δ_{i_t} differential deflection of horizontal tail used for roll control, degrees

$C_{Y_\beta} = \frac{\partial C_Y}{\partial \beta}$, per degree

δ_{sp} spoiler deflection, degrees

Λ wing leading-edge sweep, degrees

c local airfoil chord, feet (centimeters)

ϕ roll angle, degrees

Subscript:

s denotes stability axes

APPARATUS AND MODEL

A drawing of the 1/20-scale model used in the investigation is presented in figure 2(a) and a photograph of the model is presented in figure 3. Dimensional characteristics are listed in table I. The model was made of molded glass fiber and represented a 1/20-scale version of the proposed airplane configuration.

The model had a variable-sweep wing with outboard pivots, a horizontal tail, and a single vertical tail. The wing sweep could be varied in flight from 20° to 72° for the model with the trailing-edge flaps retracted. The wing pivot was located 95.29 inches (242.04 cm) aft of the nose apex and at span station 12.40. (See fig. 2(a).) The wing was

constructed to represent the bending and twist associated with 1g flight for 20° sweep condition. A drawing showing wing sections for the movable panels is presented in figure 2(b). Thrust was provided by ejector-type nozzles located in each of the four nacelles. These ejectors were designed to simulate the nozzle geometry in the engine exit properly. (See fig. 2(c).)

To facilitate model configuration changes, the wing of the model was designed with removable leading and trailing edges. To convert the model from the clean to the landing configuration, the clean leading and trailing edges of the wing and strake ($\Lambda = 20^{\circ}$) were replaced with the leading edges having slats and trailing edges having flaps. Sketches showing the leading-edge slats and trailing-edge flaps along with gaps and deflection angles are presented in figure 4. The trailing-edge flap was a double-slotted flap with the flap vane having a deflection of 30° and the flap segment having a deflection of 50°. (See fig. 4(a).) The leading-edge slat was constructed in two pieces with the inboard or strake section constructed as shown in figure 4(b) and the outboard section constructed as shown in figure 4(c).

The model had a conventional vertical tail with rudder. Pitch control was provided by an all-movable horizontal tail and roll control was provided by spoilers and aileron surfaces on the wing which were operative throughout the sweep range. For a few flights with 72° wing sweep, the area of the horizontal tail was increased so that it could be used for additional roll control and would provide adequate roll control effectiveness. (See fig. 2(d).)

The flight tests were made in the Langley full-scale tunnel by using the technique described in reference 2. A sketch of the flight test setup is presented in figure 5. All force tests were made in the Langley full-scale tunnel with a sting-support system and internal strain-gage balances.

TESTS

Flight Tests

Flight tests were made to determine the dynamic stability and control characteristics and the general flight behavior of the model. The model behavior during flight was observed by the pitch pilot, located at the side of the test section, and by the yaw and roll pilot located in the rear of the test section. (See fig. 5.) The results obtained in the flight tests were primarily in the form of qualitative ratings of the model flight behavior based on pilots' opinions. Motion-picture records were obtained in the tests for subsequent study and to verify and correlate the ratings for the different flight conditions.

The flight tests were made over a lift-coefficient range from about 0.6 to 1.65 for four specific sweep angles ($\Lambda = 20^{\circ}$, 30°, 42°, and 72°). Transitions through the sweep

range from 20° to 72° and back to 20° were made at lift coefficients of 0.70 and 0.85. The effects of trailing-edge flaps on the flight characteristics were also determined. For most flights the model was ballasted with the center of gravity at $0.45\bar{c}$ (8-percent static margin) of the 20° sweep condition, and the center of gravity moved rearward with increasing sweep because of the rearward shift of the wing weight. (See table II.)

Longitudinal control and trim were achieved through symmetrical deflection of the all-movable horizontal tail. For most of the flights lateral-directional control was obtained by using differential aileron deflection, spoiler deflection, and simultaneous rudder deflection; however, a few flights were made using ailerons, spoilers, or rudder alone. The control deflections (full off or full on) used in most of the flights were $\pm 3^{\circ}$ change in tail incidence for pitch control, $\pm 25^{\circ}$ on each aileron for roll control, and $\pm 18^{\circ}$ for rudder control. A spoiler deflection of 60° was used. In some of the flights with 72° sweep, the horizontal-tail area was increased and differential deflection of this surface was used for additional lateral control.

Force and Tuft Tests

In order to document the aerodynamic characteristics of the flight test model and to aid in interpretation of the flight-test results, force tests were made to determine the static stability characteristics of the model. Force tests were also made with simulated thrust conditions for thrust coefficients C_T of 0.11, 0.30, and 0.52. All force tests were made at a dynamic pressure of 3.30 lb/ft^2 (158.0 N/m^2) which corresponds to a Reynolds number per foot of 3.36×10^5. The model was so small in proportion to the tunnel test section that no wind-tunnel corrections were needed or made.

Tuft tests were made, for the clean and landing configuration with $\Lambda = 20^{\circ}$ and 30°, to determine the airflow and stall patterns of the model to provide an aid for interpretation of the flight test results. These tuft tests were made at the same dynamic pressure as the static-force tests.

RESULTS OF TUFT AND FORCE TESTS

Tuft Tests

Figures 6(a) and 6(b) show that for the clean configuration with 20° and 30° sweep, there was a very abrupt onset of stall over a large part of the variable-sweep panel at angles of attack of 12° to 14°.

Comparison of the pictures of figures 6(a) and 6(c) for 20° sweep and figures 6(b) and 6(d) for 30° sweep shows that the use of leading-edge slats changed the stall from a leading-edge stall to a trailing-edge stall and made the stall progression much more gradual, particularly for 30° sweep.

The data of figure 6(e) show that the stall of the landing configuration (leading-edge slats and trailing-edge flaps extended) was a trailing-edge stall and the stall onset was more gradual than that for the clean configuration. It is also evident from figure 6(e) that the flow over the flap was relatively undisturbed at the higher angles of attack. Even though the main part of the wing was stalled, the flow through the slots of the flaps apparently was strong enough to keep the flow attached to the flaps.

Force Tests

Static longitudinal stability and control, power off.- The effects of wing sweep on the static longitudinal stability characteristics of the model in the clean configuration with power off are presented in figure 7. The data show that the model with 20° sweep was longitudinally stable at low angles of attack ($\alpha < 4^{\circ}$), was essentially neutrally stable for $\alpha = 4^{\circ}$ to $\alpha = 10^{\circ}$, and was longitudinally unstable at higher angles of attack. An increase in the wing sweep angle produced a delay in the onset of static longitudinal instability for the configurations of the test.

In an effort to improve the aerodynamic characteristics of the model, the leading-edge slats were installed on the strake and variable-sweep panels. A comparison is made in figure 8 between the slats-retracted and slats-extended conditions for the four sweep angles. Also presented for the 20° sweep angle are data for the landing configuration. The data of figure 8 show that the addition of the leading-edge slats markedly delayed the onset of the pitch-up tendency to higher angles of attack. Adding both the leading-edge slats and trailing-edge flaps resulted in a marked increase in longitudinal stability at low angles of attack but this configuration showed a destabilizing break in the pitching-moment curve and static longitudinal instability at moderate and high angles of attack similar to those of the clean configuration.

Static longitudinal stability and control, power on.- Presented in figures 9 to 13 are the effects of simulated thrust conditions on the static longitudinal stability and control characteristics of the model. These data show that the effect of the simulated thrust was to increase the static longitudinal stability throughout the angle-of-attack range and to delay and minimize markedly the pitch-up for all wing sweep conditions tested with flaps up. There is also a small increase in control effectiveness with power at low angles of attack (figs. 12 and 13), probably due to some induced velocity at the tail. The power-on control effectiveness increases about 50 percent with increasing α (for positive i_t), probably because of an increase in this induced velocity as the tail moves down into the jet. This increase in control effectiveness corresponds to the small general increase in stability with increased power. The large effect of power on pitch-up probably resulted from the fact that the jet exhaust prevents the vortex off the strake from producing downwash at the tail and thereby makes the horizontal tail more effective. Even though the

simulated jet effects are favorable from low-speed stability considerations, this condition would probably present serious heating problems on the horizontal-tail structure at supersonic flight conditions. The data of figure 10(e) show that the large horizontal tail, which was used on the model for increased roll control during the flight tests, showed about the same effects of power as the design tail. As expected, however, the large tail increased the longitudinal stability of the model throughout the angle-of-attack range.

Static lateral-directional stability and control.- The effects of wing sweep on the static lateral-directional stability parameters C_{Y_β}, C_{n_β}, and C_{l_β} are presented in figure 14 for the model in the clean and landing configurations with power off. The data presented in figure 14 were determined from the incremental differences in C_l, C_n, and C_Y measured over the angle-of-attack range at fixed sideslip angles of 5° and -5°. These data show that for the clean configuration with sweep angles up to 42° the model became directionally unstable $(-C_{n_\beta})$ at angles of attack near 20°. This angle of attack is at or above the stall ($\alpha = 12^\circ$ to 14°) for the movable wing panels and not in the normal flight range. For the 72° sweep configuration, the model was directionally unstable at angles of attack above 26°.

A comparison of the data of figures 14(a) and 14(b) shows that the addition of the leading-edge slats generally delayed the onset of directional instability to a higher angle of attack except for the 72° sweep case where the addition of the slats was destabilizing. The addition of the slats generally increased the positive effective dihedral at the higher angles of attack for the sweep conditions of the tests, probably because it increased the range of angles of attack over which the movable panels were not stalled. A comparison of the data of figures 14(a) and 14(c) shows that the landing configuration was directionally stable to a higher angle of attack than that for the clean configuration.

Presented in figures 15 to 17 are the effects of simulated thrust on the static lateral-directional stability characteristics of the model. The data show no significant effect of power.

The results of tests to determine the effect of sweep on the aileron control effectiveness of the model are presented in figure 18. The data show that the ailerons were effective at minimum sweep angles but the effectiveness decreased with increased sweep until the ailerons were barely effective at maximum sweep. The yawing moments produced by aileron deflection were generally proverse over the angle-of-attack range for which the movable wing panels were unstalled.

Presented in figure 19 are the results of tests to determine the spoiler control effectiveness of the model. These data show that the spoiler was very effective at low sweeps ($\Lambda = 20^\circ$, 30°, and 42°) at low angles of attack ($\alpha < 15^\circ$) and that the effectiveness diminished progressively with increasing angle of attack. For the 72° sweep configuration,

however, the spoiler was almost completely ineffective as a roll control for the entire test angle-of-attack range. The addition of the flaps made the spoilers more effective at low angles of attack but made little change in the effectiveness at the higher angles.

The results of tests to determine the rudder control effectiveness are presented in figures 20 and 21 for both static and simulated thrust conditions. The data show that the rudder was effective for directional control over the test angle-of-attack range. Generally, the use of simulated thrust had little effect on the rudder control at the lower angles of attack ($\alpha < 20^{\circ}$); however, simulated thrust caused the rudder effectiveness to increase at the higher angles of attack.

The data presented in figures 22(a) and 22(b) show the control effectiveness resulting from differential deflection of the horizontal tail for roll control for the 72° sweep condition. These data show that the design tail was completely ineffective as a roll control whereas the large tail gave relatively large rolling moments and proverse yawing moments over the test angle-of-attack range. Increasing thrust is shown to increase substantially the rolling effectiveness of the large tail as was the case for the pitch control effectiveness of the horizontal tail. This increase in control effectiveness of the horizontal tail is believed to result from a jet-induced increase in dynamic pressure at the tail.

FLIGHT TEST RESULTS AND DISCUSSION

A motion-picture film supplement covering the flight tests of the model has been prepared and is available on loan. A request card form and a description of the film are found at the end of this report.

Interpretation of Flight Test Results

In the flying model technique there are several factors which must be considered in correlating the results of the model to those of a full-scale airplane. The first factor, and probably most important, is that the angular motions of a dynamic model are much more rapid than those of its full-scale counterpart, which gives the model pilot less time in which to apply a corrective control. Also, the pilot of the model is remotely located, which makes it impossible for him to feel an acceleration as the pilot of a full-scale aircraft can. The lack of feel of the acceleration introduces considerable lag in the application of the control by the model pilot since he must, instead, rely on visual observations of some model displacements before he recognizes the need for corrective control. In addition, the model must be flown within the confines of the tunnel test section; this restriction prohibits the model pilot to allow the development of certain mild drifting motions or slight changes in speed which would be of little concern to the pilot of a

full-scale airplane operating in open air. These factors, which combine to make the model more difficult to fly than the full-scale airplane, are offset somewhat by the use of flicker (full on or off) control to minimize the time lag involved in obtaining corrective response.

In the past it has been found that the flying-model technique gave a good qualitative indication of the dynamic behavior of an aircraft and of the relative ease of control. The models flown were about 6 feet in length and were generally 1/10-scale versions of fighter-type aircraft or moderately sized transports or bombers. The fact that good correlation between the models and aircraft flight results was obtained is an indication that the fast motions of the model were properly offset by the increase in control sensitivity to give a good simulation of the aircraft behavior. Recently, however, when these models were used to simulate larger aircraft, such as the supersonic transport, it was found that the model flight test results were somewhat optimistic. For example, in the model flight tests these configurations were generally found to have satisfactory dynamic behavior whereas simulator studies showed them to have poor flight behavior because of sluggish initial control response. (See refs. 3, 4, and 5.) Analysis of these results indicates that the apparent discrepancy between the model and simulator flight data is related to the improper control power simulation in the model. That is, the flicker control used to offset the fast model motions gave too much control to simulate properly the sluggish control response generally characteristic of very large airplanes with high moments of inertia.

In the simulator studies (for example, see ref. 5) it was found that when the control surface to column gearing was increased to give large increases in the initial control surface deflection, the flight behavior was greatly improved and the simulator and model flight test results were brought into much better agreement. On the basis of these results, it appears, therefore, that the model flight results presented herein are somewhat optimistic for the basic airplane configuration, but they should give a fairly good indication of the flight behavior of the airplane configuration with the increased gearing found necessary in simulator studies to achieve satisfactory control response.

Longitudinal Stability and Control

Wing sweep transitions were made at constant lift coefficients of 0.70 and 0.85 with the center of gravity located at $0.45\bar{c}$ for the 20° sweep condition. The transitions were started at 20° wing sweep, and the sweep was varied to 72° and then back to 20°. Because the transitions were made at constant lift coefficients and because of the slight increase in static longitudinal stability with increasing wing sweep (see fig. 7), it was necessary to change trim throughout the transition; however, this procedure did not present any problem during the flights because the model motions were well damped in pitch and the

control response was good. The model was very easy to fly and required very little attention of the longitudinal pilot to maintain smooth flight during these wing-sweep transitions.

The effects of lift coefficient on the longitudinal characteristics were determined with fixed-sweep conditions of 20°, 30°, 42°, and 72° with the model ballasted to put the center of gravity at $0.45\bar{c}$ for the 20° sweep configuration. These tests were made for a range of lift coefficients from about 0.60 up to the point at which stability or control difficulty made flight impossible. Most of the flights were made with the slats extended to provide a better flying configuration since the slats made the stall more gradual and minimized the abrupt roll off and wing dropping motion associated with this type of stall. At 20° wing sweep the model was dynamically longitudinally stable and easy to fly. Very little effort was required of the longitudinal pilot to fly the model through an angle-of-attack range from 10° up to 30° where flights were generally terminated by a divergence in yaw. The significant point of these results is that the model flew satisfactorily at high angles of attack where the static data of figure 10 show the model to be statically longitudinally unstable in the power-off condition. This result is attributed mainly to the large stabilizing effect of power in the high angle-of-attack range, which is also shown by the data of figure 10. Another interesting point is that the model could be flown reasonably well over this angle-of-attack range even though there was extensive stalling of the movable wing panels. This result does not indicate that the pilot of a full-scale airplane of this configuration would be satisfied to fly the airplane in this range, but it does indicate that the airplane is stable and controllable far beyond the conditions to which buffeting and the other irregular motions normally associated with stalling would limit ordinary operation.

Increasing the wing sweep made the model behavior appear to be better throughout the flight range. The pilots' comments indicated that as the wing sweep increased, the dynamic longitudinal stability of the model increased and the model became easier to fly. The pilots' comments ranged from "easy to fly" at 30° sweep to "very stable and easy to fly" at 72° sweep. These results are in good agreement with the static-force test results of figure 10 which show increasing static longitudinal stability with increasing sweepback.

The model was also flown with the trailing-edge flaps extended (landing configuration, $\Lambda = 20^{\circ}$) with the center of gravity located at $0.45\bar{c}$. In the angle-of-attack range from 6° to 8° where the model had static longitudinal stability and the wings were essentially unstalled, the flight behavior was satisfactory. The longitudinal motions were well damped and the model was very easy to fly. As the angle of attack was increased above 8°, however, the longitudinal flight behavior of the model deteriorated and at an angle of attack of about 20°, the model became very difficult to fly because of static longitudinal instability.

As part of the flight-test investigation, tests were made to determine the effect of center-of-gravity position on the longitudinal flight characteristics of the model for the 20° sweep condition with the leading-edge slats extended. These tests were made at an angle of attack of about 15°. The results of these tests showed that the model had good dynamic longitudinal stability characteristics, adequate control, and was easy to fly with the center of gravity in the range from $0.45\bar{c}$ to $0.51\bar{c}$ (8 to 2 percent static margin). In the center-of-gravity range from $0.53\bar{c}$ to $0.57\bar{c}$ (0 to -4 percent static margin) there was a marked deterioration in both the longitudinal stability and control, and the model required careful attention to fly. As the center of gravity was moved rearward to $0.61\bar{c}$ (-8 percent static margin), the model became extremely difficult to fly and required constant attention to the controls to maintain flight and, in cases where large disturbances were encountered, control of the model could not be maintained.

Lateral-Directional Stability and Control

As previously mentioned, wing-sweep transitions were made at lift coefficients of 0.70 and 0.85. There were no serious lateral stability and control problems encountered in making transitions from 20° to 42° sweep. As the sweep was increased past 42°, there was a marked deterioration in both the roll control effectiveness and Dutch roll damping which made flights almost impossible.

For a wing sweep of 20° with the leading-edge slats extended, the model was reasonably easy to fly, and exhibited good Dutch roll damping, good directional stability, and good lateral-directional control in the angle-of-attack range from 10° to 16°. For this condition, the ailerons, spoilers, and rudder were used simultaneously for lateral-directional control. The reasonably good lateral-directional flight behavior of the model in this range of angle of attack is surprising in view of the rather extensive stalling of the movable wing panels indicated by the tuft tests. It can only be conjectured that the reason that the flight behavior was not poor was that the stall progression was very gradual with slats extended; thus, there were no abrupt changes in moment with small changes in angle of attack. Another possible explanation of this result is that the airflow in the tunnel is fairly gusty; therefore, the behavior of a model, at best, is somewhat erratic and not greatly different from that caused by a very gradual stall progression. When the speed was reduced to correspond to an angle of attack of 20°, there was some evidence of a random wing dropping motion, but in the slats-extended configuration, this motion was relatively mild and could be easily counteracted with corrective control. There was no indication of low Dutch roll damping over any of the angle-of-attack range, and the control effectiveness was adequate for satisfactory control of the model even though there was a deterioration in control effectiveness with decreasing speed. At an angle of attack of 20° there was some indication of low directional stability evidenced by a tendency for

the nose of the model to wander randomly in yaw. This yawing tendency became worse as the speed was reduced and at an angle of attack of about 27°, the model diverged in yaw against full corrective control.

Increasing the sweep to 30° and 42° had very little effect on the lateral flight characteristics of the model. In the lower angle-of-attack range the only change noted in flight behavior for this sweep range was a slight decrease in control effectiveness with increased sweep. The model had good Dutch roll damping and the general flight behavior was considered to be satisfactory. As the angle of attack was increased, the roll control effectiveness deteriorated to the extent that at an angle of attack of about 24°, the control was barely adequate for flying the model at the 42° sweep condition. In the angle-of-attack range from about 20° to 24°, there was a progressive decrease in the directional stability (see fig. 16(c)), and at an angle of attack of 27°, the model diverged in yaw.

Increasing the sweep to 72° resulted in the model having very poor lateral-directional flight behavior because of a large-amplitude Dutch roll oscillation and very weak roll control from the spoilers and ailerons. (See figs. 18 and 19.) This combination of low damping and weak control made the model extremely difficult to fly in the angle-of-attack range from 15° to 20° and most flights were terminated at a slightly higher angle of attack ($\alpha = 22°$) because the pilot lost control of the model and it diverged out of the tunnel airstream.

In order to investigate the 72° sweep condition more closely, a roll damper using differential deflection of the horizontal tail was installed in the model. In order to utilize the horizontal tail for roll damping, it was necessary to increase the size of this surface. This approach was taken rather than resort to the ailerons and spoilers because these surfaces were ineffective at high sweep angles. With the roll damper installed, the Dutch roll oscillation was stabilized over the test angle-of-attack range, and differential deflection of the horizontal tail with simultaneous deflection of the rudder provided satisfactory lateral-directional control.

The flight characteristics of the model were also determined for the landing configuration (roll damper off). In the angle-of-attack range from 6° to 8°, the model had good Dutch roll damping, good directional stability, and good roll control. Despite the good stability and control characteristics, however, the pilot felt that the model was somewhat more difficult to fly than in the clean condition because of a random wing dropping which was much more severe than that noted for the clean configuration. It is believed that this random wing dropping was mainly associated with the unsteady flow and intermittent stalling of the variable-sweep wing panels and was aggravated by the addition of the trailing-edge flaps. At an angle of attack of 10°, the wing dropping was less of a problem but the model was still difficult to fly smoothly because of a random yawing motion. As the angle of attack was increased up to 20°, there was evidence of low Dutch

roll damping and low directional stability and a marked decrease in control effectiveness. Sustained flights were possible, however, despite this deterioration in dynamic stability and control through careful attention to the controls.

One significant point noted in the investigation was that the model diverged in yaw at an angle of attack higher than that indicated by static data. This same characteristic is shown by the results of previous investigations (ref. 6) and is attributed to the favorable effect of the positive effective dihedral parameter $-C_{l_\beta}$ on the directional stability of the model under dynamic conditions. This parameter contributes to the directional stability under dynamic conditions through inertia coupling and can become significant for highly swept configurations. An example of the $C_{n_{\beta,\text{dynamic}}}$ for the present model in the 20° sweep condition with leading-edge slats extended is shown in figure 23. A comparison of these data with those of figure 14 shows that the angle of attack for zero directional stability was considerably higher for the dynamic case ($\alpha = 35^\circ$) as compared with the static case ($\alpha = 25^\circ$). Actually, the model diverged at an angle of attack of 27° which is between these two conditions. One possible reason why the model could not be flown up to the angle of attack for zero $C_{n_{\beta,\text{dynamic}}}$ is that there was a noticeable deterioration in lateral control as the angle of attack for the divergence was approached. It is possible that with more control, the model flight tests would have been in better agreement with the $C_{n_{\beta,\text{dynamic}}}$ data of figure 23.

CONCLUSIONS

From the force- and flight-test investigation to determine the low-speed stability and control characteristics of a 1/20-scale model of a proposed supersonic transport with a variable-sweep wing, the following conclusions were drawn:

1. The dynamic longitudinal stability and control characteristics of the model were generally satisfactory over the test angle-of-attack range for all sweep conditions except for the landing configuration at high angles of attack where the model was statically longitudinally unstable. The effects of power were found to be generally very large and stabilizing on the longitudinal stability of the model.

2. Although appreciable longitudinal stability and trim changes were encountered during wing-sweep transitions, the pilot was able to compensate for these changes and to maintain smooth flights during transition by proper use of the pitch control.

3. In the wing-sweep ranges from 20° to 42°, the model generally had good lateral-directional characteristics; however, flights at the highest lift coefficients were generally characterized by a deterioration in Dutch roll damping and directional stability and control. These adverse characteristics, however, occurred in conditions where there was

extensive stalling of the movable wing panels and where an airplane would not normally be operated.

4. As the sweep was increased beyond 42°, there was a marked deterioration in both lateral control effectiveness and Dutch roll damping, and at maximum sweep ($\Lambda = 72^{\circ}$) an unstable Dutch roll oscillation together with very weak lateral control made flights almost impossible.

5. The use of differential deflection of a large horizontal tail for roll control together with the use of a roll damper provided satisfactory lateral flight behavior for the 72° sweep condition.

Langley Research Center,
National Aeronautics and Space Administration,
Langley Station, Hampton, Va., July 15, 1968,
720-01-00-08-23.

REFERENCES

1. Mechtly, E. A.: The International System of Units - Physical Constants and Conversion Factors. NASA SP-7012, 1964.

2. Paulson, John W.; and Shanks, Robert E.: Investigation of Low-Subsonic Flight Characteristics of a Model of a Hypersonic Boost-Glide Configuration Having a 78° Delta Wing. NASA TN D-894, 1961. (Supersedes NASA TM X-201.)

3. Staff of the Langley Research Center: Determination of Flight Characteristics of Supersonic Transports During the Landing Approach With a Large Jet Transport In-Flight Simulator. NASA TN D-3971, 1967.

4. Freeman, Delma C., Jr.: Low Subsonic Flight and Force Investigation of a Supersonic Transport Model With a Highly Swept Arrow Wing. NASA TN D-3887, 1967.

5. Grantham, William D.; and Deal, Perry L.: A Piloted Fixed-Base Simulator Study of Low-Speed Flight Characteristics of an Arrow-Wing Supersonic Transport Design. NASA TN D-4277, 1967.

6. Moul, Martin T.; and Paulson, John W.: Dynamic Lateral Behavior of High-Performance Aircraft. NACA RM L58E16, 1958.

TABLE I.- MASS AND DIMENSIONAL CHARACTERISTICS OF THE MODEL

Weight, lb (N)	72	(320.3)
Moment of inertia about Z-axis ($\Lambda = 20^{o}$), slug-ft^2 (kg-m^2)	13.10	(17.76)
Moment of inertia about X-axis ($\Lambda = 20^{o}$), slug-ft^2 (kg-m^2)	3.10	(4.20)
Moment of inertia about Y-axis ($\Lambda = 20^{o}$), slug-ft^2 (kg-m^2)	9.91	(13.44)
Wing ($\Lambda = 72^{o}$):		
Area (reference), ft^2 (cm^2)	12.56	(11 669)
Span (reference), ft (cm)	4.93	(150)
Mean aerodynamic chord, ft (cm)	2.995	(91.29)
Aspect ratio	1.93	
Leading-edge sweep range, deg	$\Lambda = 20$ to $\Lambda = 72$	

TABLE II.- EFFECT OF WING SWEEP ON CENTER OF GRAVITY

Wing sweep, deg	Center-of-gravity position, percent $\bar{c}$
20	45
30	46
42	47.5
72	50.5

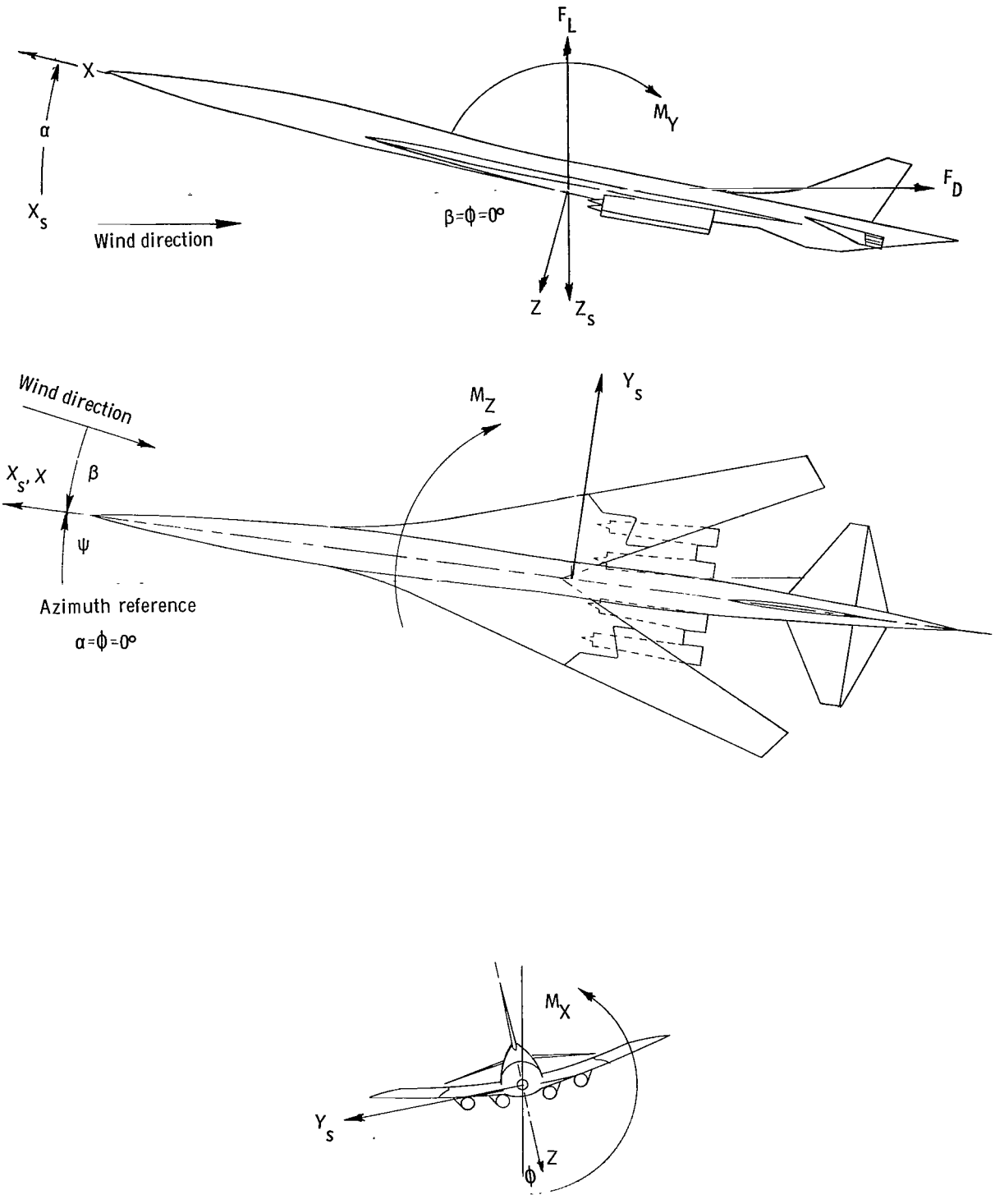

Figure 1.- System of axes used in investigation. Arrows indicate positive directions of moments, forces, and angles.

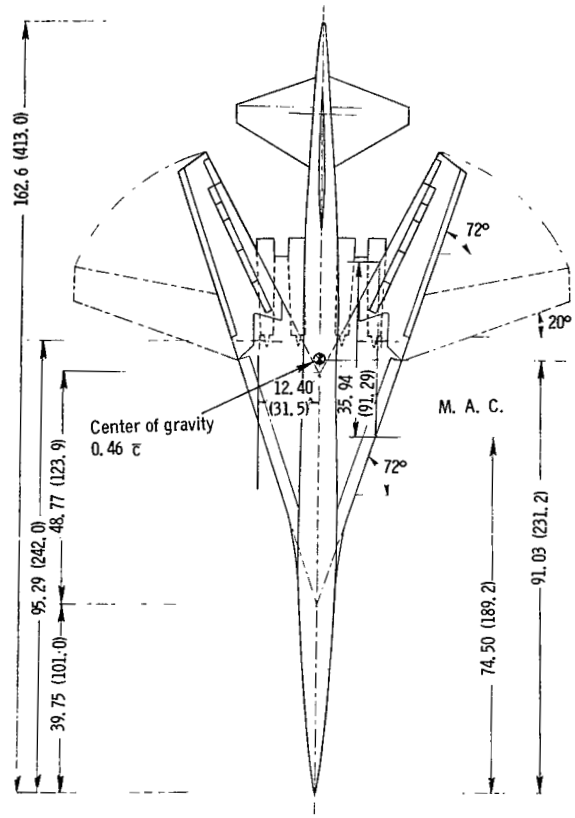

Reference dimensions (Λ=72°)

Area	12.56 ft^2 (11668.6 cm^2)
Aspect ratio	1.93
Chord	2.995 ft (91.29 cm)
Span	4.93 ft (150.30 cm)

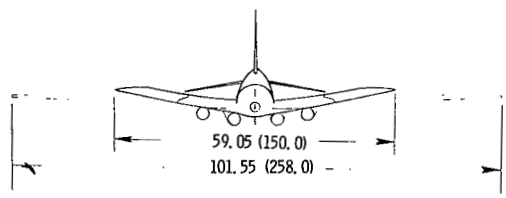

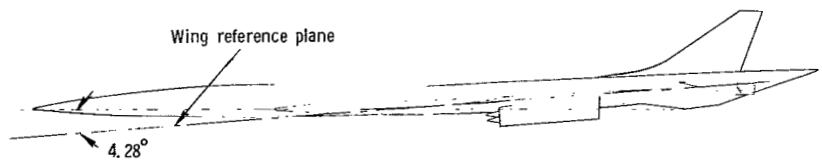

(a) Three-view drawing of model.

Figure 2.- Drawings of model used in investigation. All dimensions are in inches with centimeters given in parentheses.

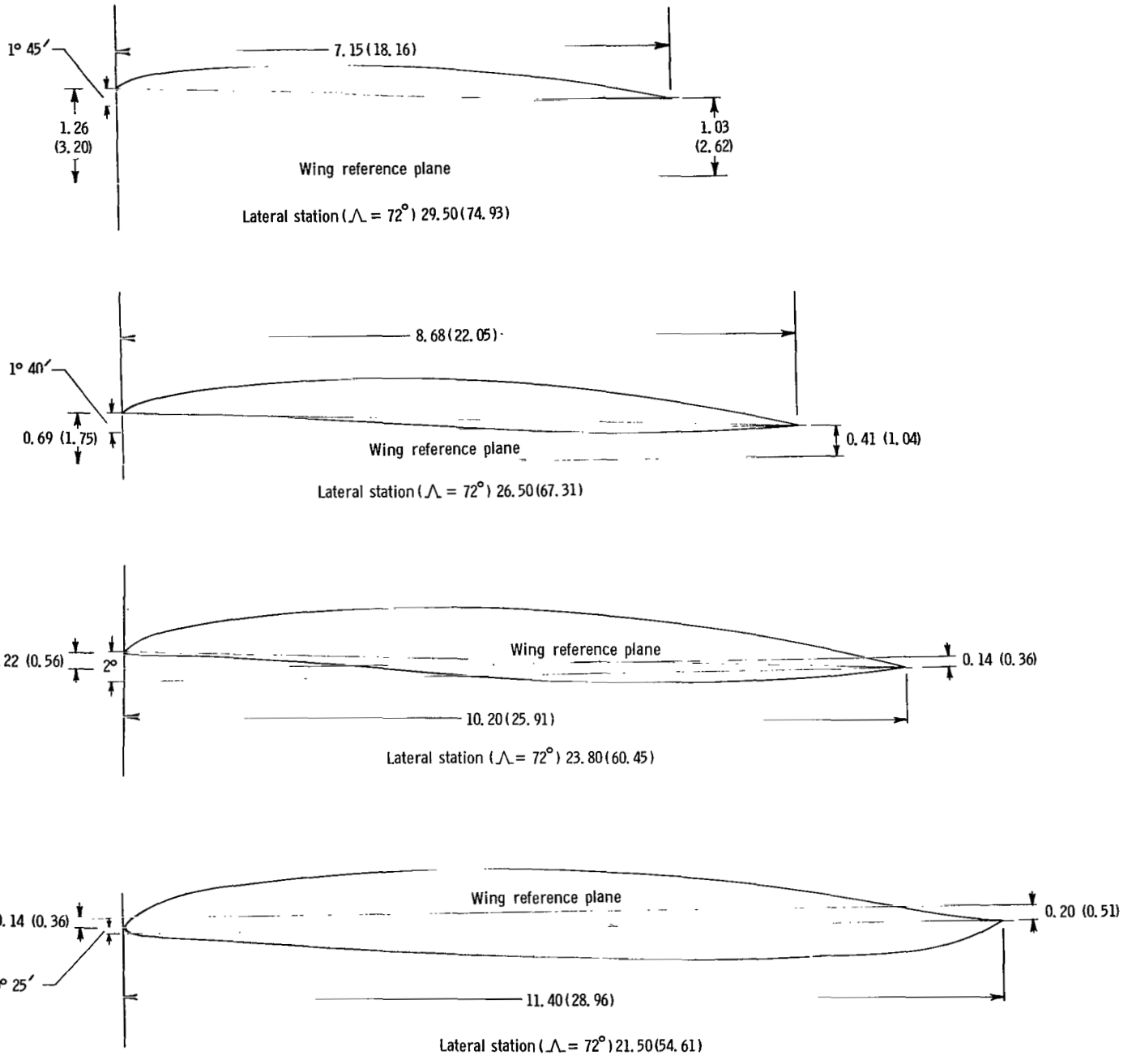

(b) Wing sections for variable-sweep panels. Sections presented were taken normal to wing leading edge at lateral stations given for wing at 72° sweep.

Figure 2.- Continued.

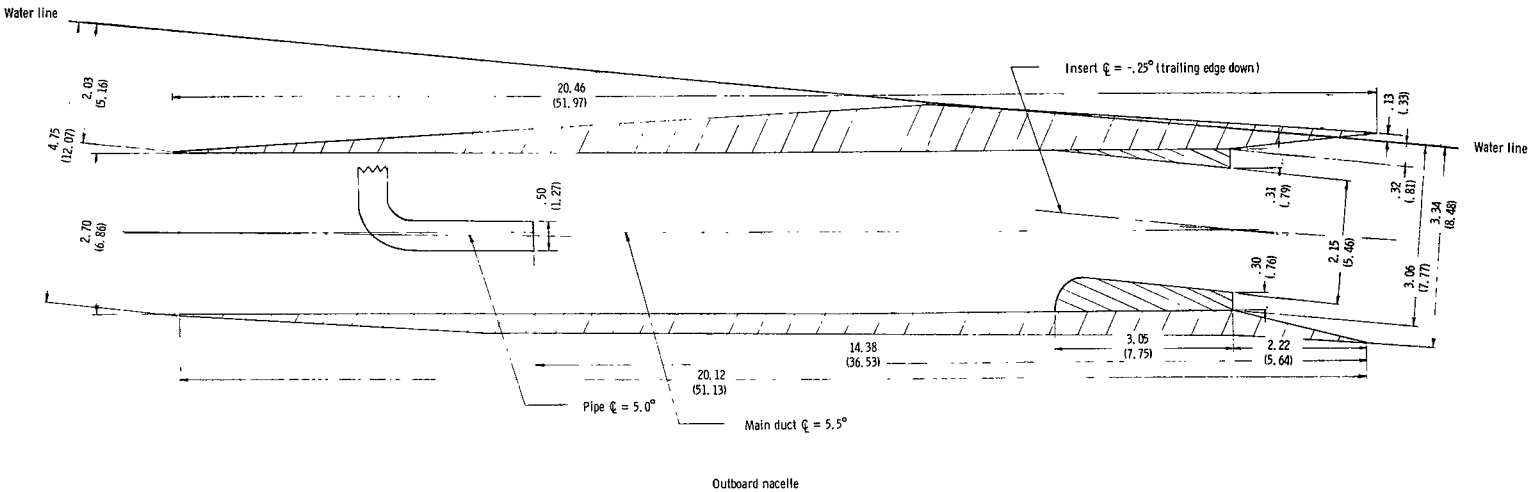

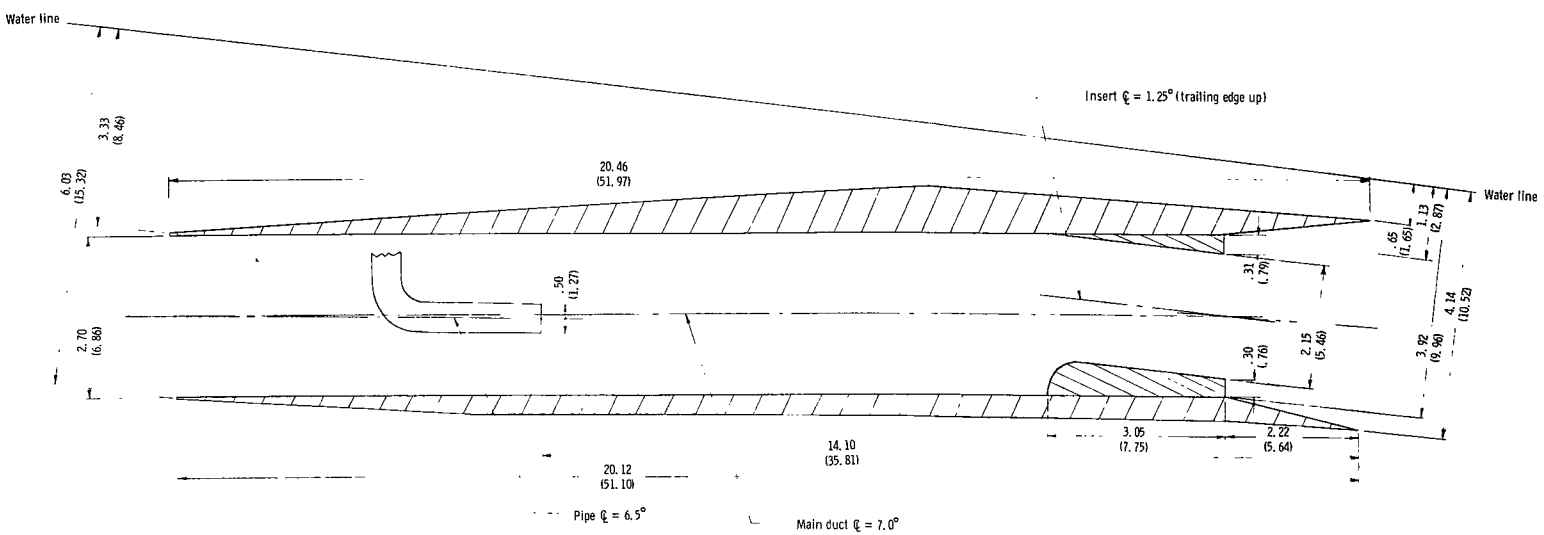

(c) Cross section of ejector used to power model.

Figure 2.- Continued.

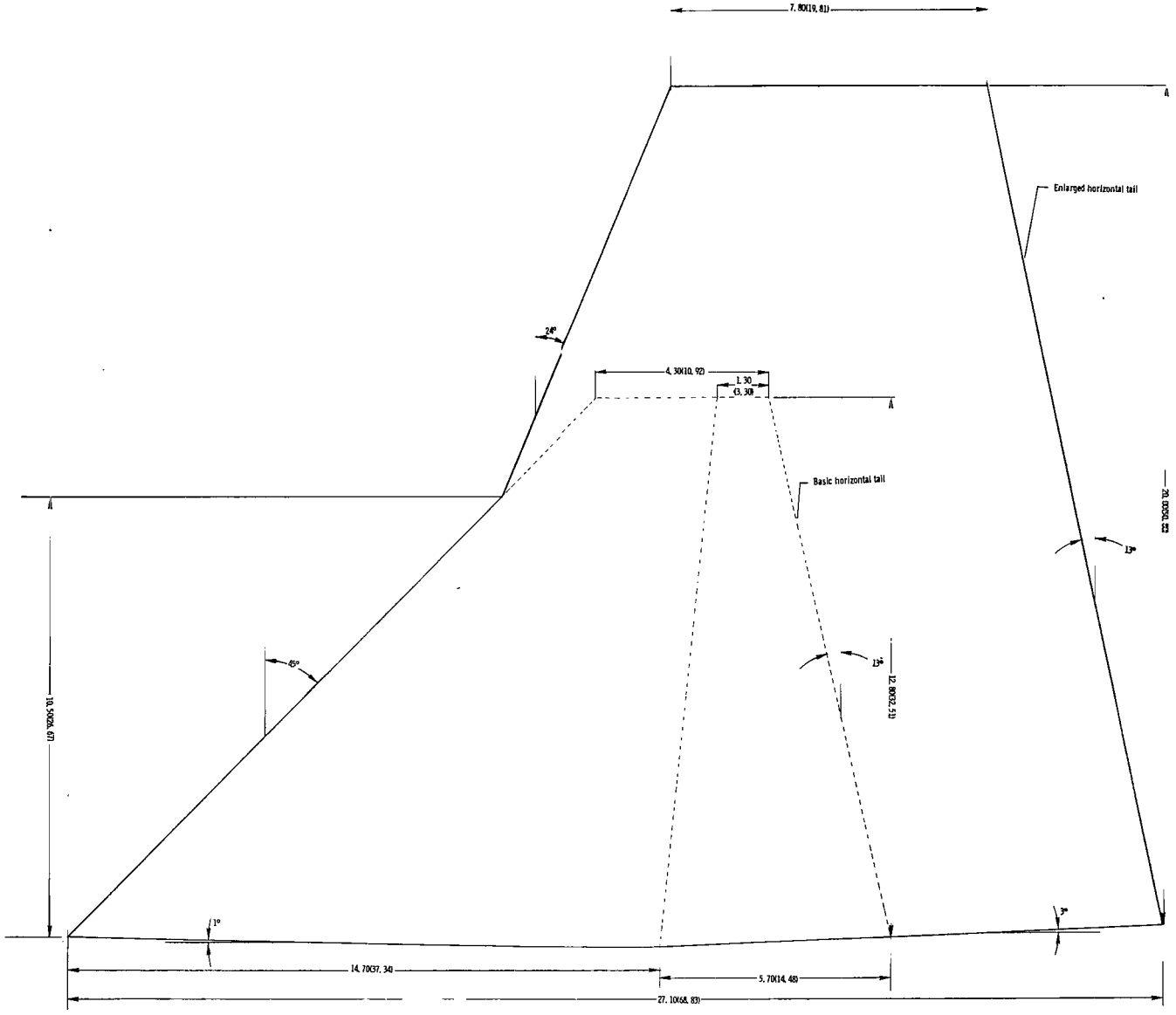

(d) Comparison of horizontal tails used in investigation.

Figure 2.- Concluded.

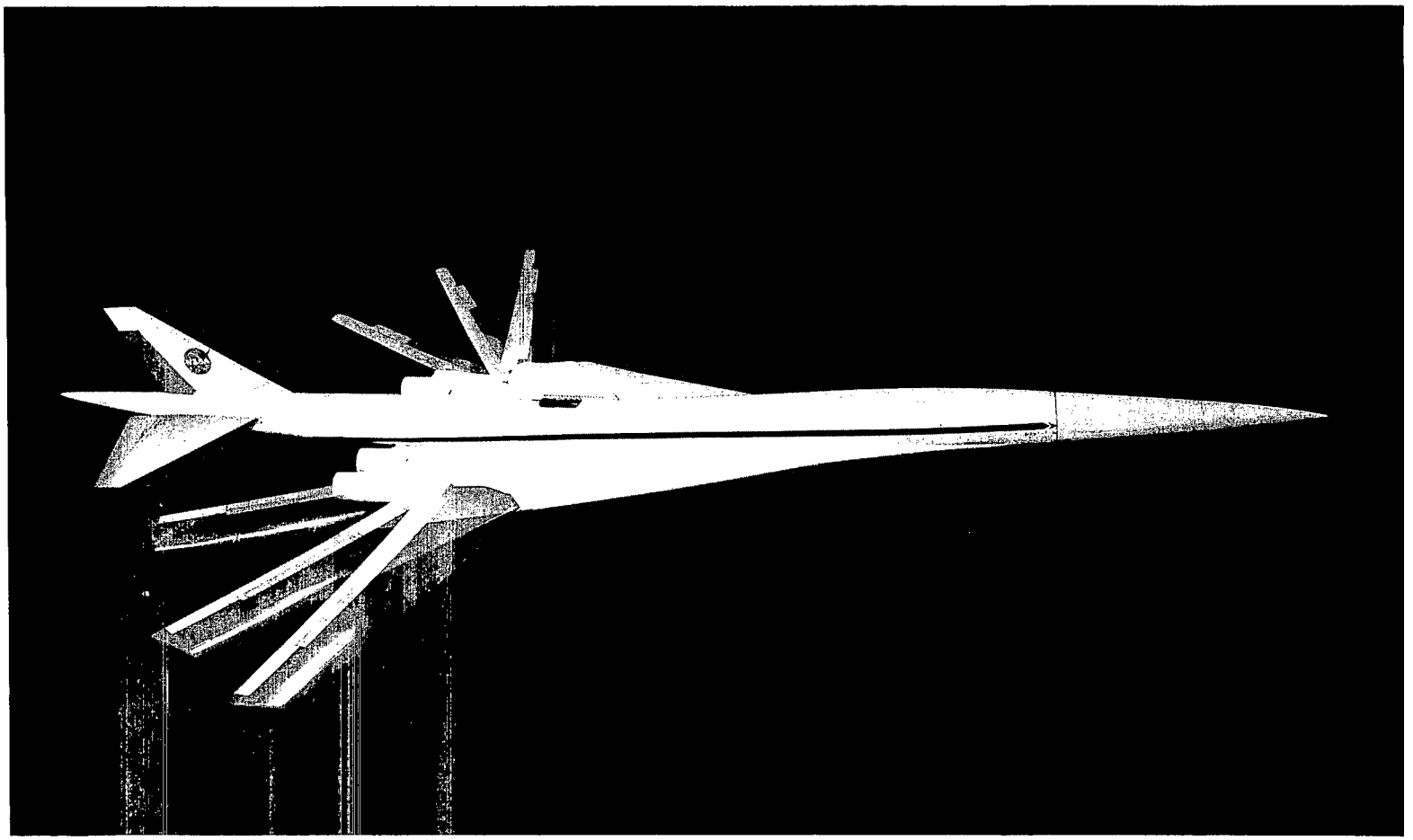

Figure 3.- Photograph of model used in investigation. L-66-2766

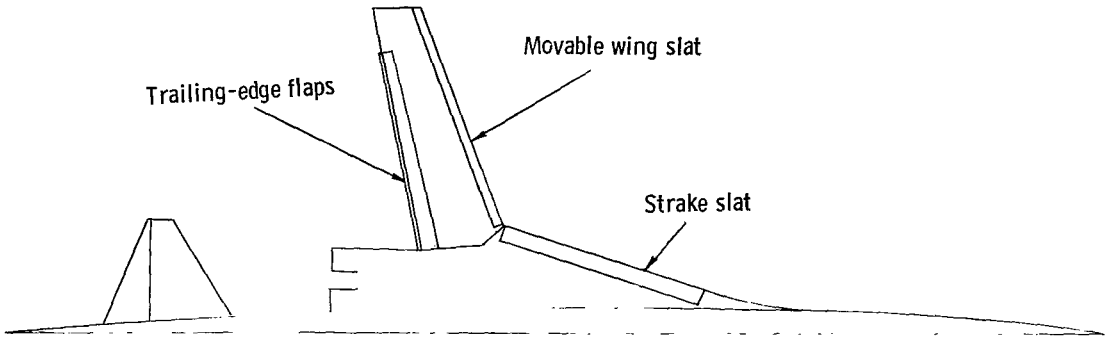

x_m	1.0	x_a	0.4
g_m	2.5	g_a	1.0

x and g dimensions are given in percent of streamwise chord (Λ = 20°).

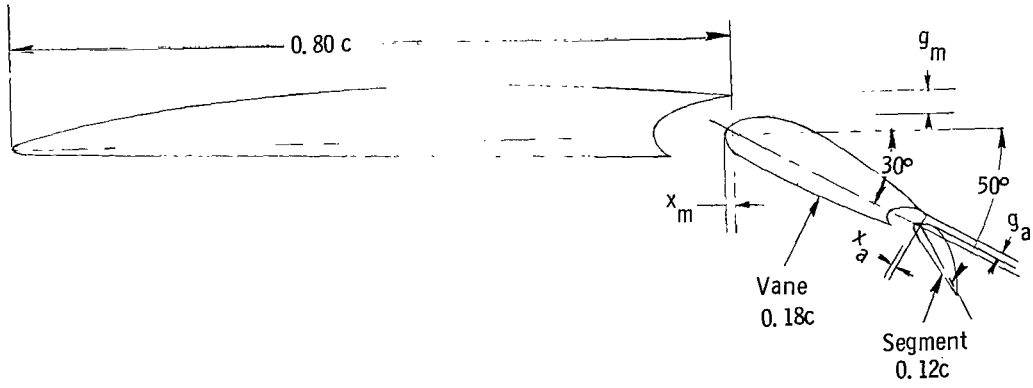

(a) Trailing-edge flap details.

Figure 4.- Slat and flap details. All dimensions are in inches with centimeters given in parentheses.

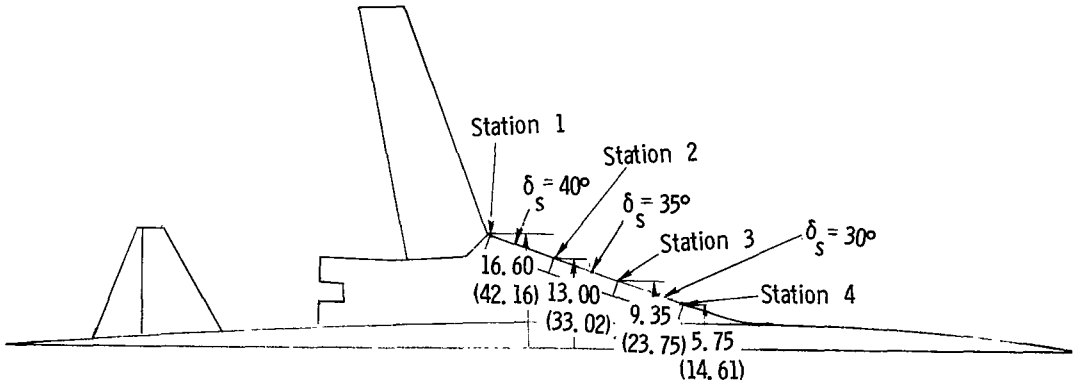

d = 0.29 (0.732)
g = 0.38 (0.953)

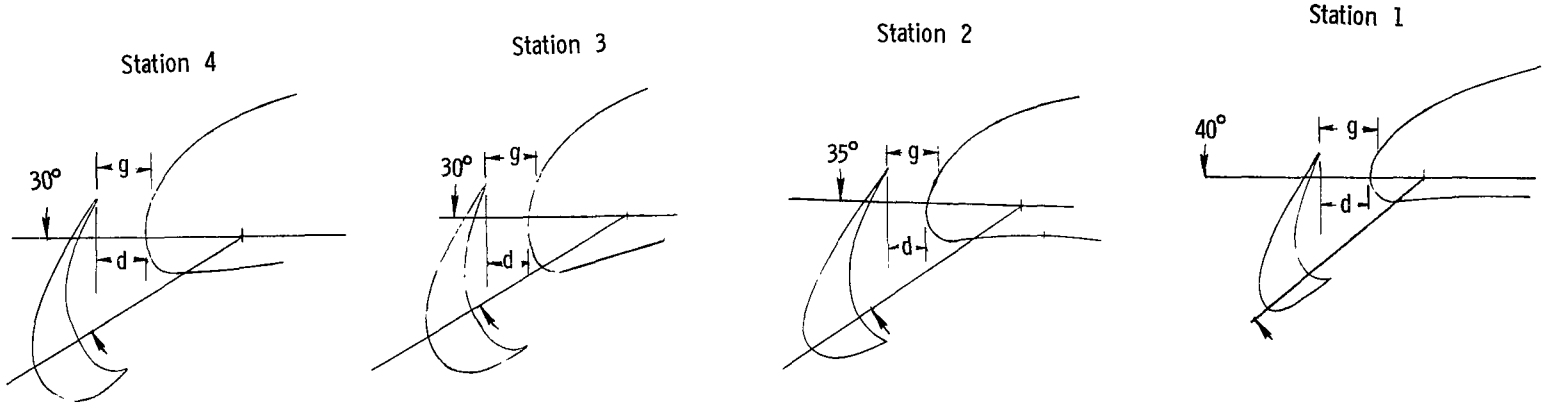

(b) Strake slat δ_s details.

Figure 4.- Continued.

Cut normal to leading edge

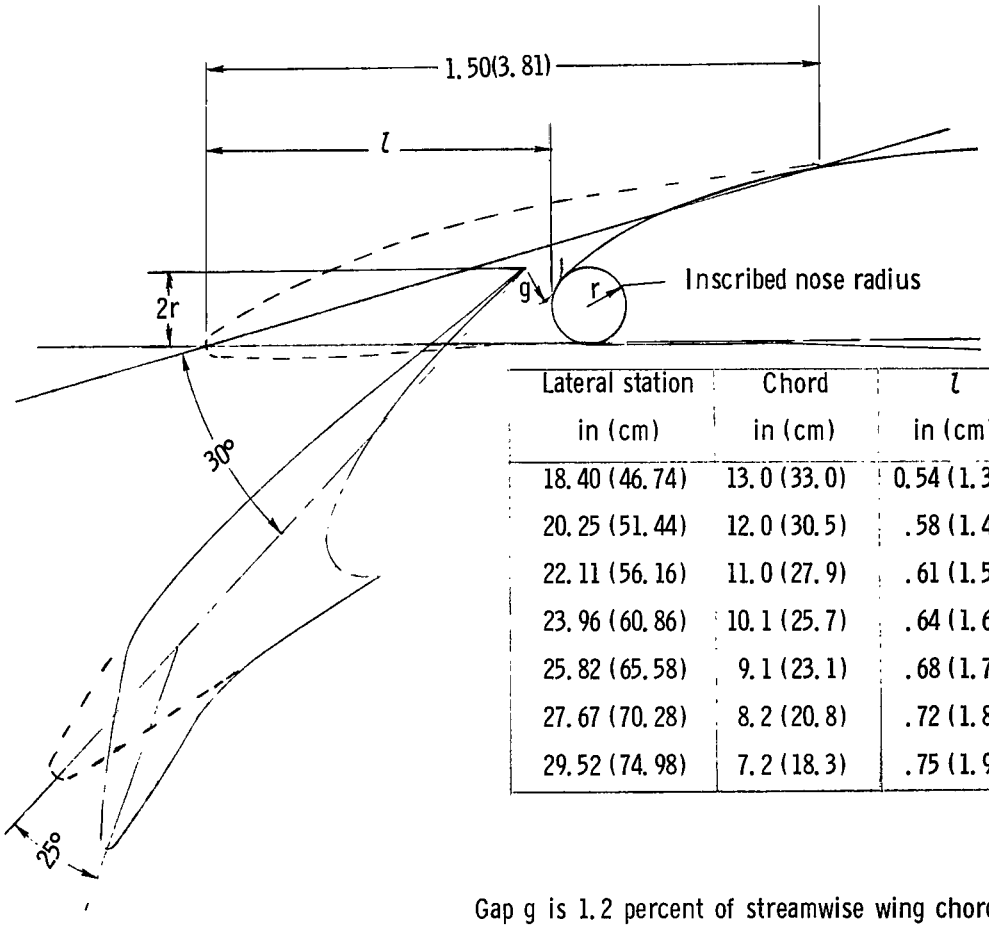

Lateral station in (cm)	Chord in (cm)	l in (cm)	r in (cm)
18.40 (46.74)	13.0 (33.0)	0.54 (1.37)	0.133 (0.338)
20.25 (51.44)	12.0 (30.5)	.58 (1.47)	.116 (.295)
22.11 (56.16)	11.0 (27.9)	.61 (1.55)	.100 (.254)
23.96 (60.86)	10.1 (25.7)	.64 (1.63)	.082 (.208)
25.82 (65.58)	9.1 (23.1)	.68 (1.73)	.066 (.168)
27.67 (70.28)	8.2 (20.8)	.72 (1.83)	.055 (.140)
29.52 (74.98)	7.2 (18.3)	.75 (1.91)	.049 (.124)

Gap g is 1.2 percent of streamwise wing chord at 20° sweep

(c) Movable wing slat.

Figure 4.- Concluded.

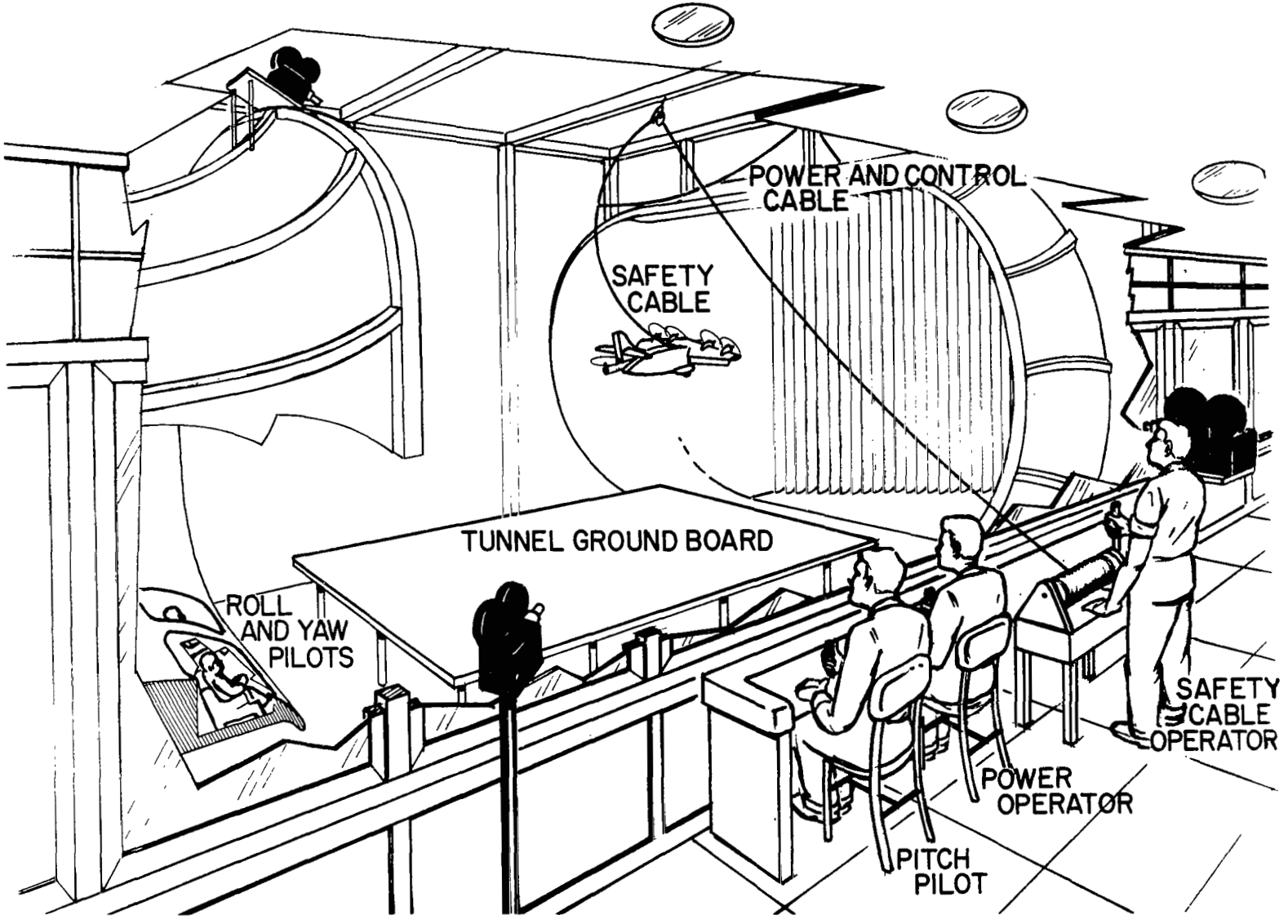

Figure 5.- Test setup for flight tests in the Langley full-scale tunnel. L-64-3008

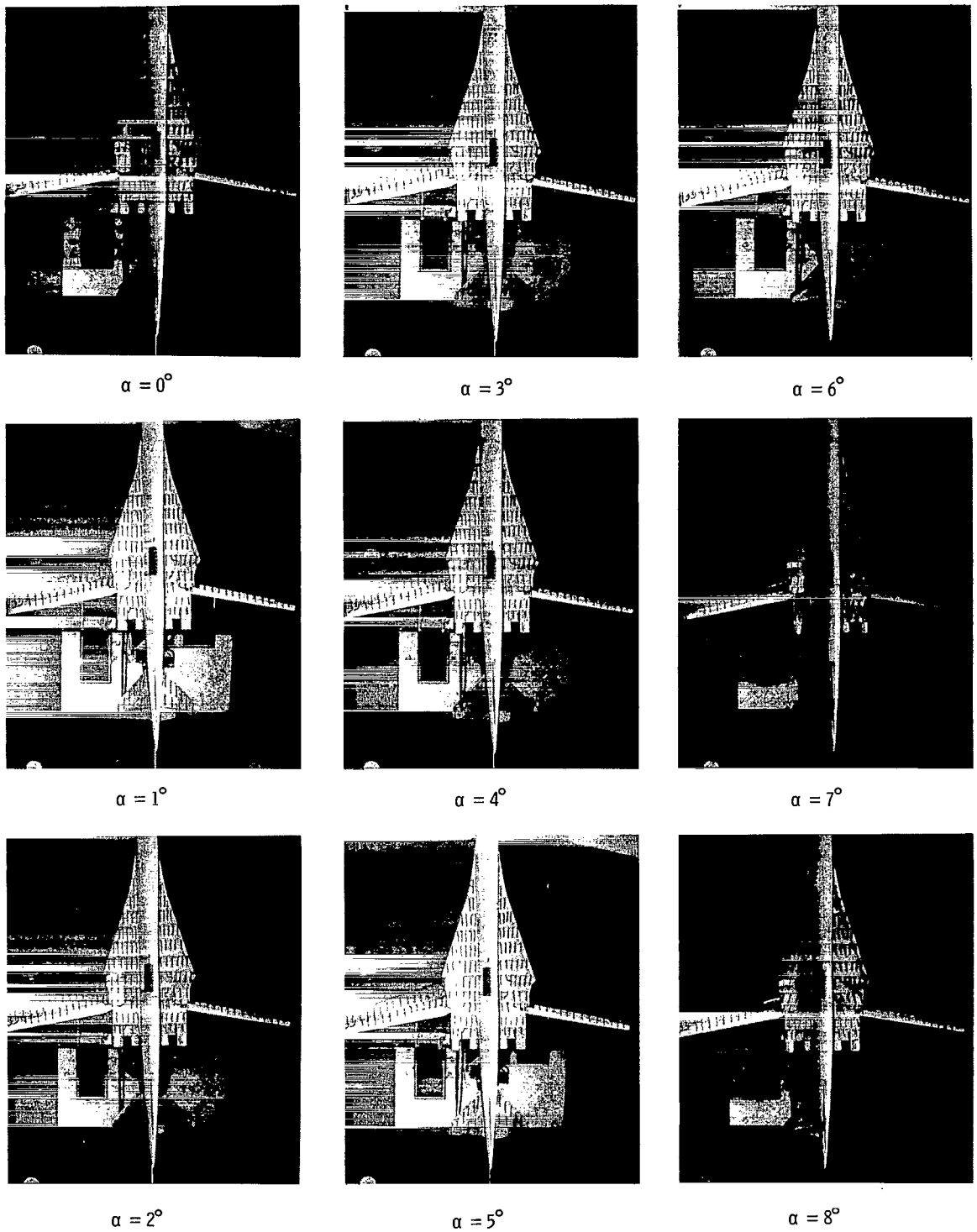

(a) Clean configuration; $\Lambda = 20^{\circ}$. L-68-5663

Figure 6.- Tuft photographs of the model. All controls zero.

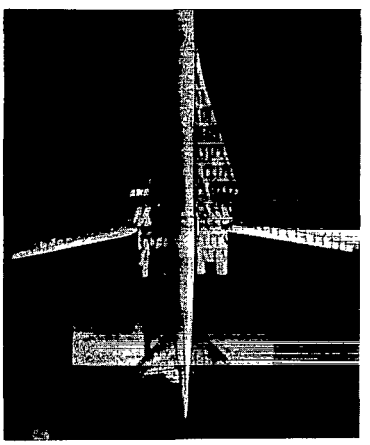

$\alpha = 9^\circ$

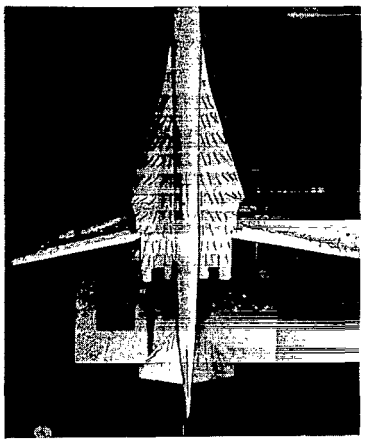

$\alpha = 14^\circ$

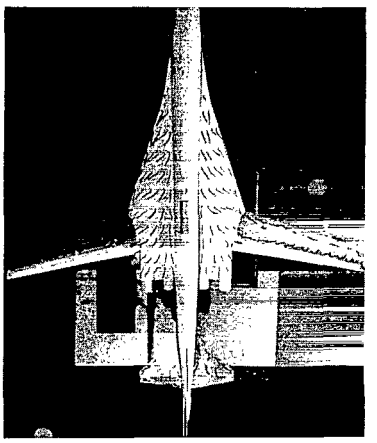

$\alpha = 20^\circ$

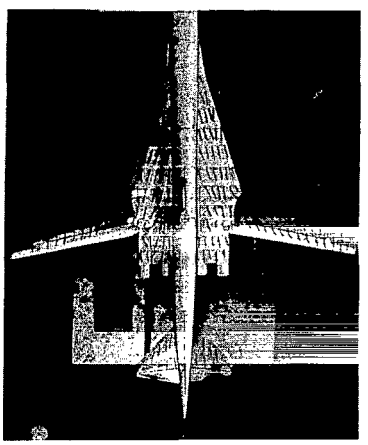

$\alpha = 10^\circ$

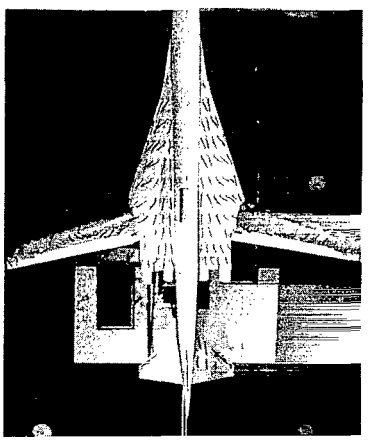

$\alpha = 16^\circ$

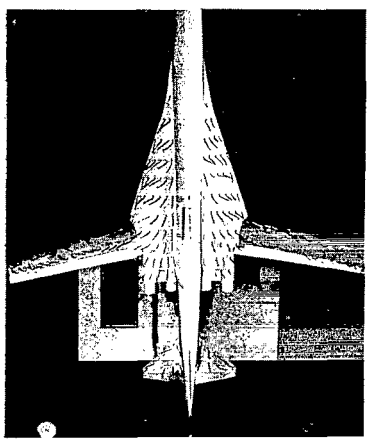

$\alpha = 24^\circ$

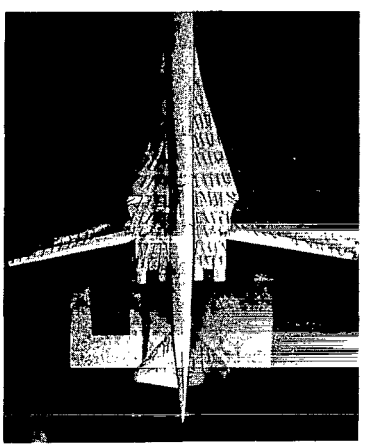

$\alpha = 12^\circ$

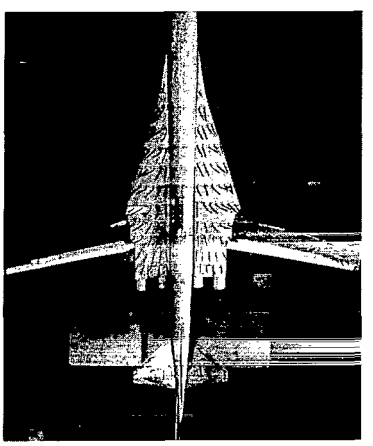

$\alpha = 18^\circ$

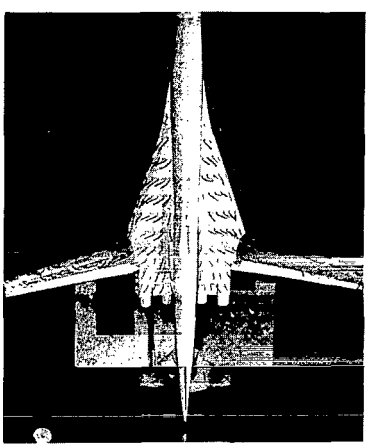

$\alpha = 28^\circ$

(a) Clean configuration; $\Lambda = 20^0$. Concluded.

L-68-5664

Figure 6.- Continued.

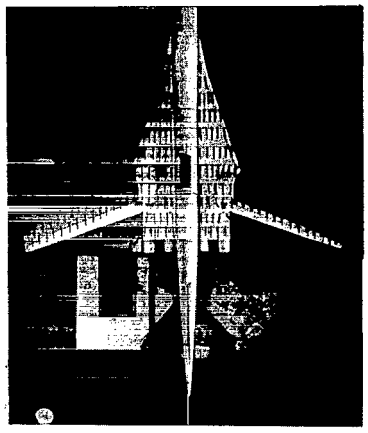

$\alpha = 0°$

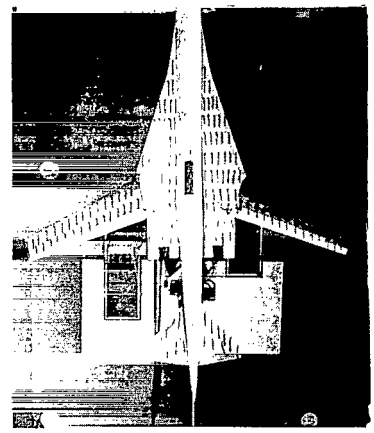

$\alpha = 3°$

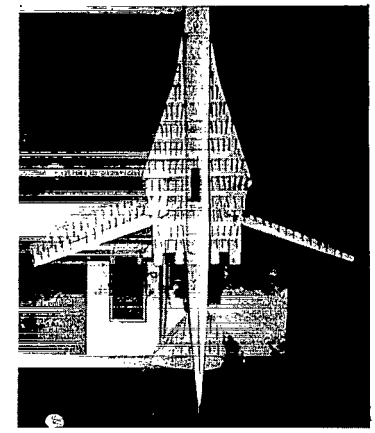

$\alpha = 6°$

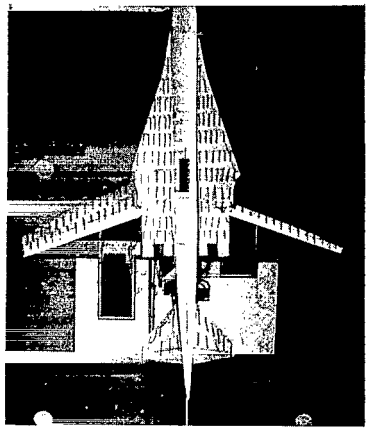

$\alpha = 1°$

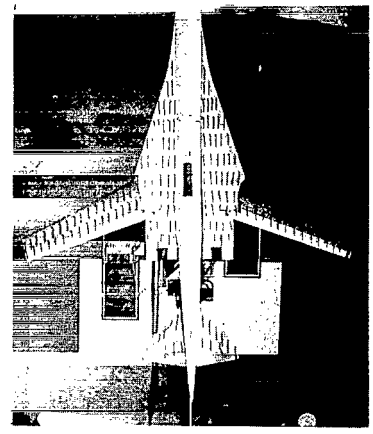

$\alpha = 4°$

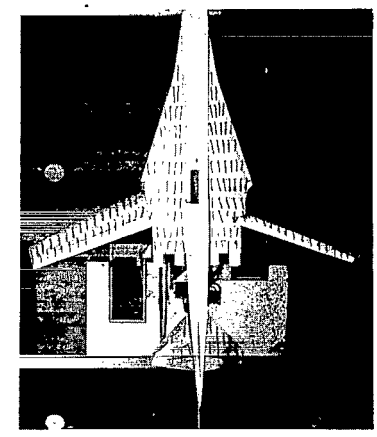

$\alpha = 7°$

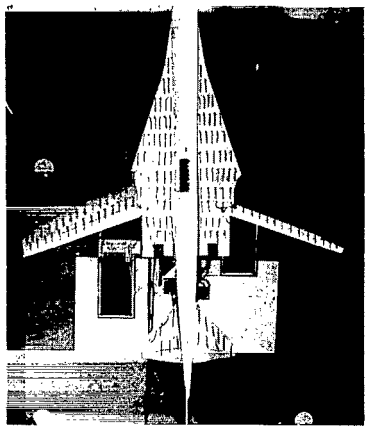

$\alpha = 2°$

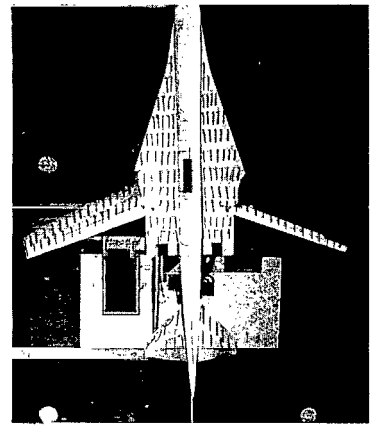

$\alpha = 5°$

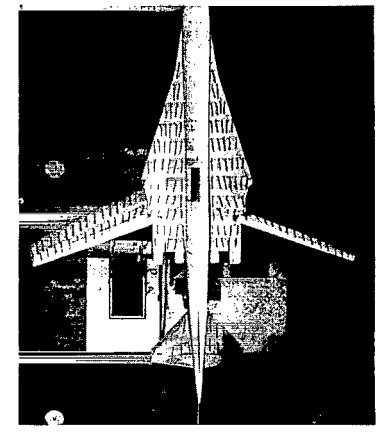

$\alpha = 8°$

(b) Clean configuration; $\Lambda = 30^{\circ}$.

L-68-5665

Figure 6.- Continued.

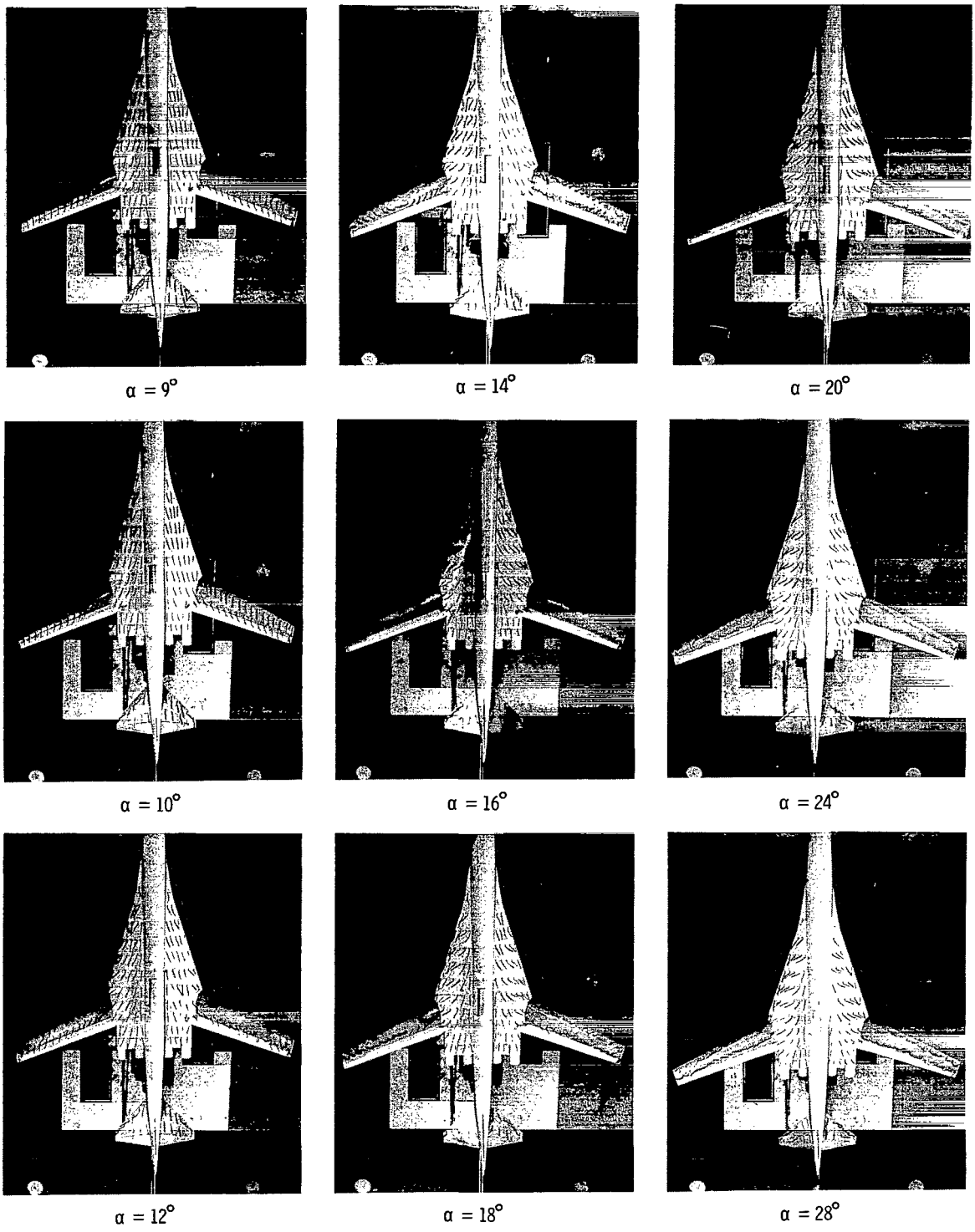

(b) Clean configuration; $\Lambda = 30^{\circ}$. Concluded. L-68-5666

Figure 6.- Continued.

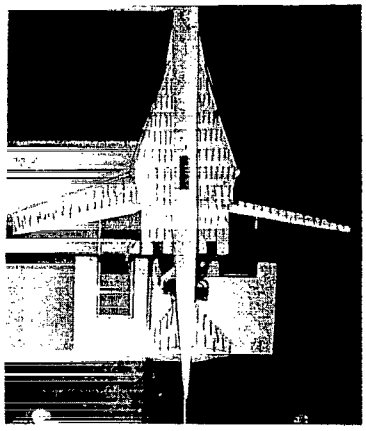

$\alpha = 0°$

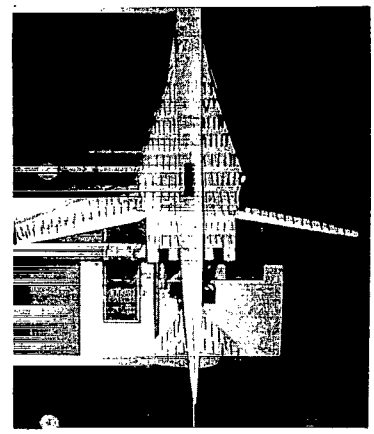

$\alpha = 3°$

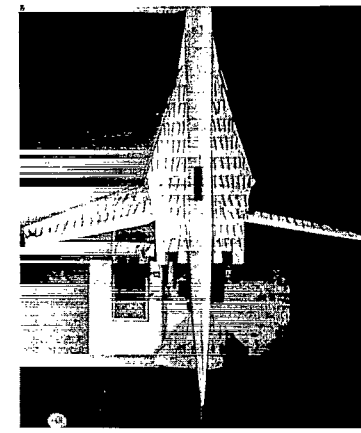

$\alpha = 6°$

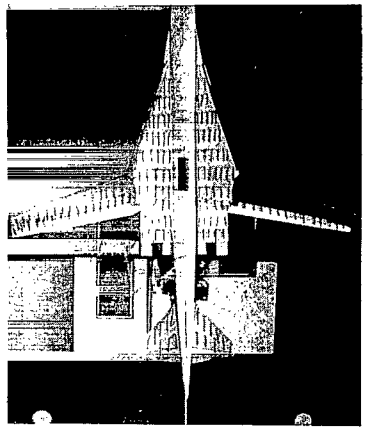

$\alpha = 1°$

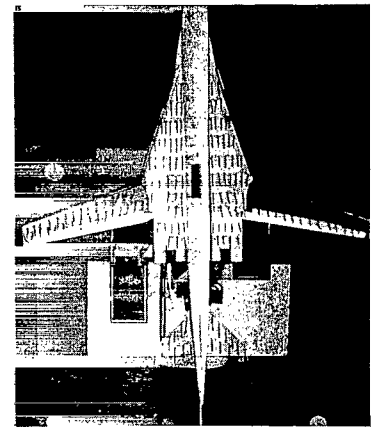

$\alpha = 4°$

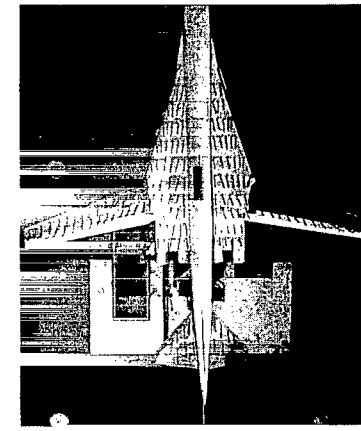

$\alpha = 7°$

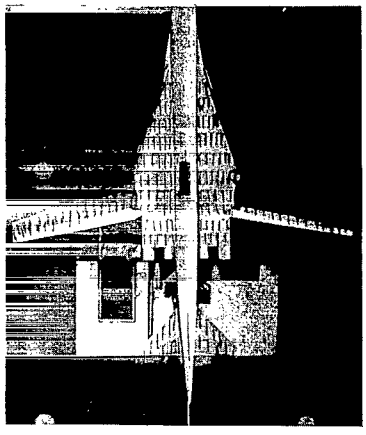

$\alpha = 2°$

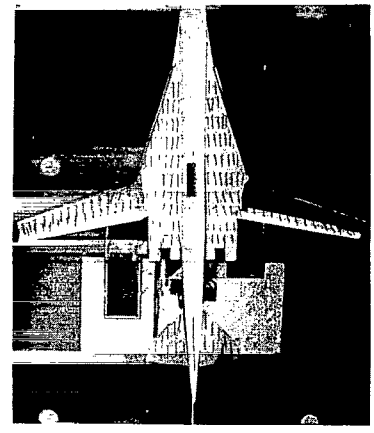

$\alpha = 5°$

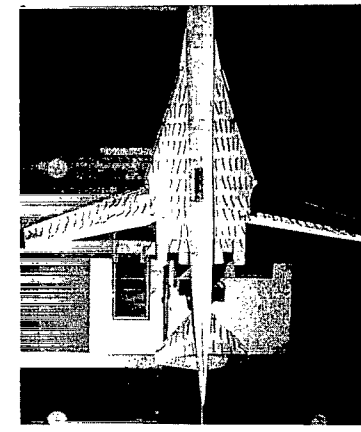

$\alpha = 8°$

(c) Slats extended; $\Lambda = 20^0$. L-68-5667

Figure 6.- Continued.

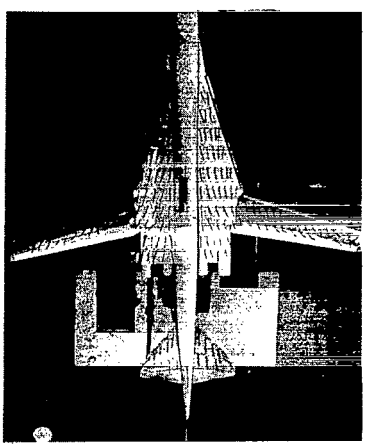

$\alpha = 9^\circ$

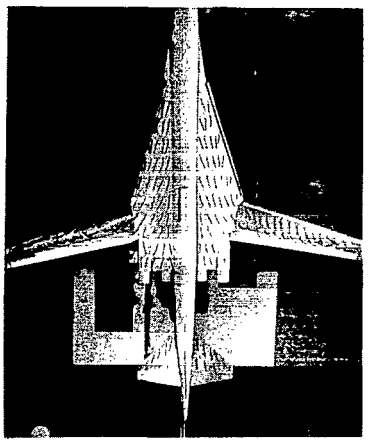

$\alpha = 14^\circ$

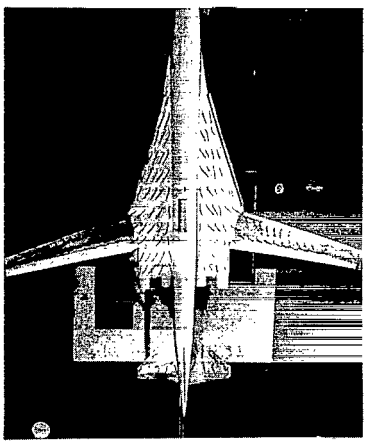

$\alpha = 20^\circ$

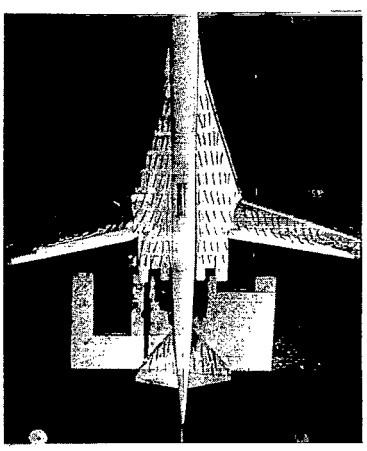

$\alpha = 10^\circ$

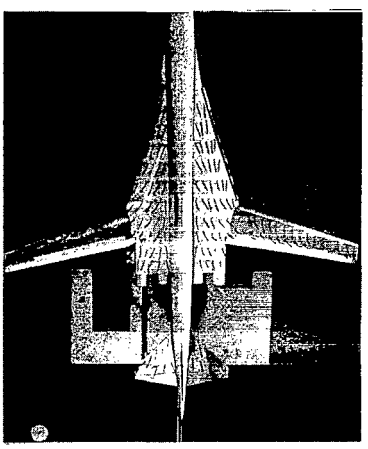

$\alpha = 16^\circ$

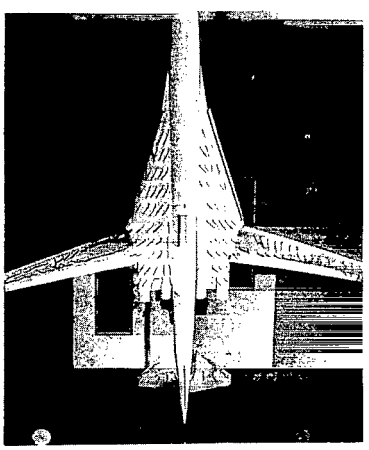

$\alpha = 24^\circ$

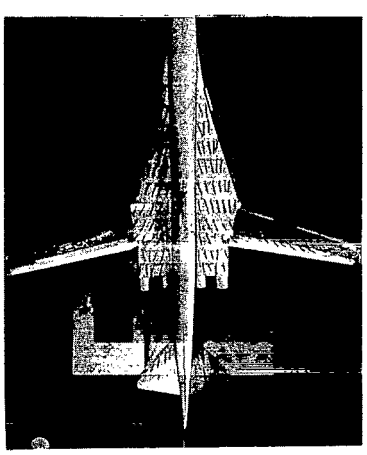

$\alpha = 12^\circ$

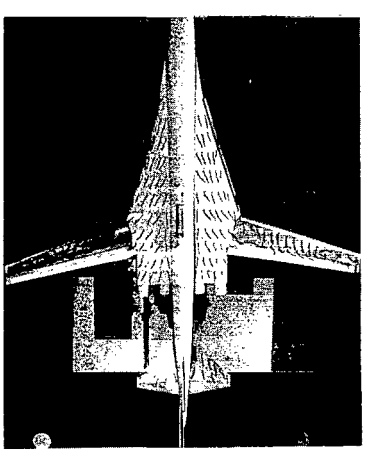

$\alpha = 18^\circ$

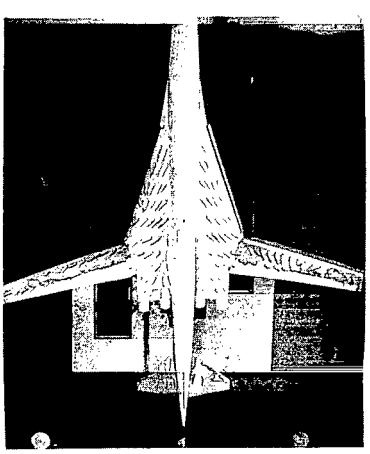

$\alpha = 28^\circ$

(c) Slats extended; $\Lambda = .20^\circ$. Concluded.

L-68-5668

Figure 6.- Continued.

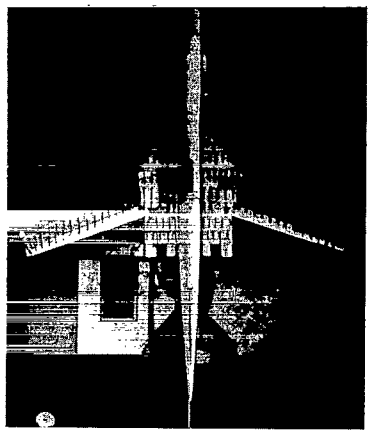

$\alpha = 0^{\circ}$

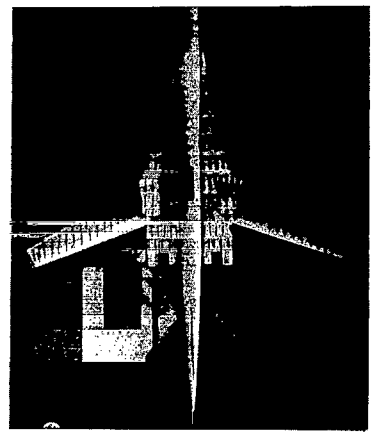

$\alpha = 3^{\circ}$

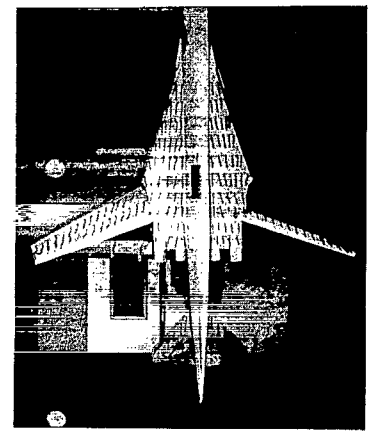

$\alpha = 6^{\circ}$

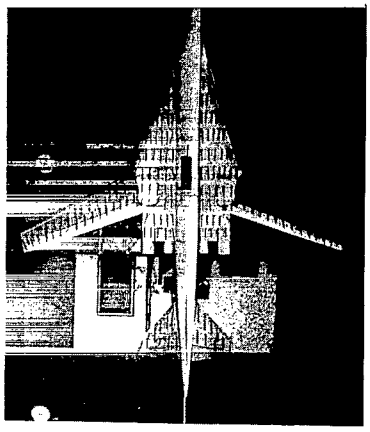

$\alpha = 1^{\circ}$

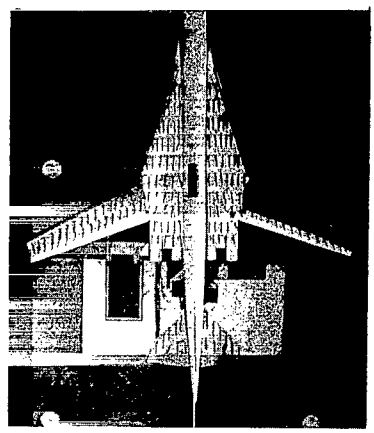

$\alpha = 4^{\circ}$

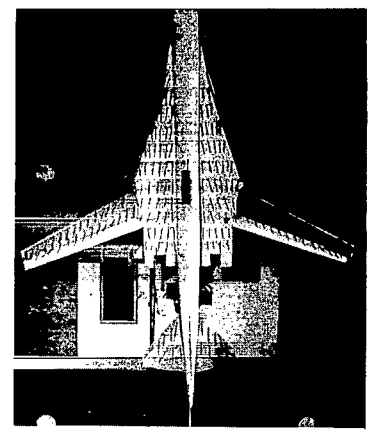

$\alpha = 7^{\circ}$

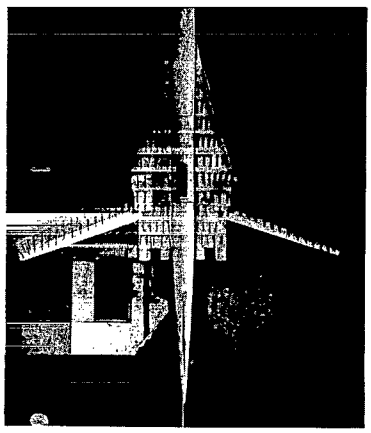

$\alpha = 2^{\circ}$

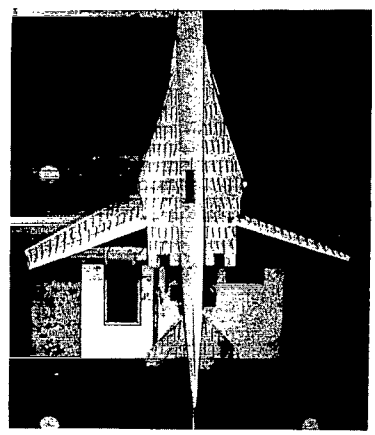

$\alpha = 5^{\circ}$

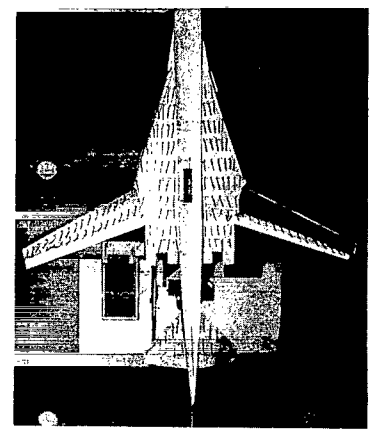

$\alpha = 8^{\circ}$

(d) Slats extended; $\Lambda = 30^{\circ}$.

L-68-5669

Figure 6.- Continued.

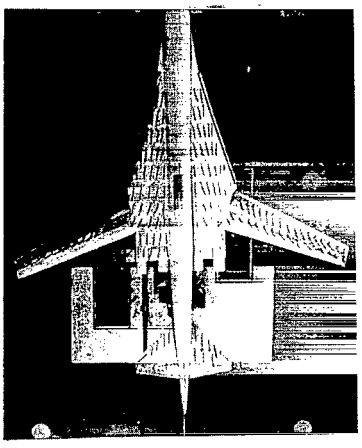

$\alpha = 9^\circ$

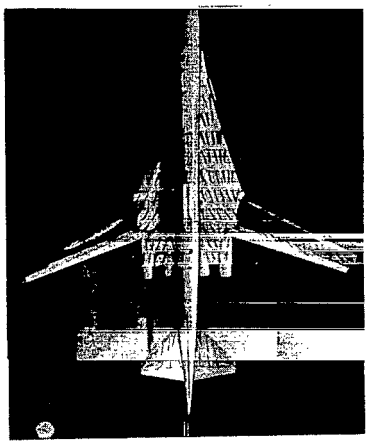

$\alpha = 14^\circ$

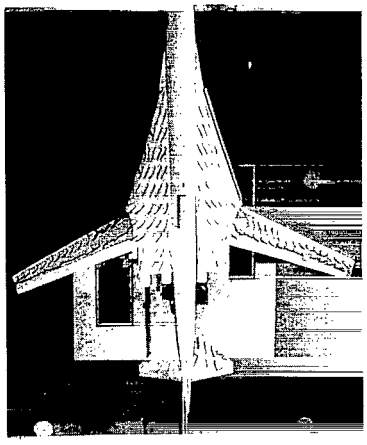

$\alpha = 20^\circ$

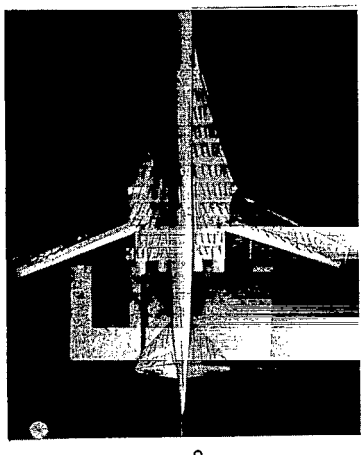

$\alpha = 10^\circ$

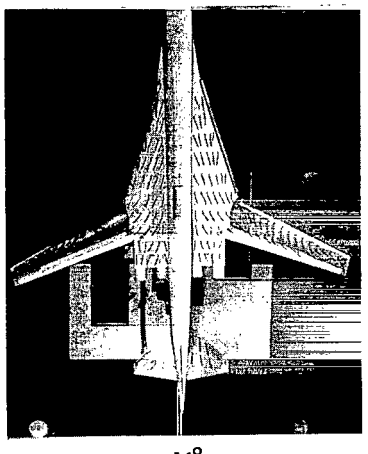

$\alpha = 16^\circ$

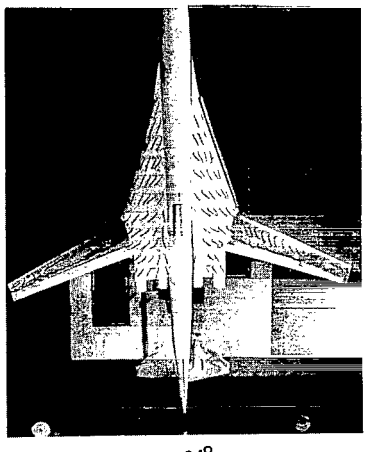

$\alpha = 24^\circ$

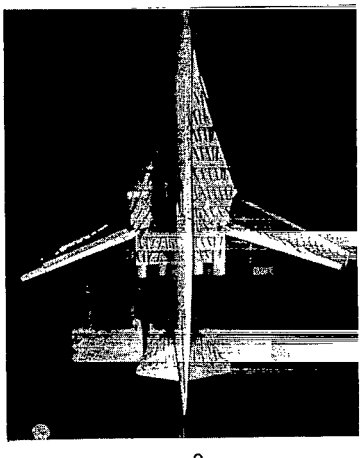

$\alpha = 12^\circ$

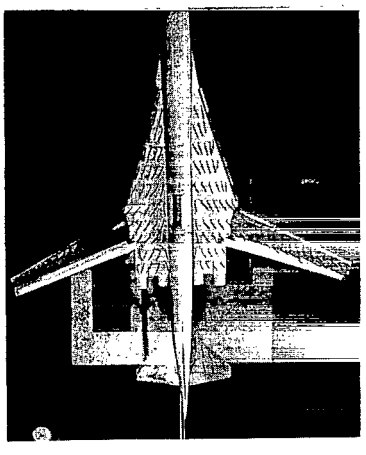

$\alpha = 18^\circ$

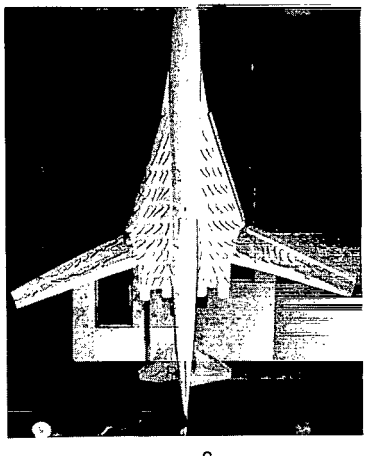

$\alpha = 28^\circ$

(d) Slat extended; $\Lambda = 30^\circ$. Concluded.

L-68-5670

Figure 6.- Continued.

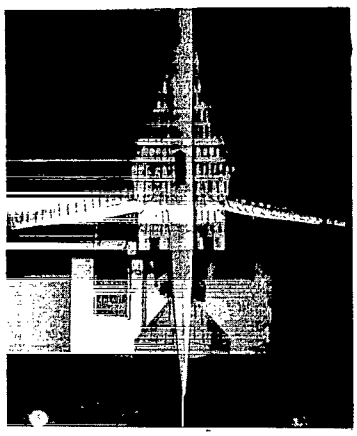

$\alpha = -5^\circ$

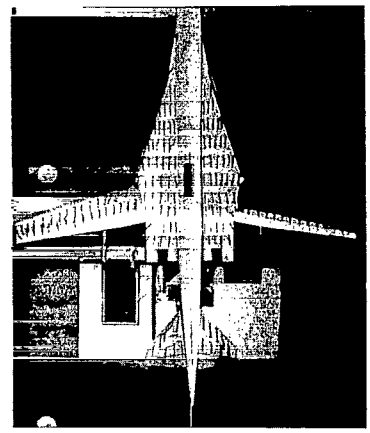

$\alpha = 1^\circ$

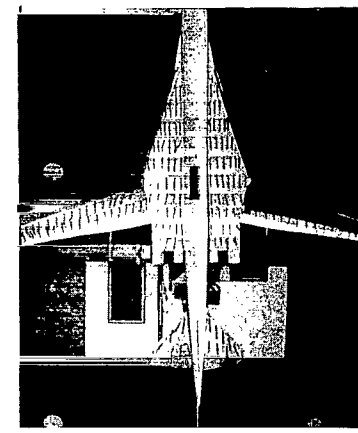

$\alpha = 4^\circ$

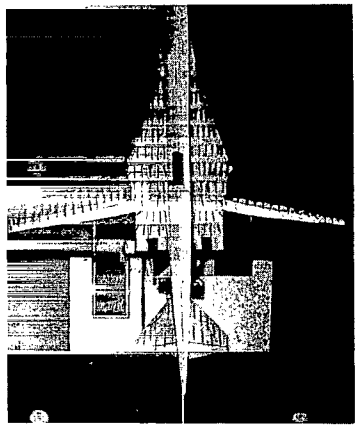

$\alpha = -3^\circ$

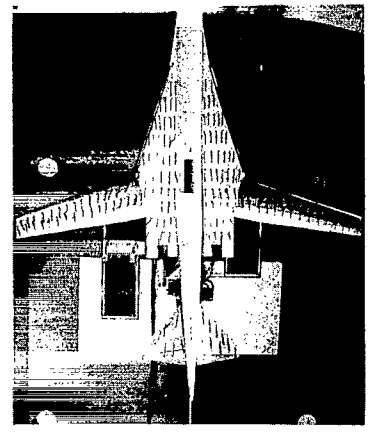

$\alpha = 2^\circ$

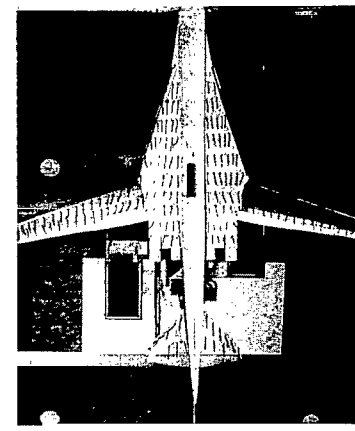

$\alpha = 5^\circ$

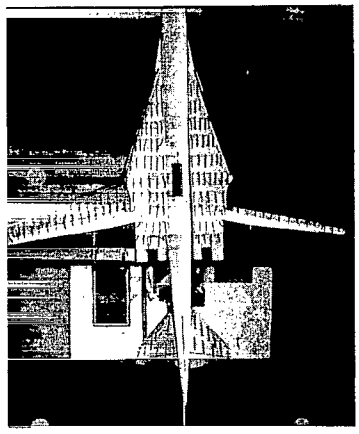

$\alpha = 0^\circ$

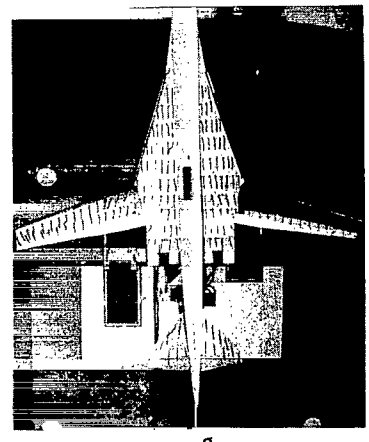

$\alpha = 3^\circ$

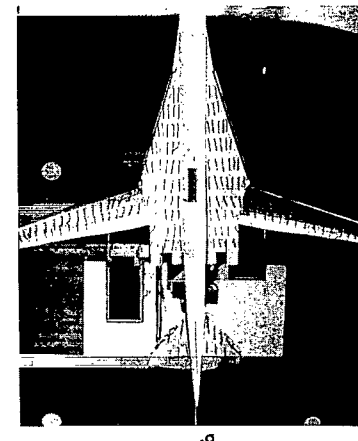

$\alpha = 6^\circ$

(e) Slats and flaps extended; $\Lambda = 20^\circ$. L-68-5671

Figure 6.- Continued.

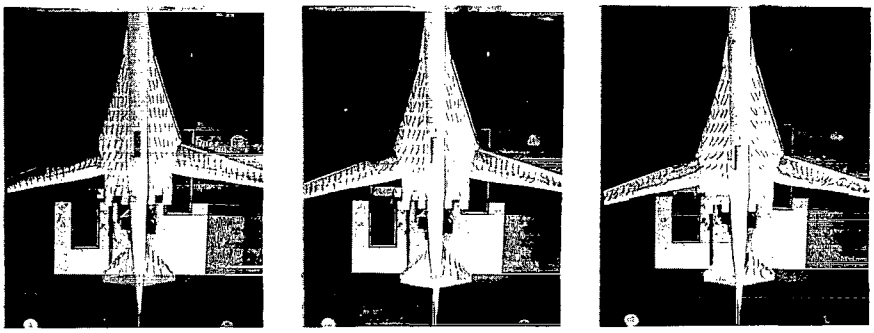

α = 7°

α = 12°

α = 20°

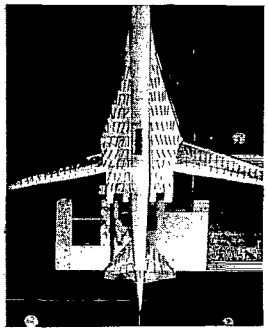

α = 8°

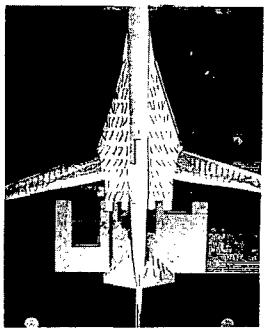

α = 14°

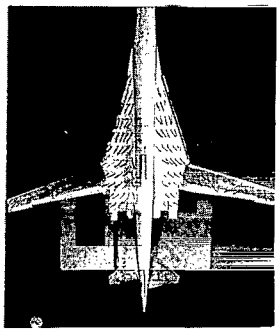

α = 24°

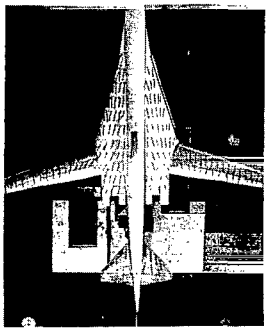

α = 9°

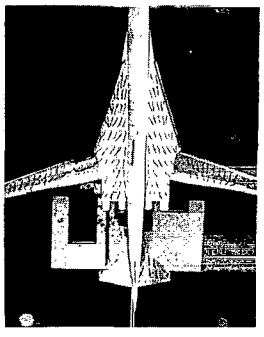

α = 16°

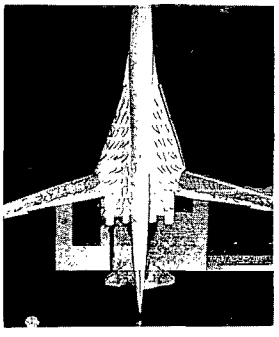

α = 28°

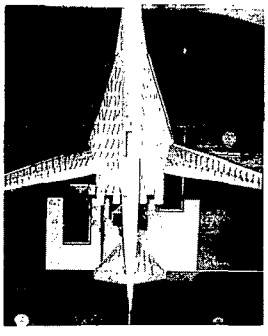

α = 10°

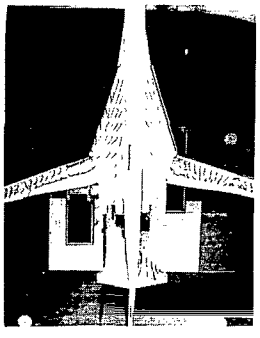

α = 18°

(e) Slats and flaps extended; Λ = 20°. Concluded.

L-68-5672

Figure 6.- Concluded.

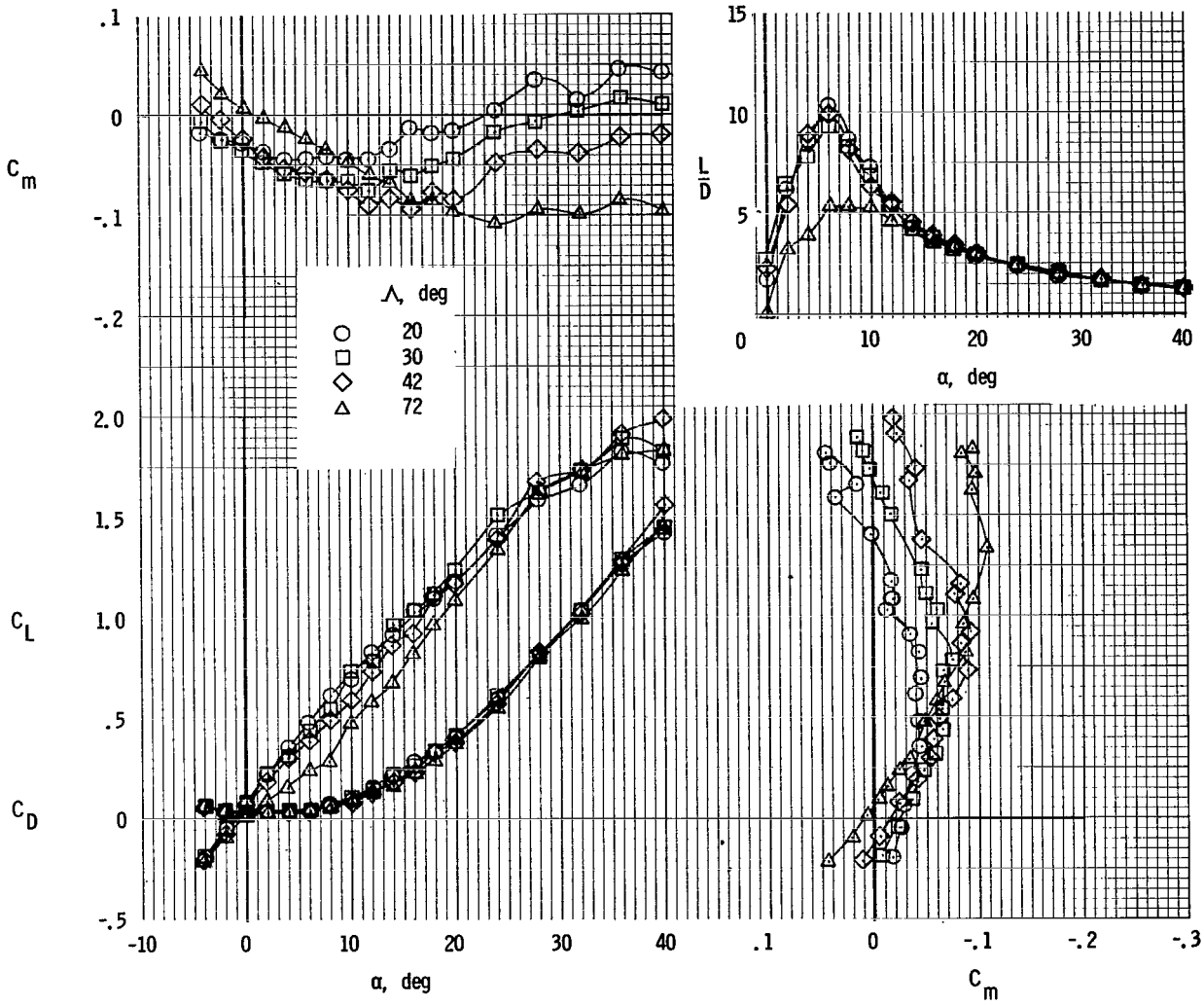

Figure 7.- Effect of wing sweep on the longitudinal stability characteristics of the model in the clean configuration. $C_T = 0$.

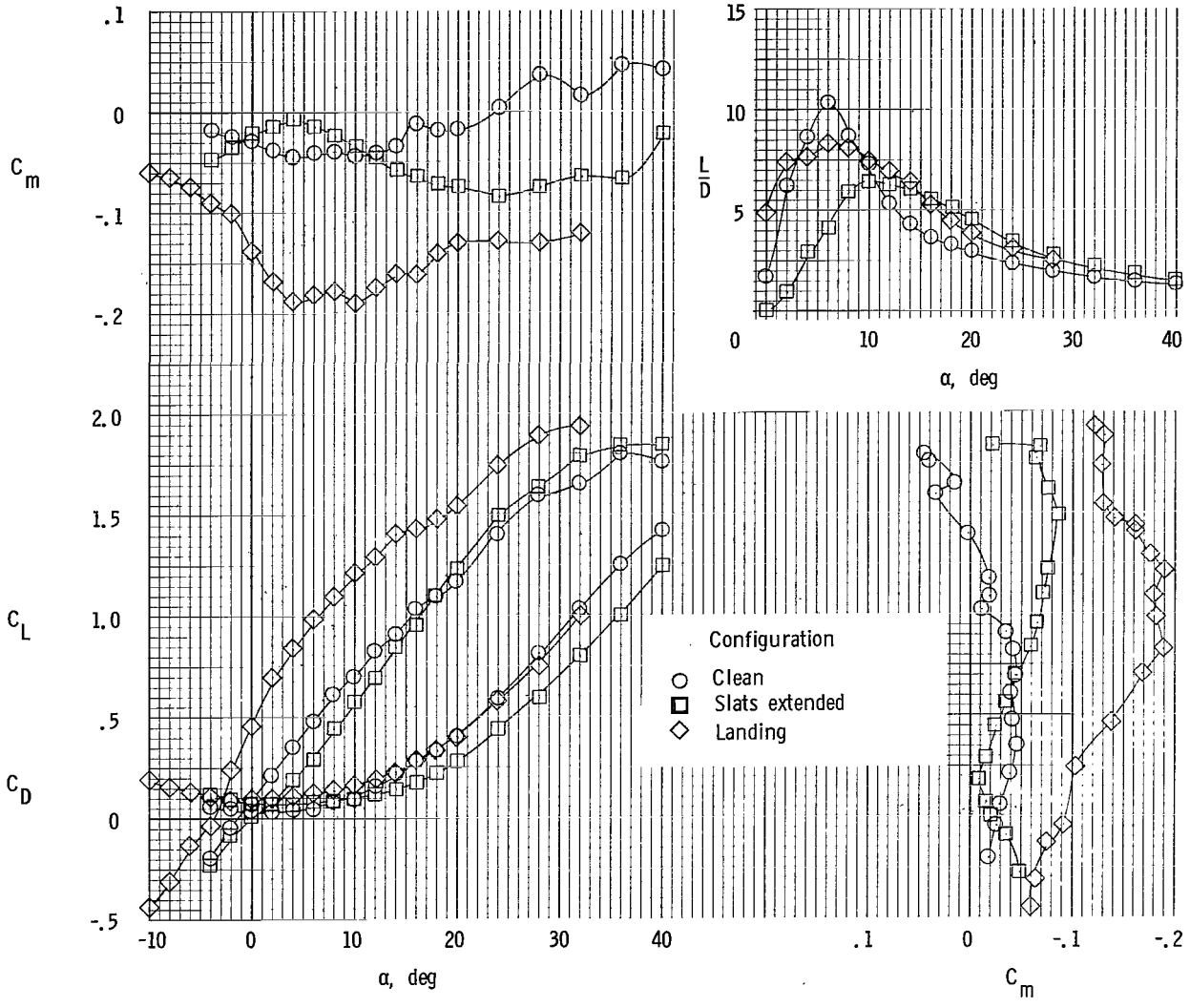

(a) $\Lambda = 20^{o}$.

Figure 8.- Effect of leading-edge slats and trailing-edge flaps on the longitudinal characteristics of the model. $C_T = 0$.

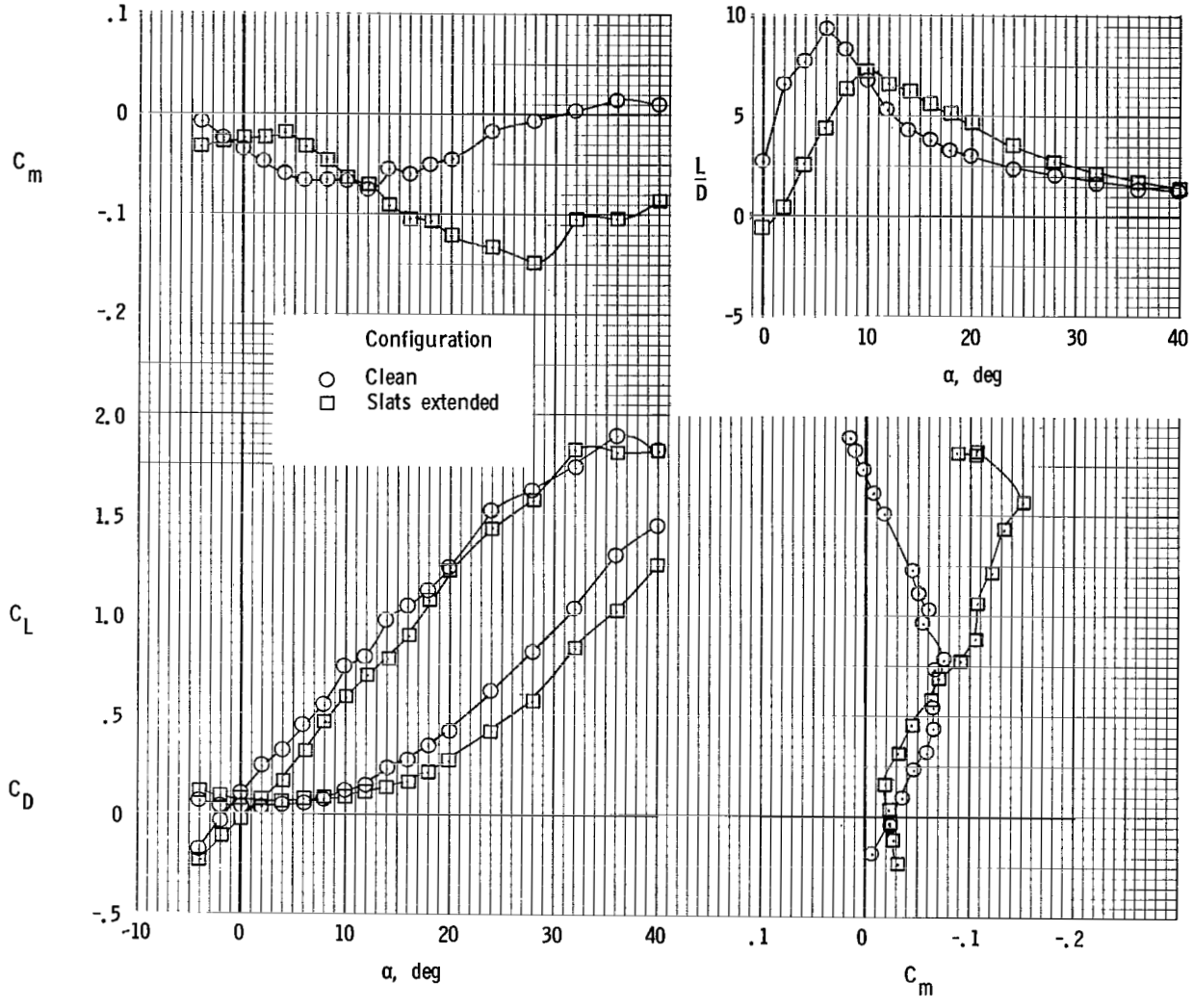

(b) $\Lambda = 30^0$.

Figure 8.- Continued.

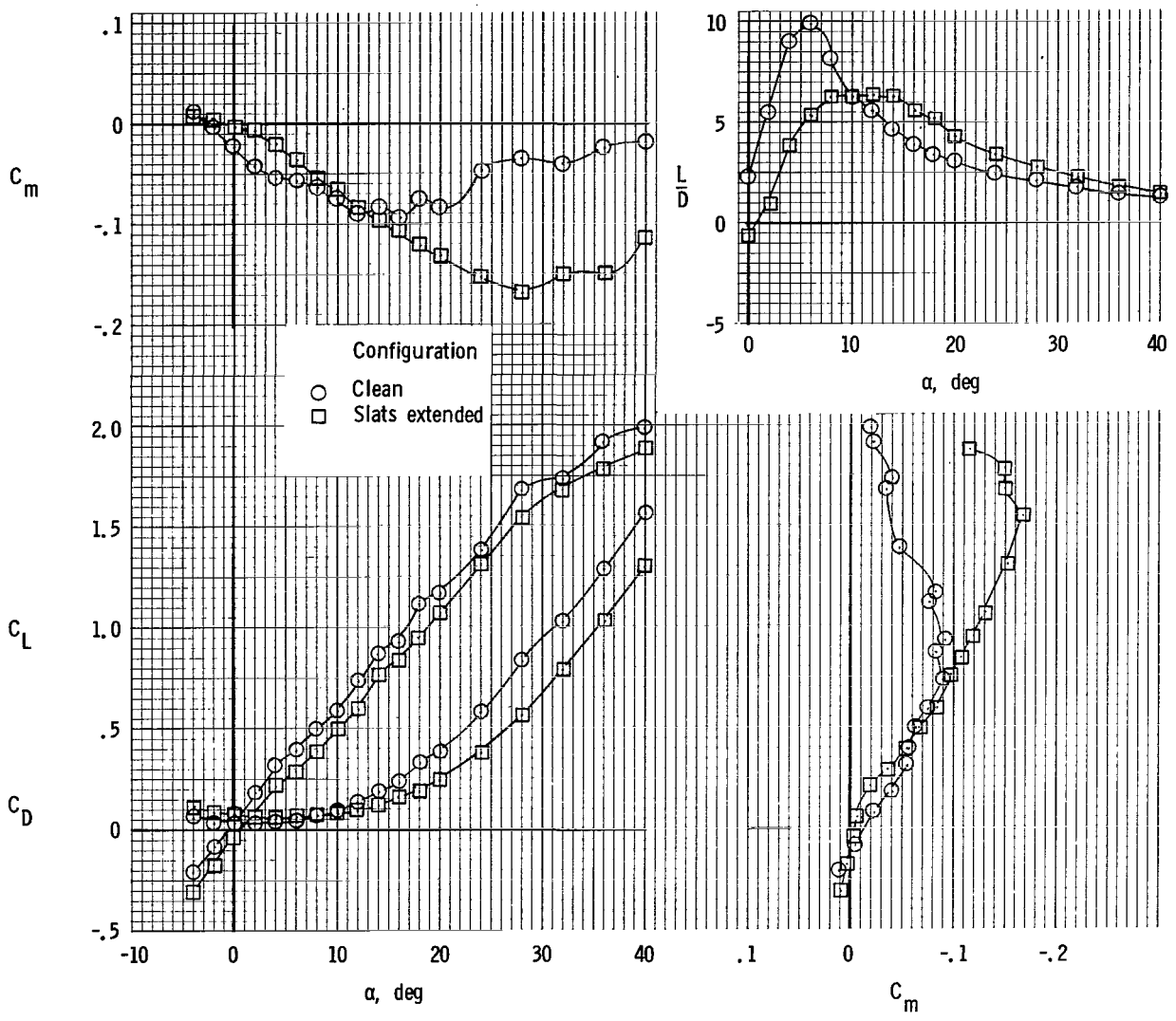

(c) $\Lambda = 42^{o}$.

Figure 8.- Continued.

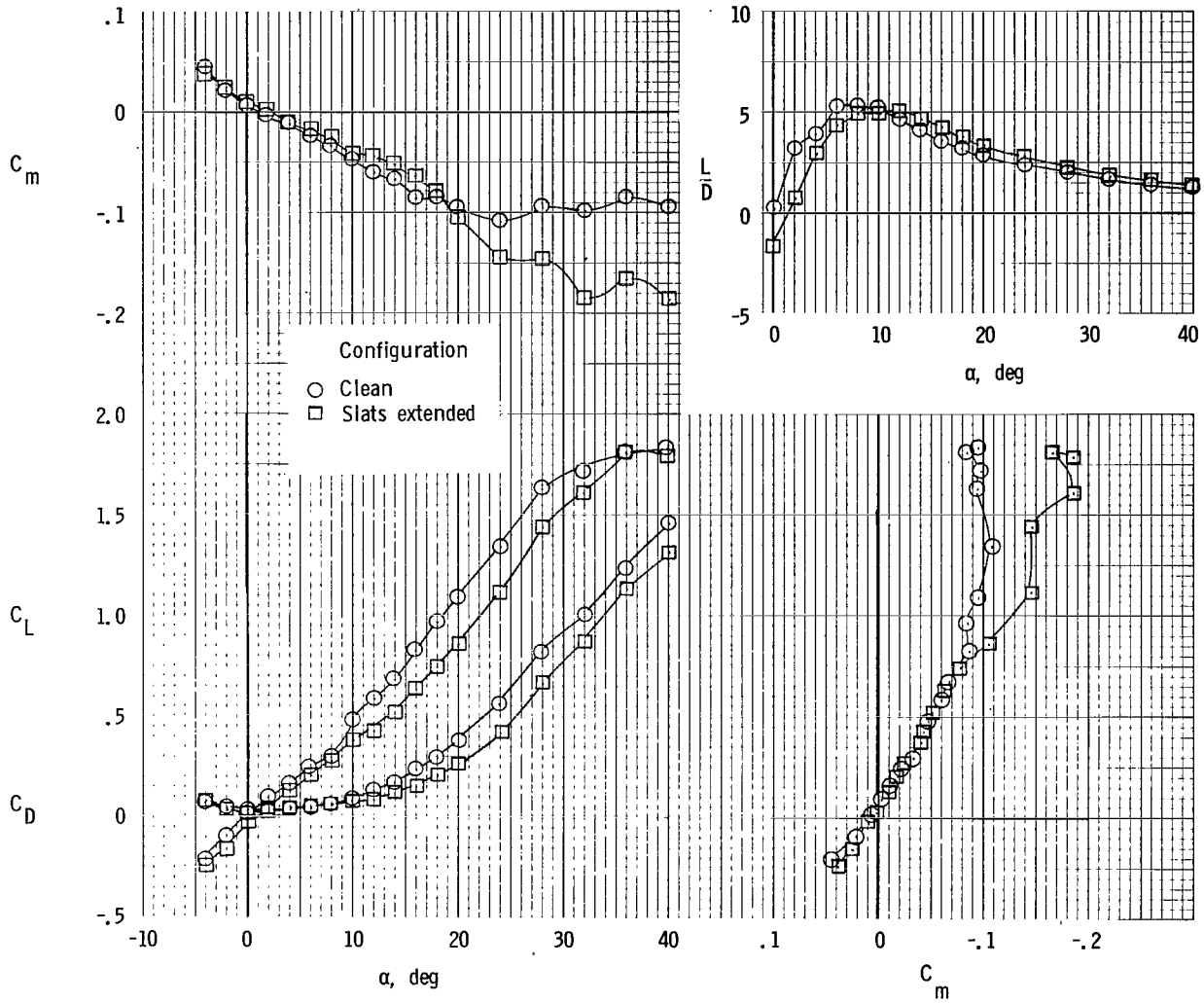

(d) $\Lambda = 72^{o}$.

Figure 8.- Concluded.

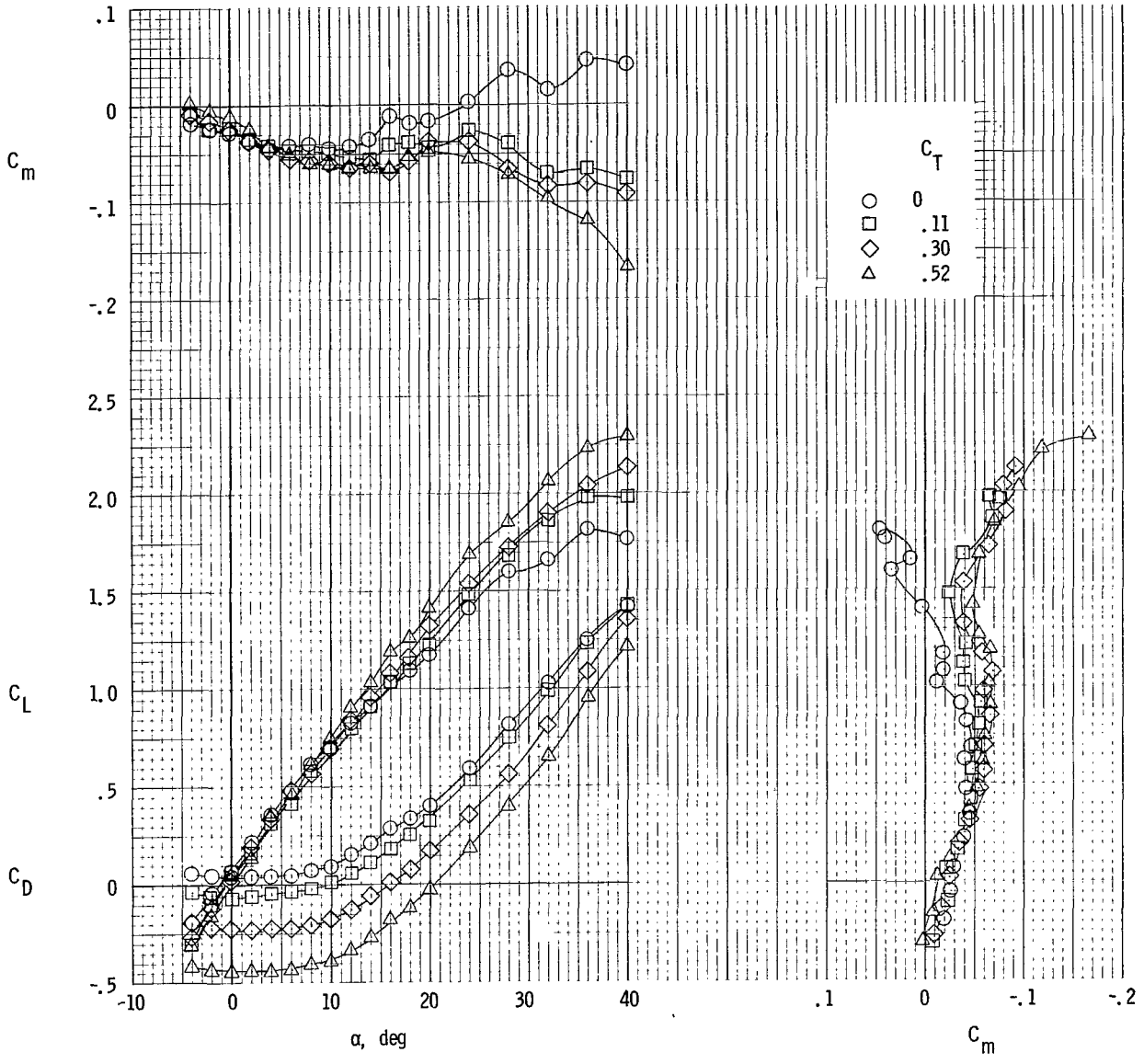

(a) Clean configuration; $\Lambda = 20^{o}$.

Figure 9.- Effect of power on the static longitudinal stability characteristics of the model. $i_t = 0^{o}$.

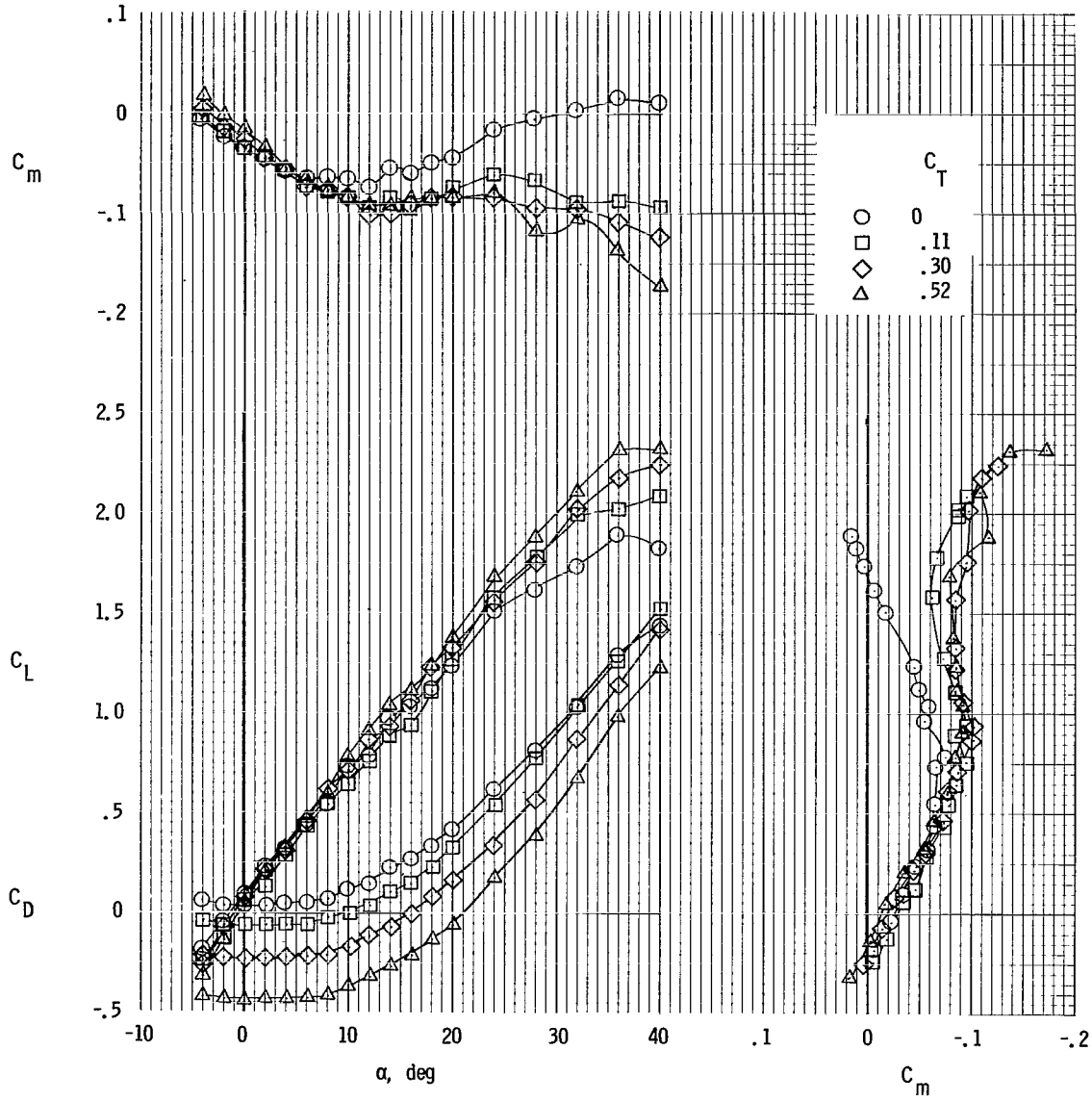

(b) Clean configuration; $\Lambda = 30^{o}$.

Figure 9.- Continued.

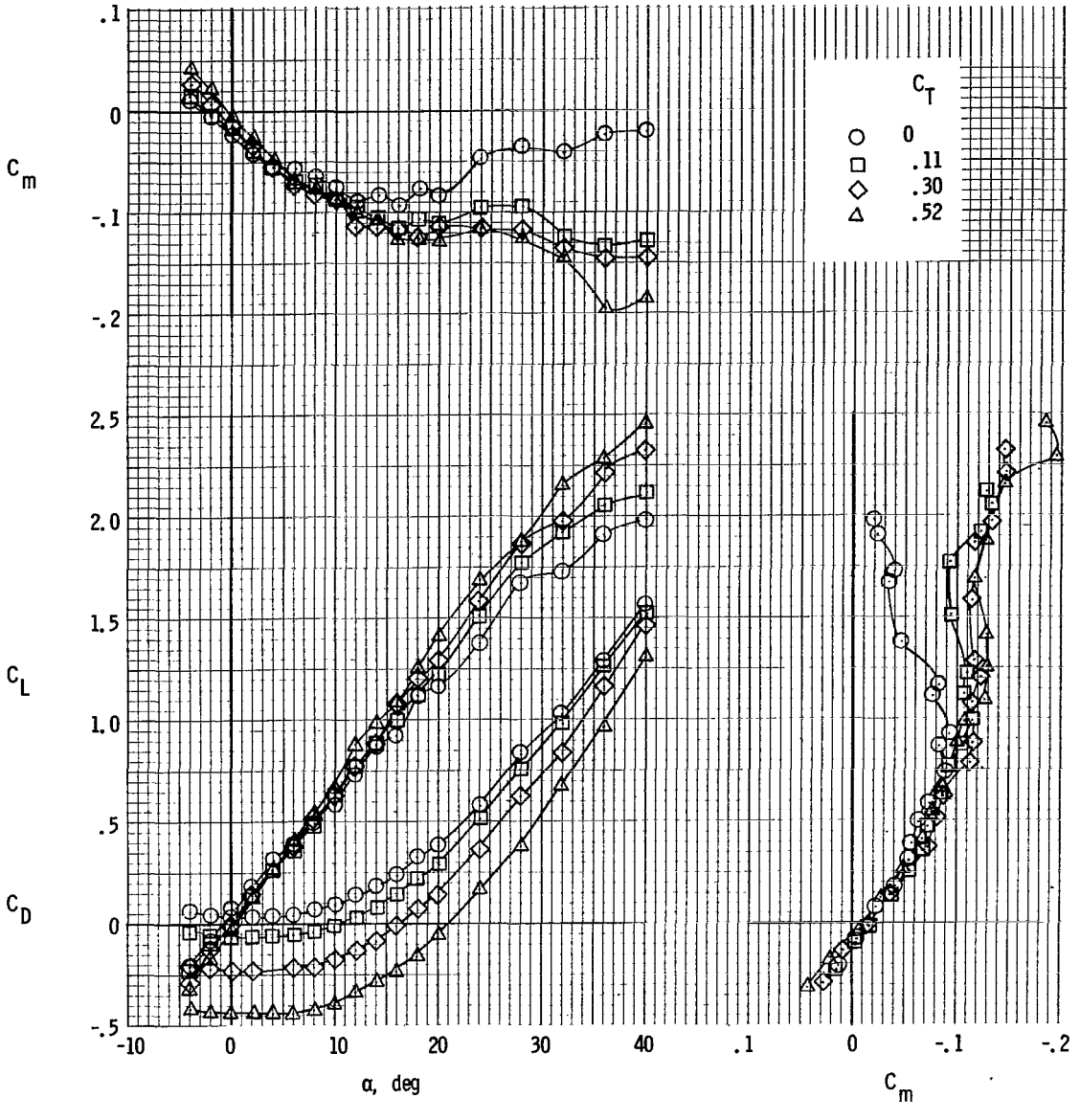

(c) Clean configuration; $\Lambda = 42^{o}$.

Figure 9.- Continued.

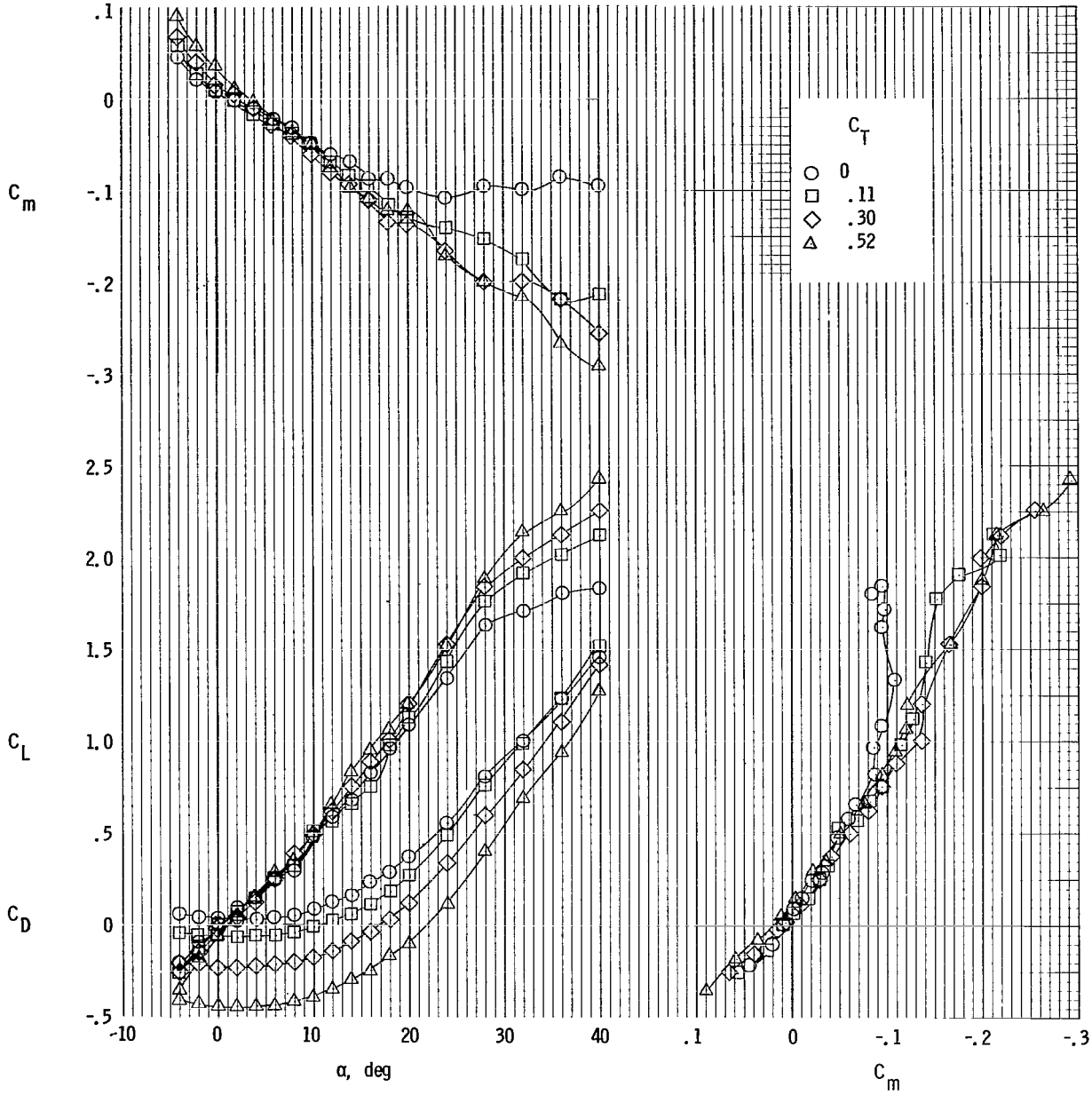

(d) Clean configuration; $\Lambda = 72^0$.

Figure 9.- Concluded.

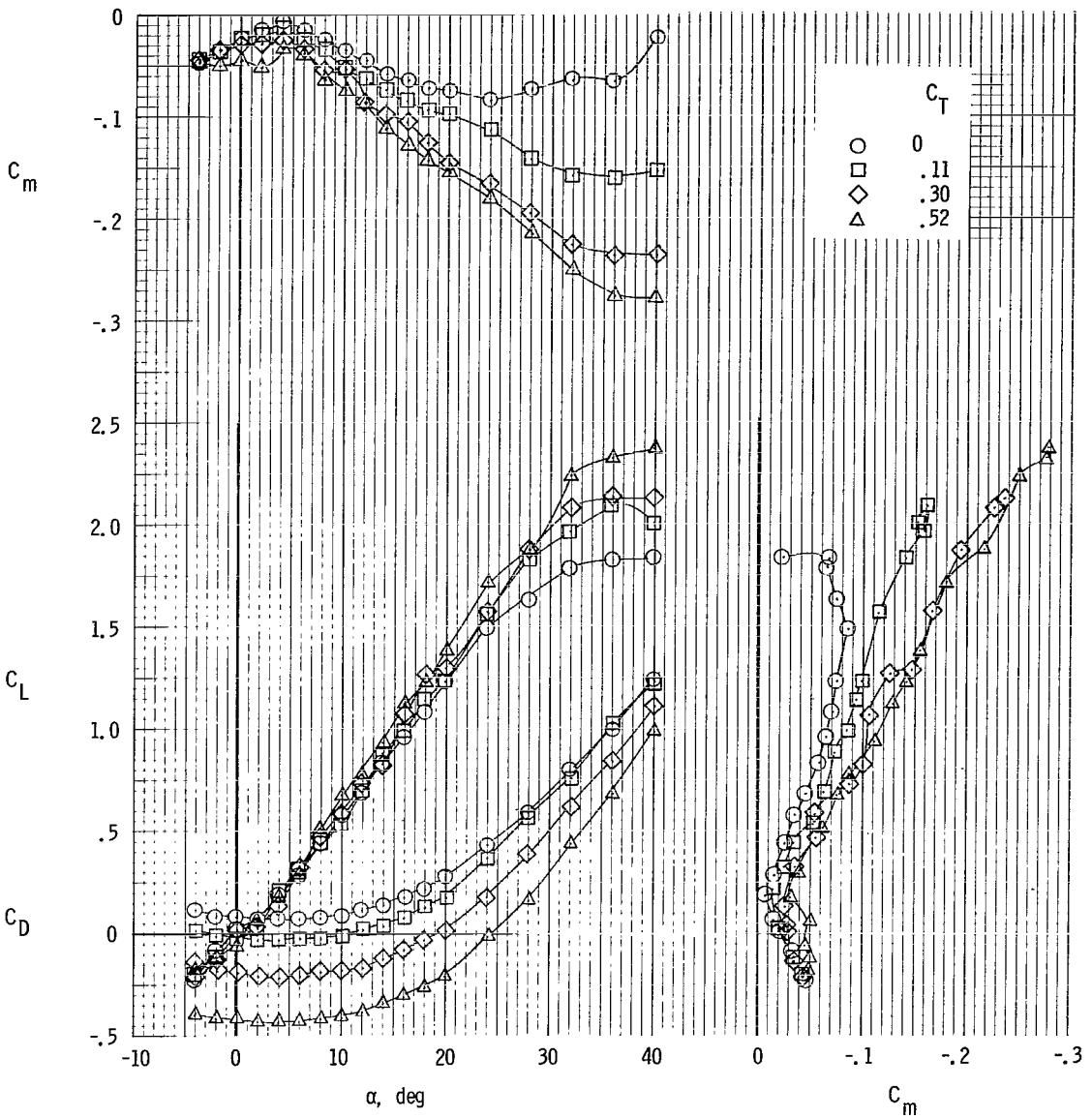

(a) Slats extended; $\Lambda = 20^{o}$.

Figure 10.- Effect of power on static longitudinal stability characteristics of model. $i_t = 0^{o}$.

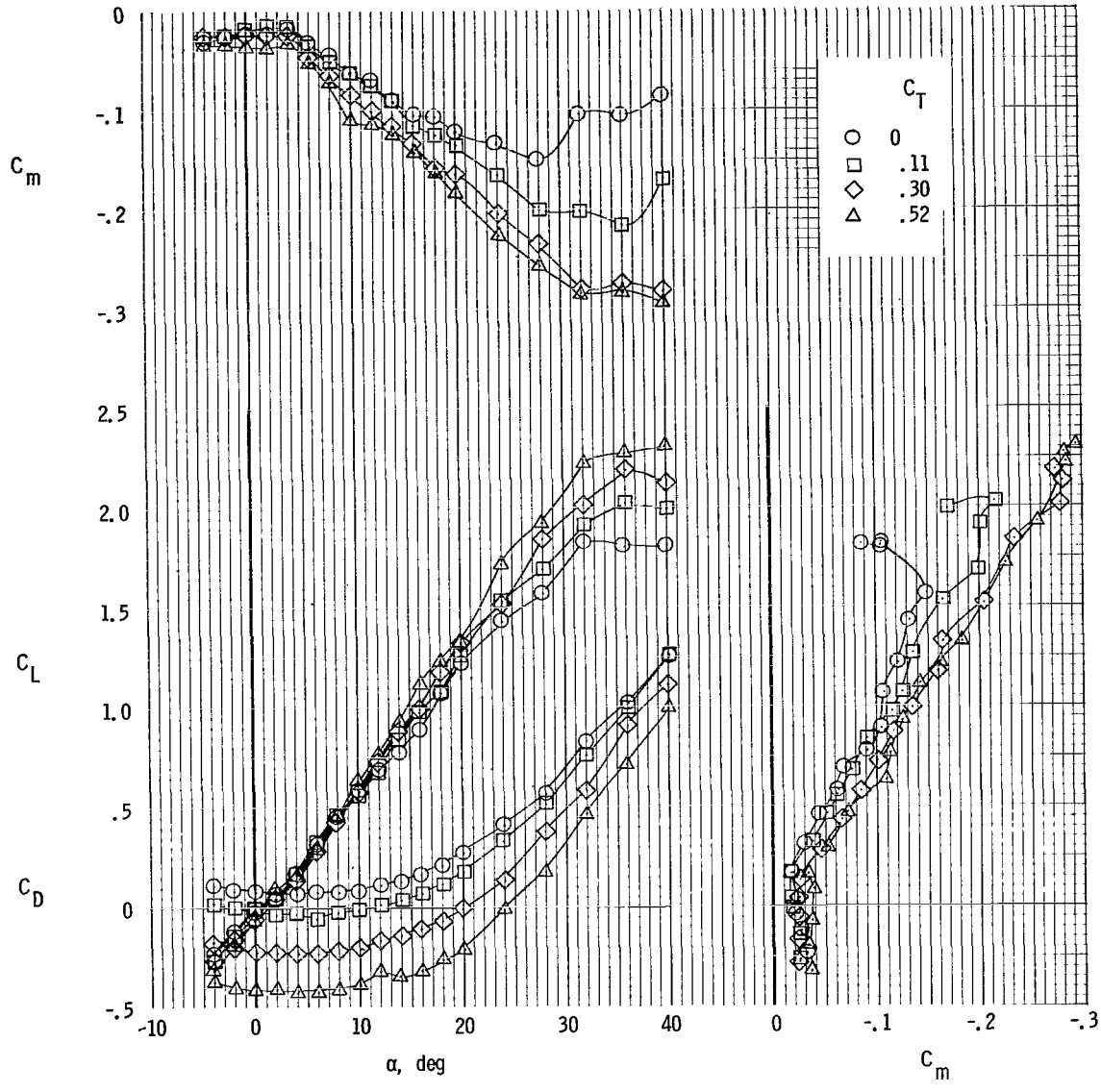

(b) Slats extended; $\Lambda = 30^{o}$.

Figure 10.- Continued.

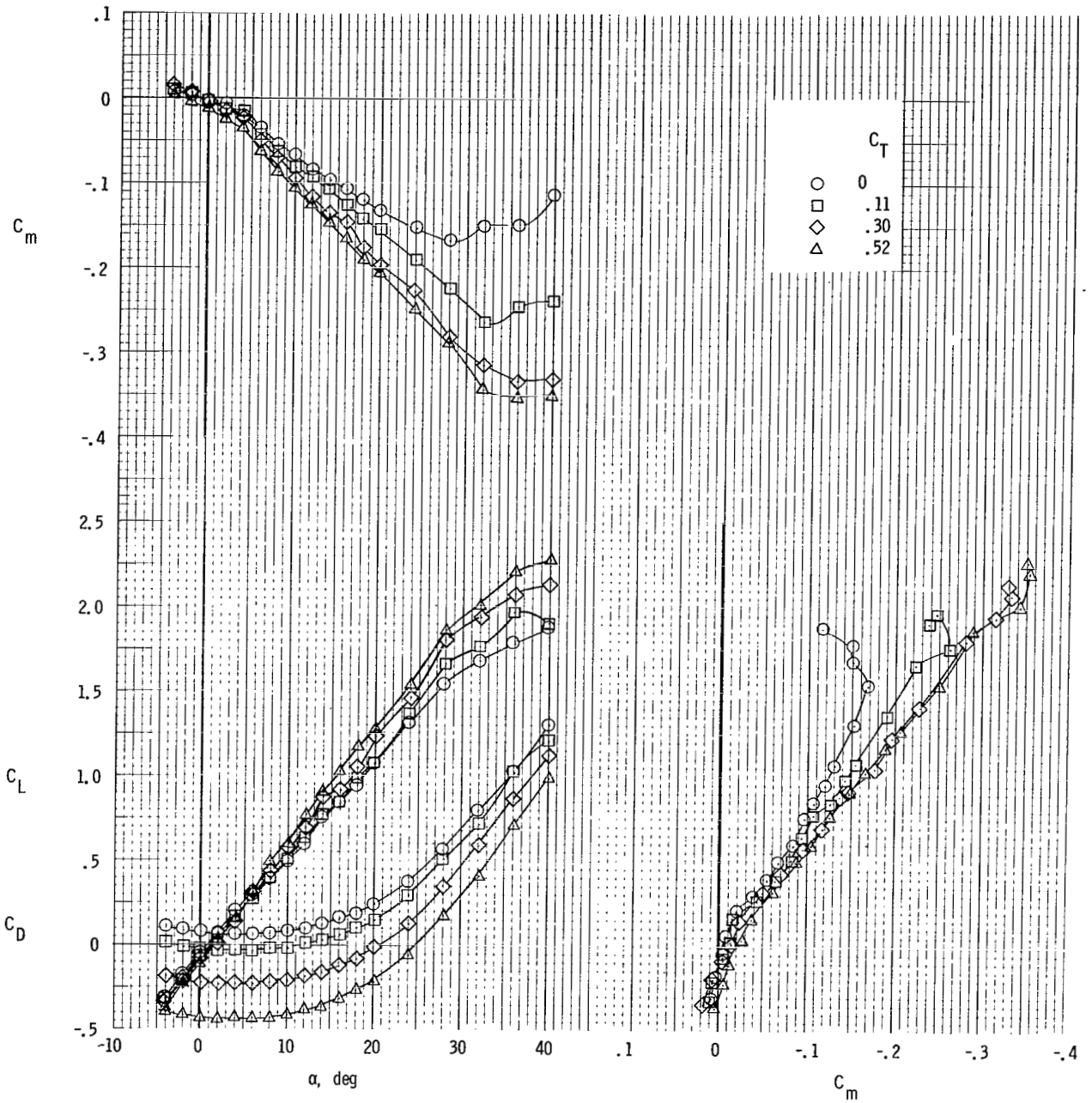

(c) Slats extended; $\Lambda = 42^{o}$.

Figure 10.- Continued.

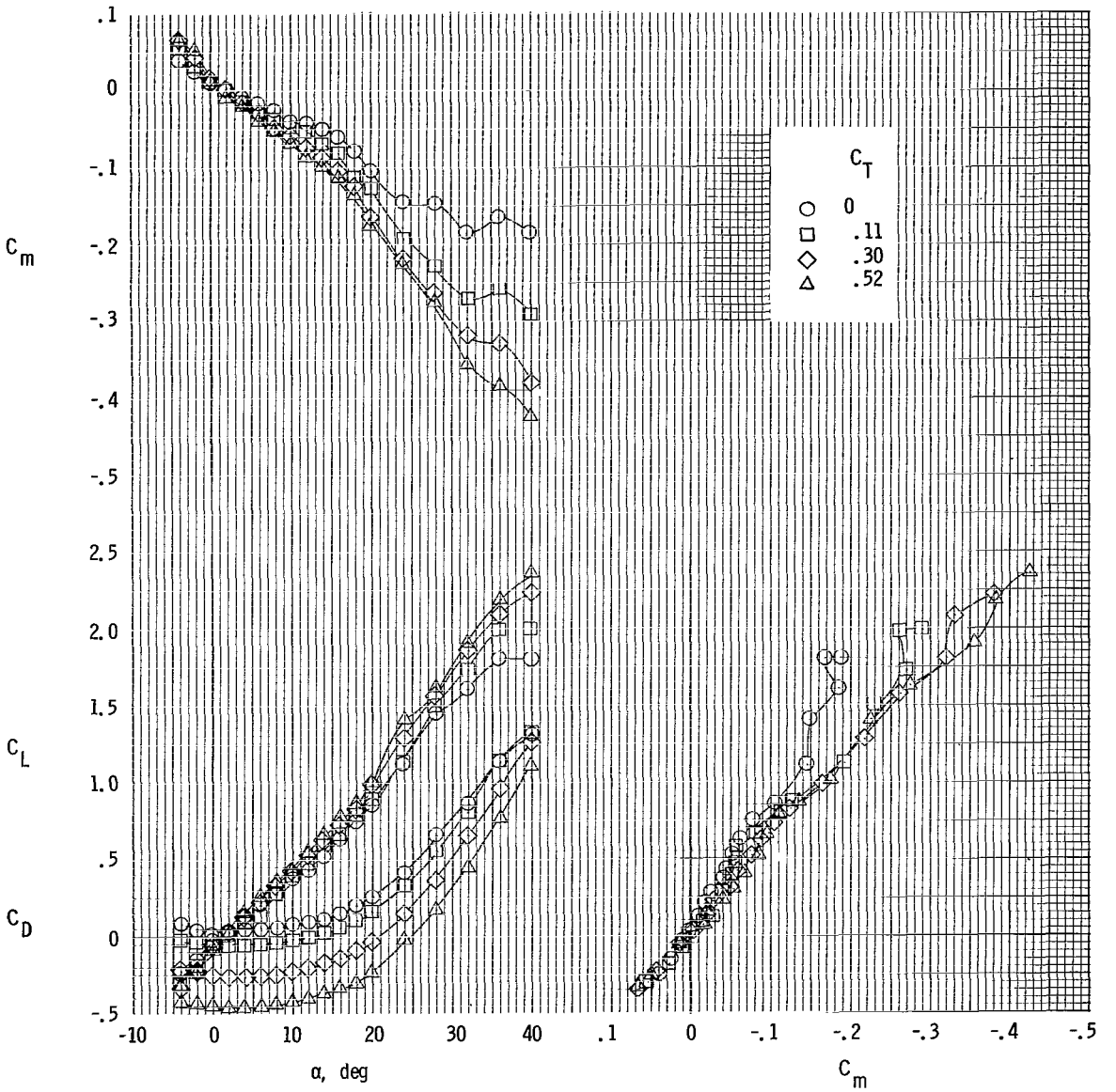

(d) Slats extended; $\Lambda = 72^{o}$.

Figure 10.- Continued.

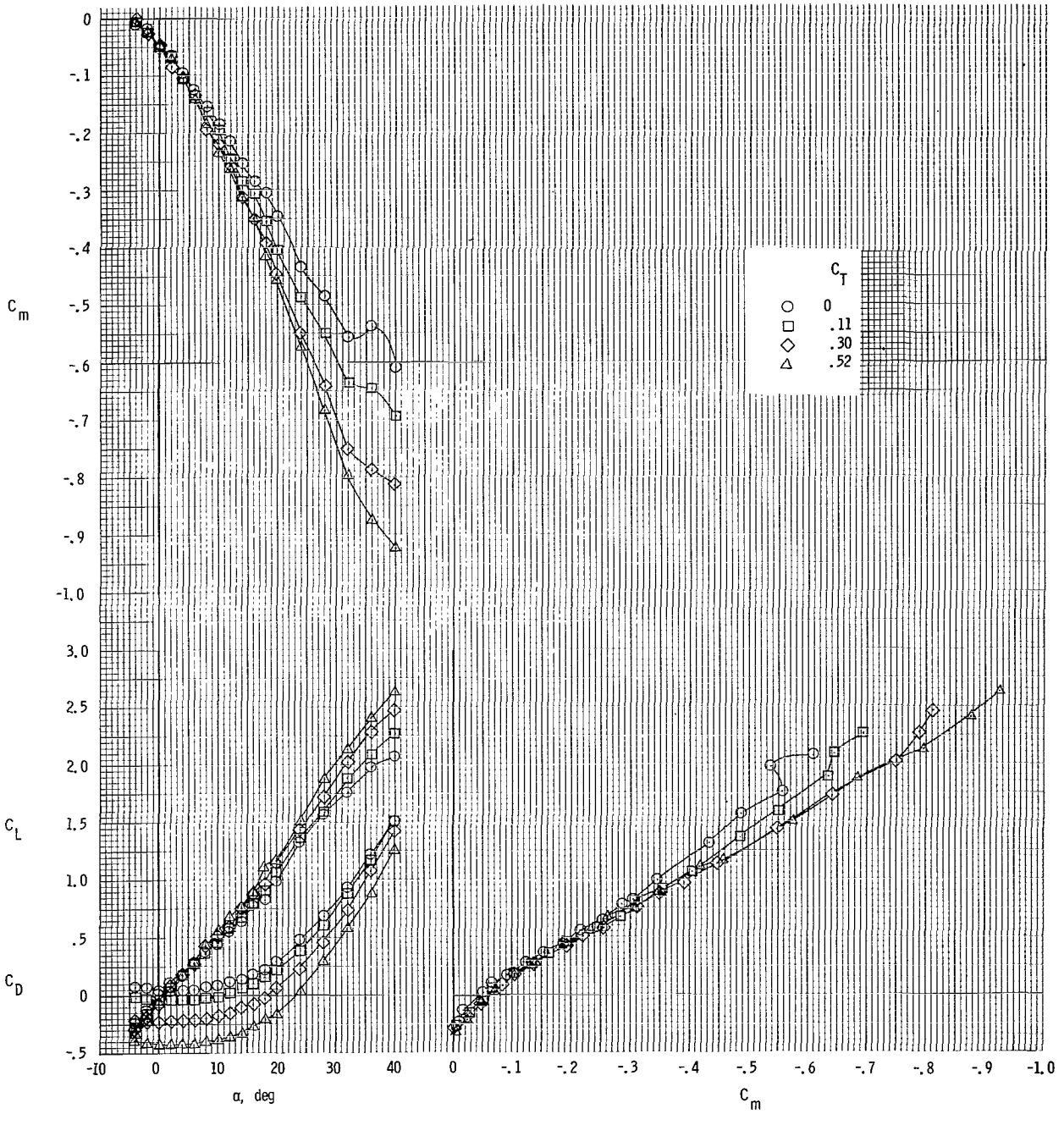

(e) Slats extended; large horizontal tail; $\Lambda = 72^{o}$.

Figure 10.- Concluded.

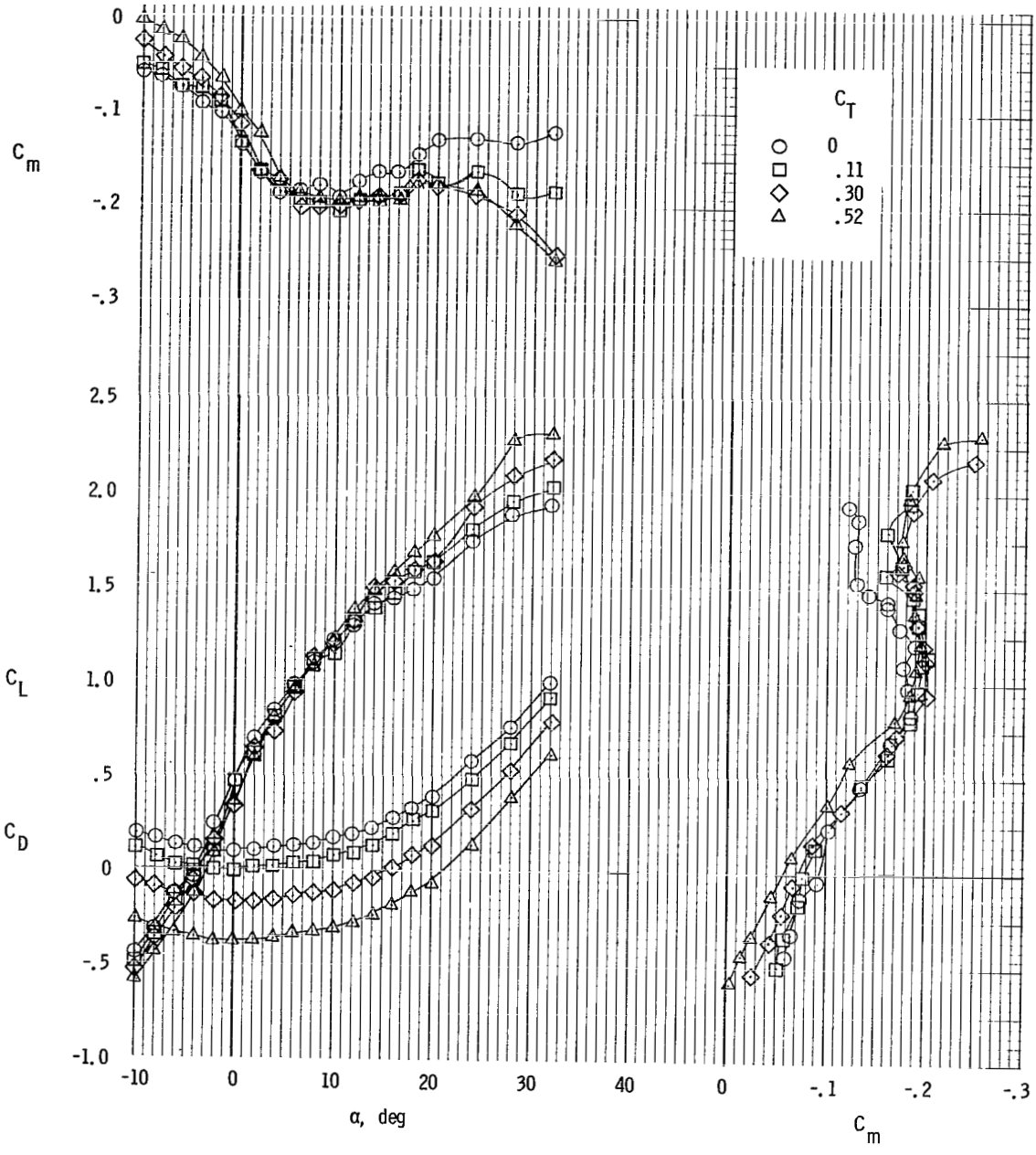

Figure 11.- Effect of power on static longitudinal stability characteristics of model. $i_t = 0^o$; landing configuration; $\Lambda = 20^o$.

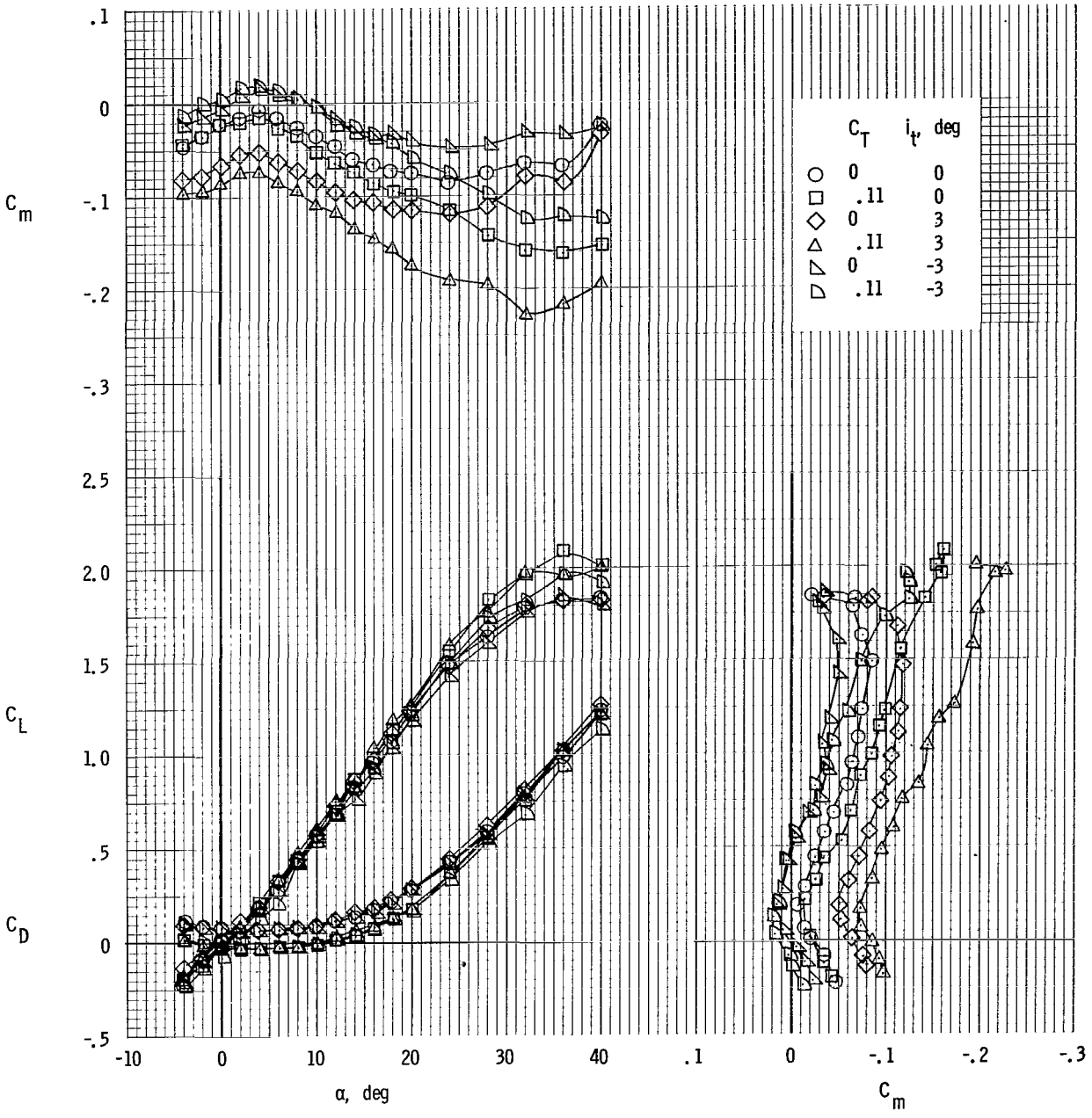

(a) Slats extended; $\Lambda = 20^{o}$.

Figure 12.- Effect of power on longitudinal control characteristics of model.

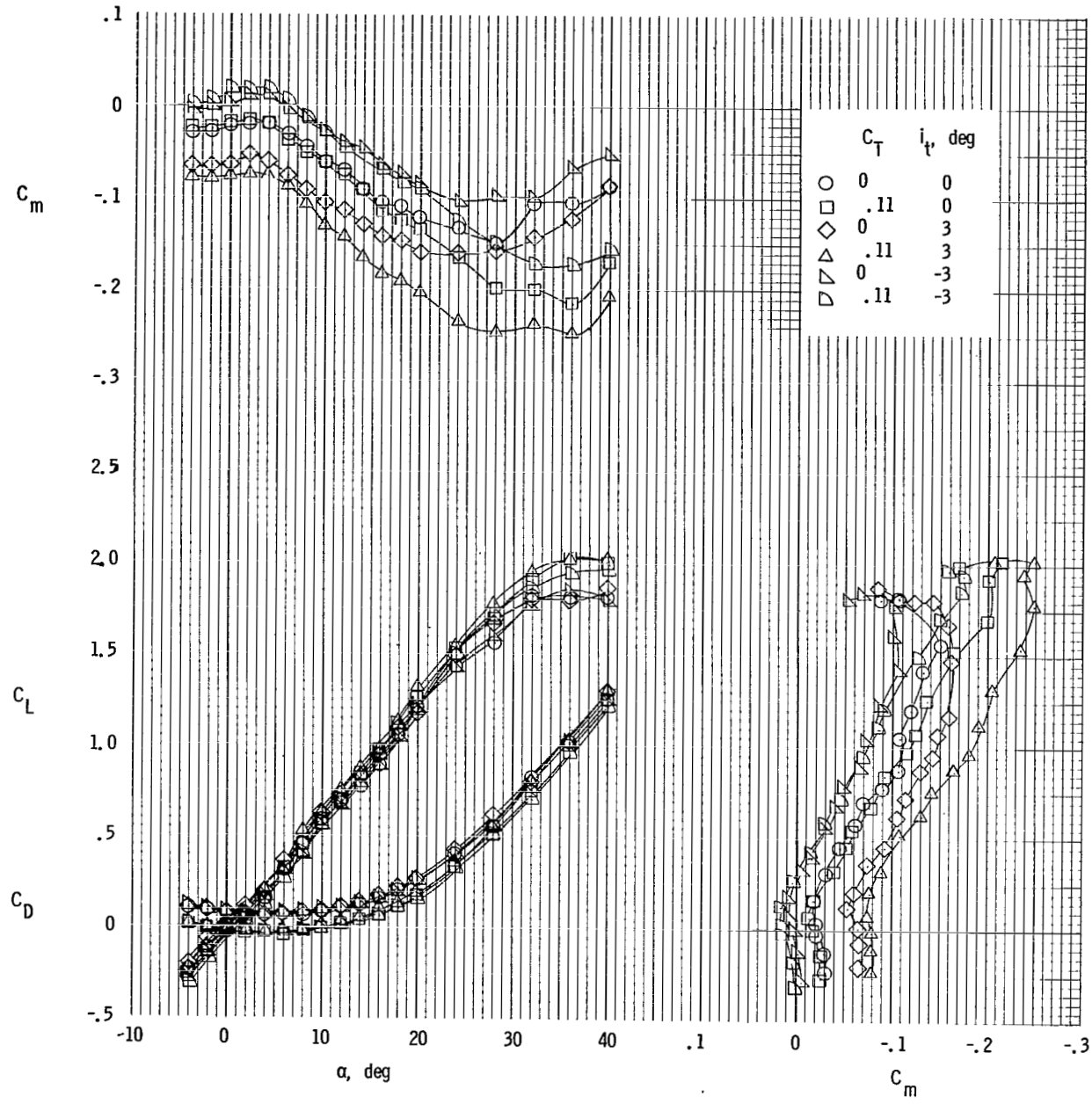

(b) Slats extended; $\Lambda = 30^{o}$.

Figure 12.- Continued.

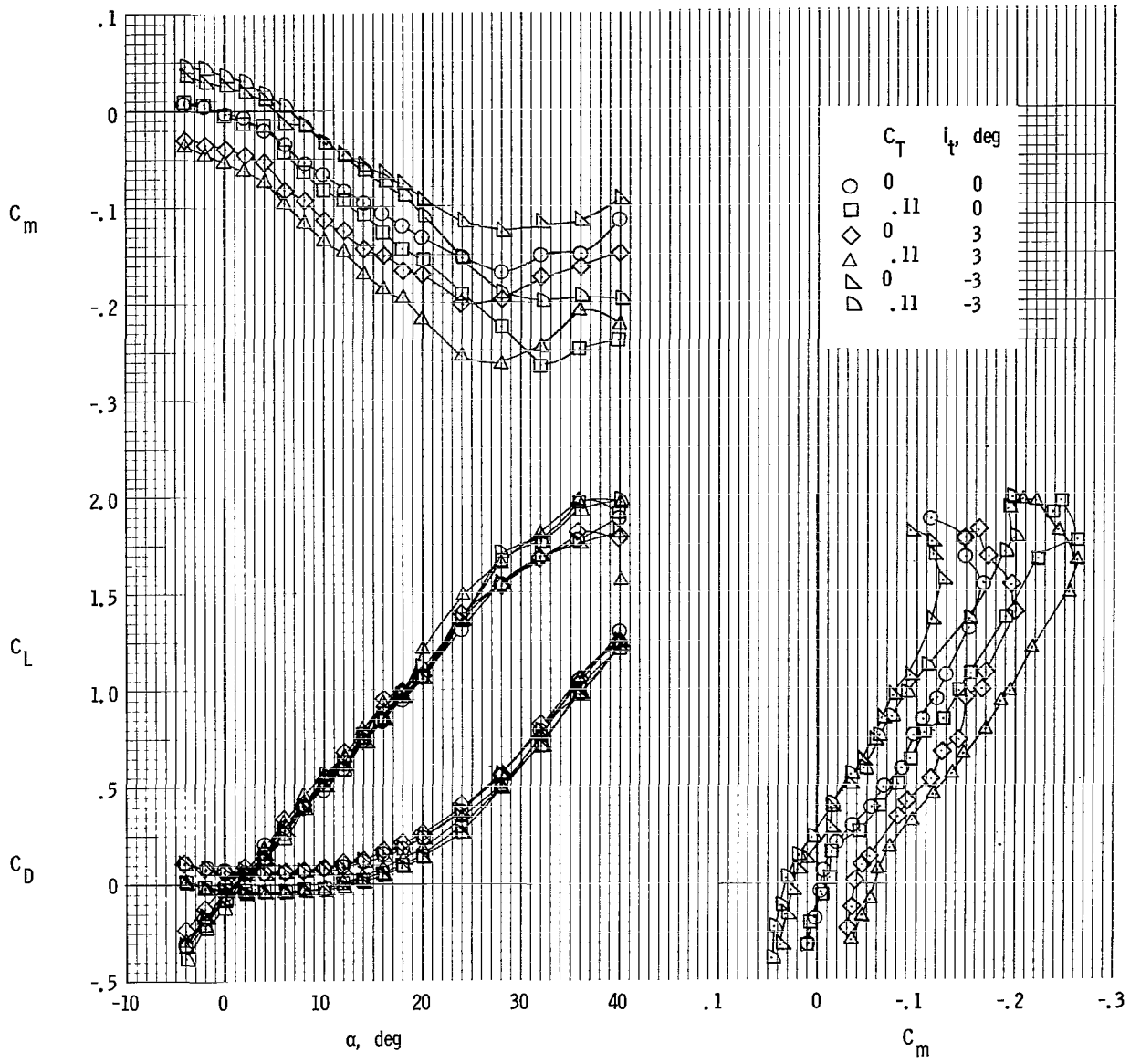

(c) Slats extended; $\Lambda = 42^{o}$.

Figure 12.- Continued.

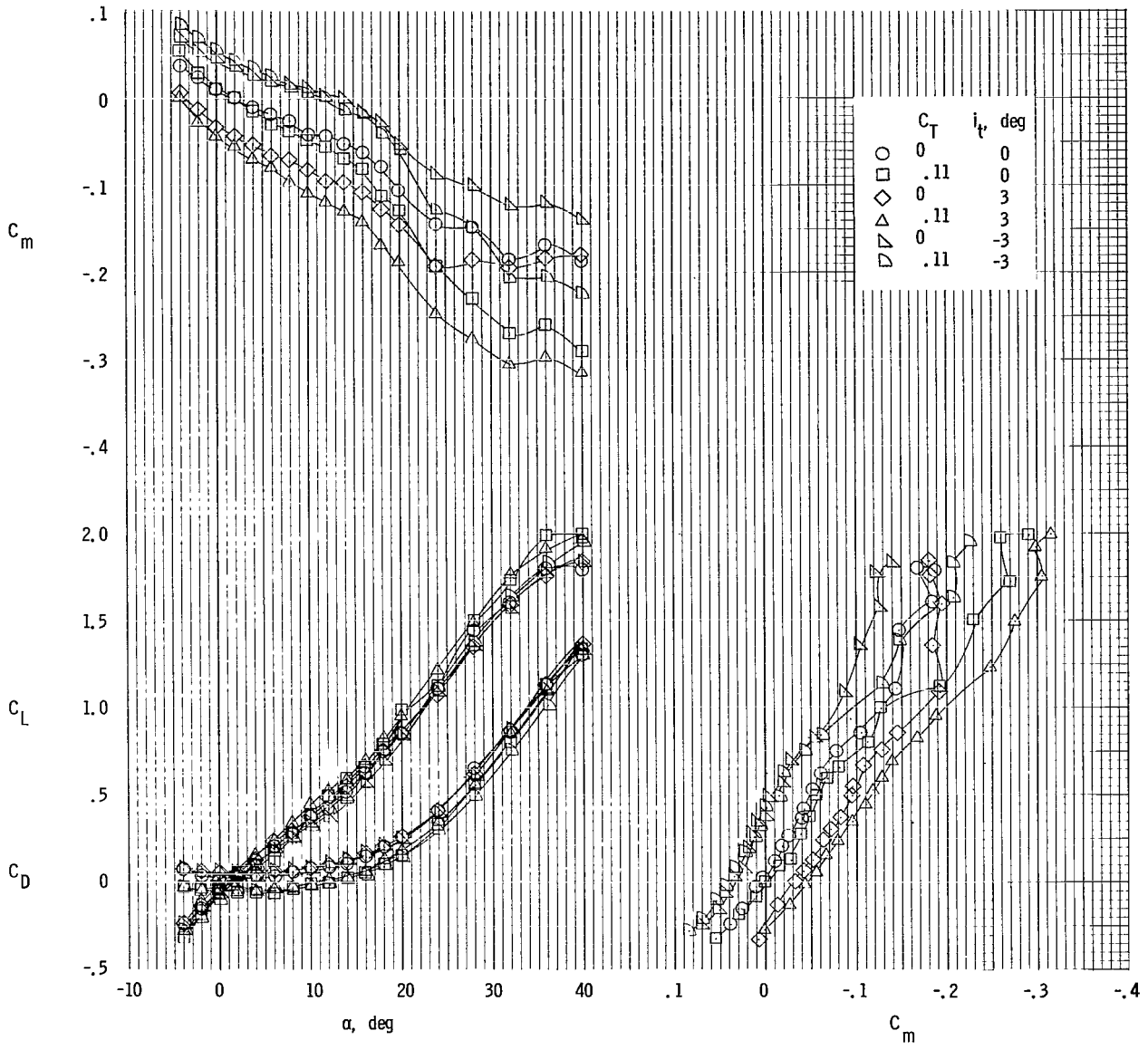

(d) Slats extended; $\Lambda = 72^{o}$.

Figure 12.- Continued.

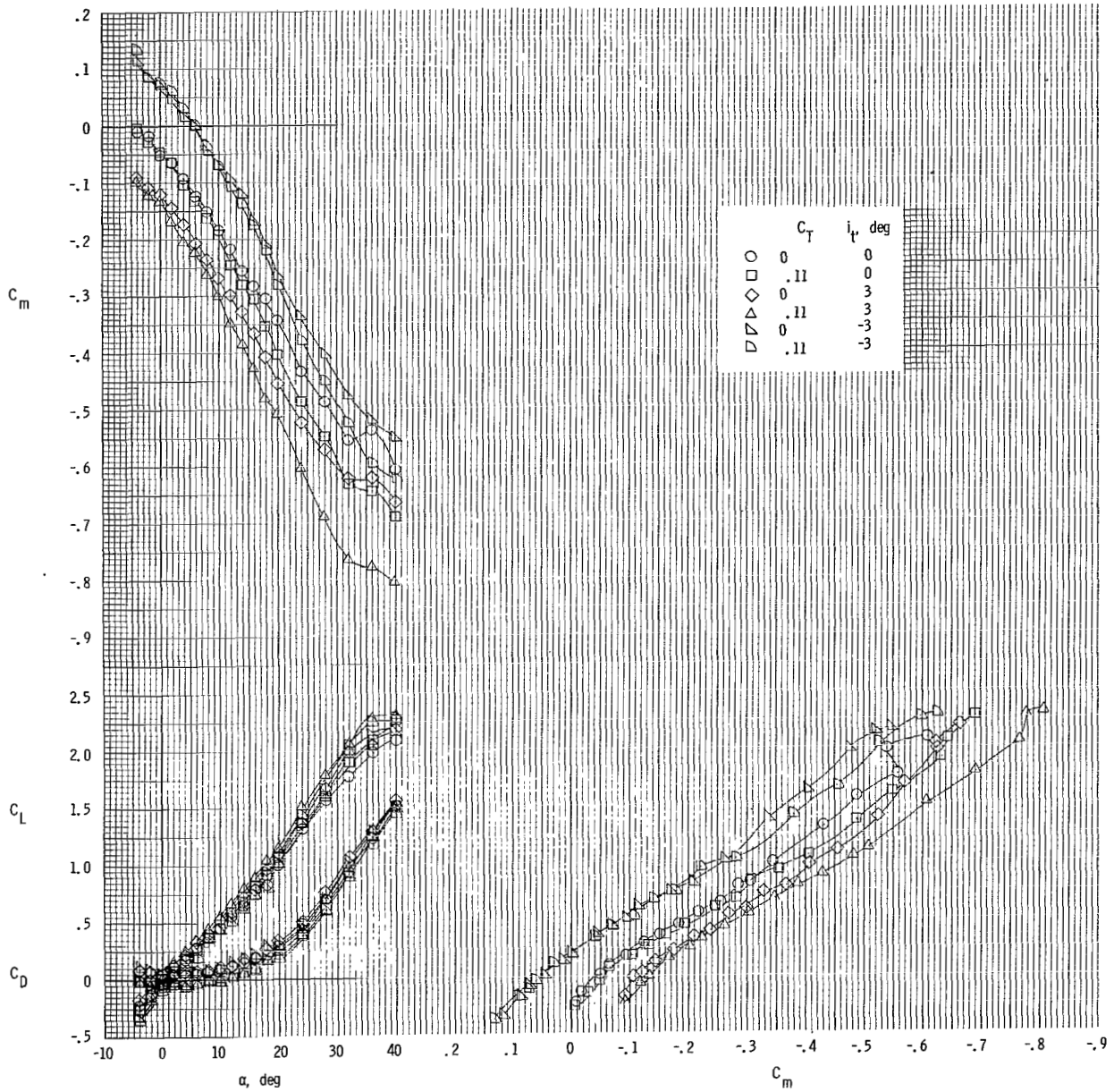

(e) Slats extended; large horizontal tail; $\Lambda = 72^{0}$.

Figure 12.- Concluded.

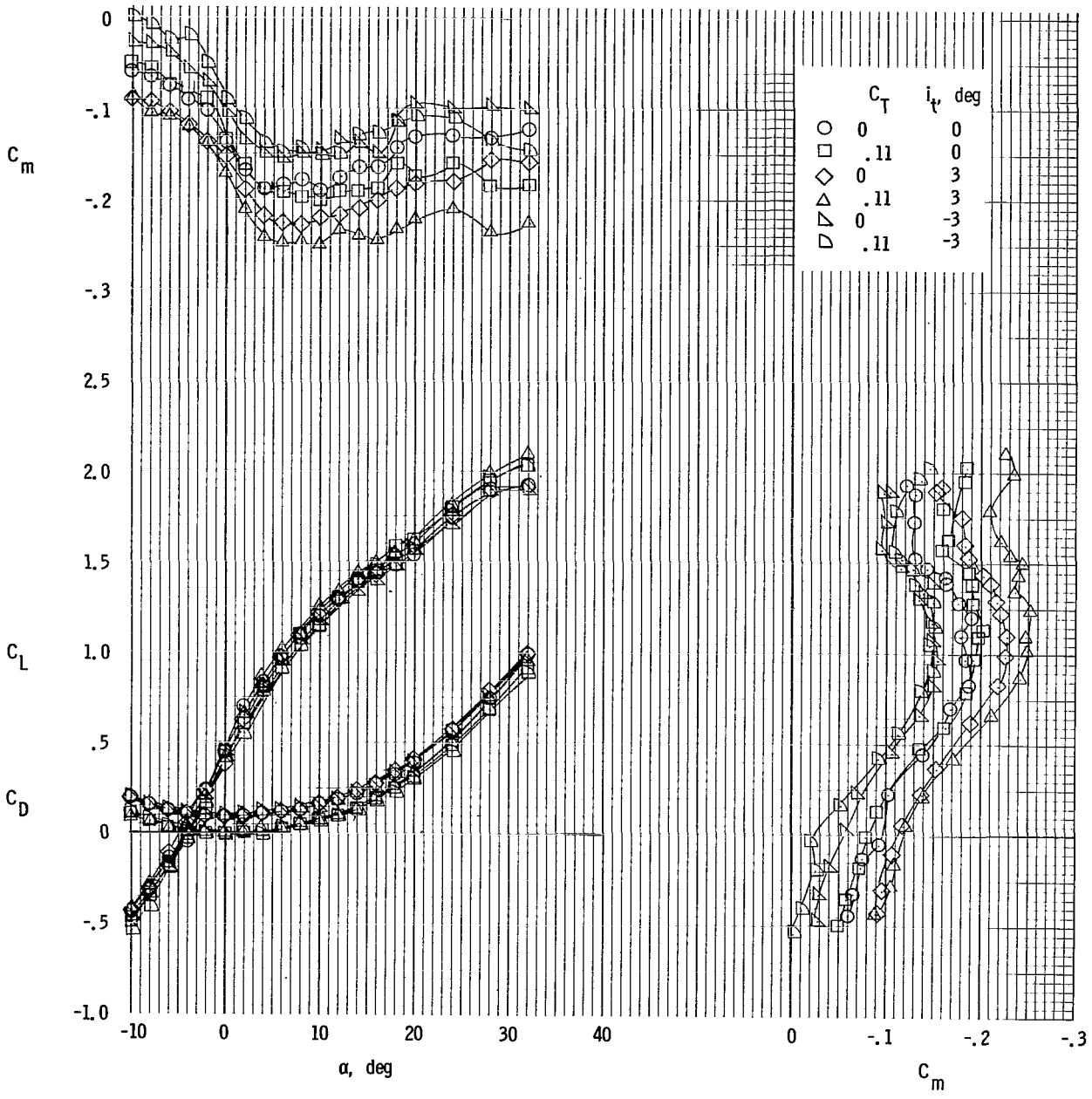

Figure 13.- Effect of power on longitudinal control characteristics of model. Landing configuration; $\Lambda = 20^0$.

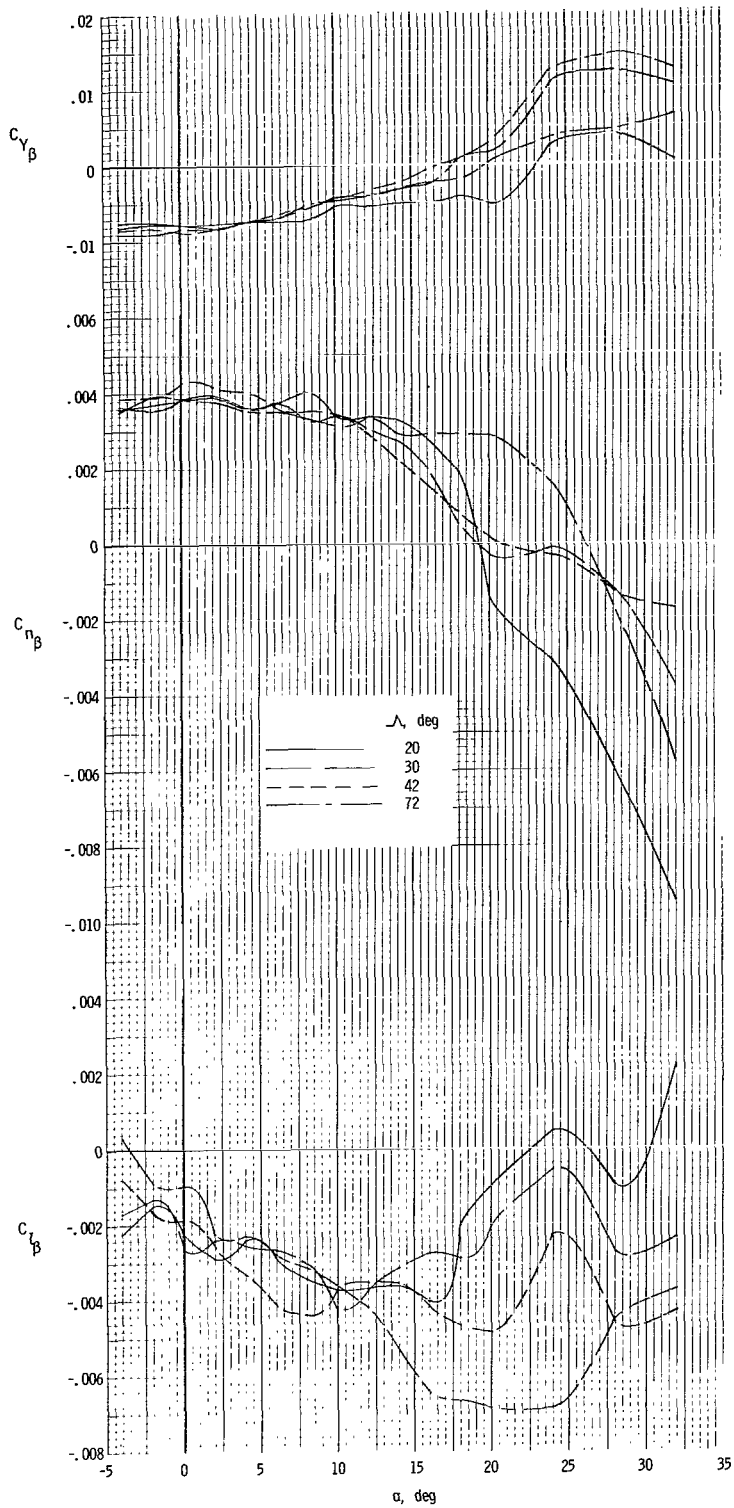

(a) Clean configuration.

Figure 14.- Static lateral stability characteristics of the model.

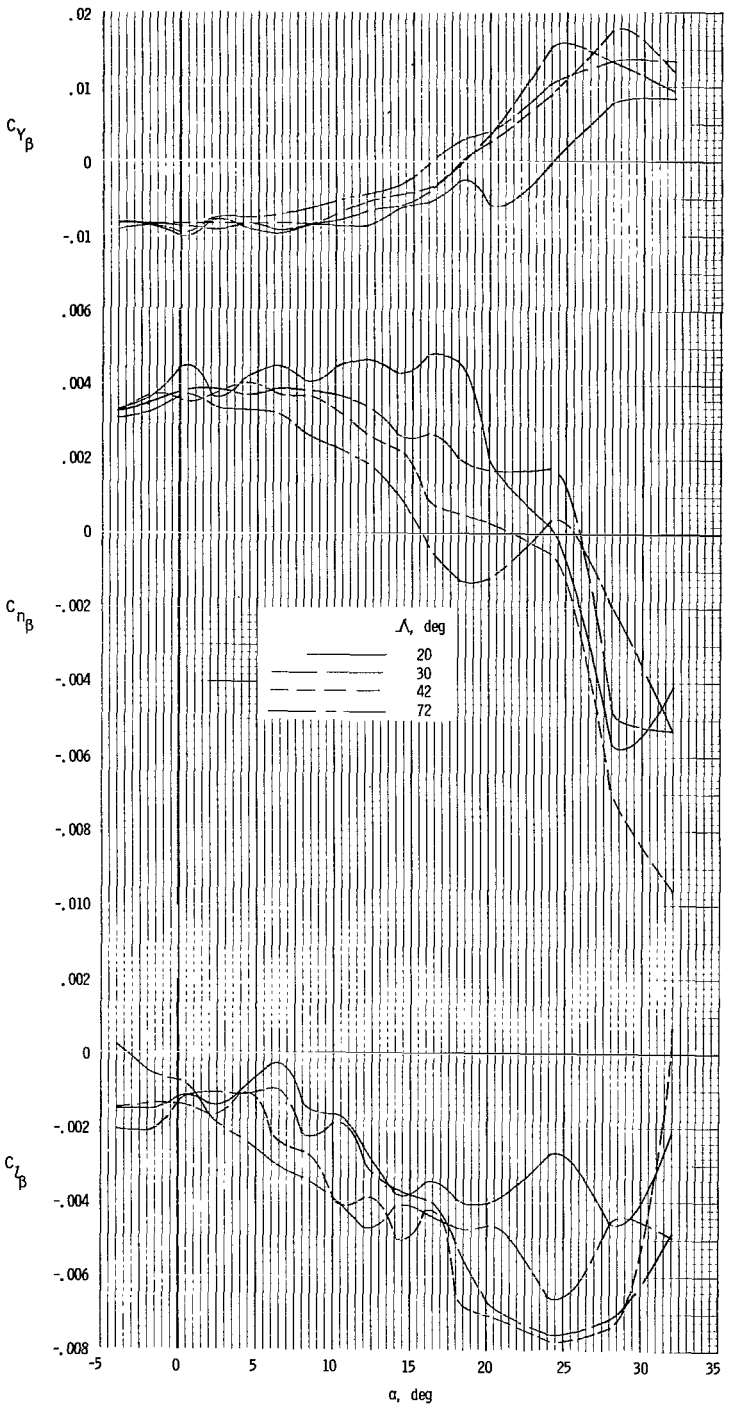

(b) Slats extended.

Figure 14.- Continued.

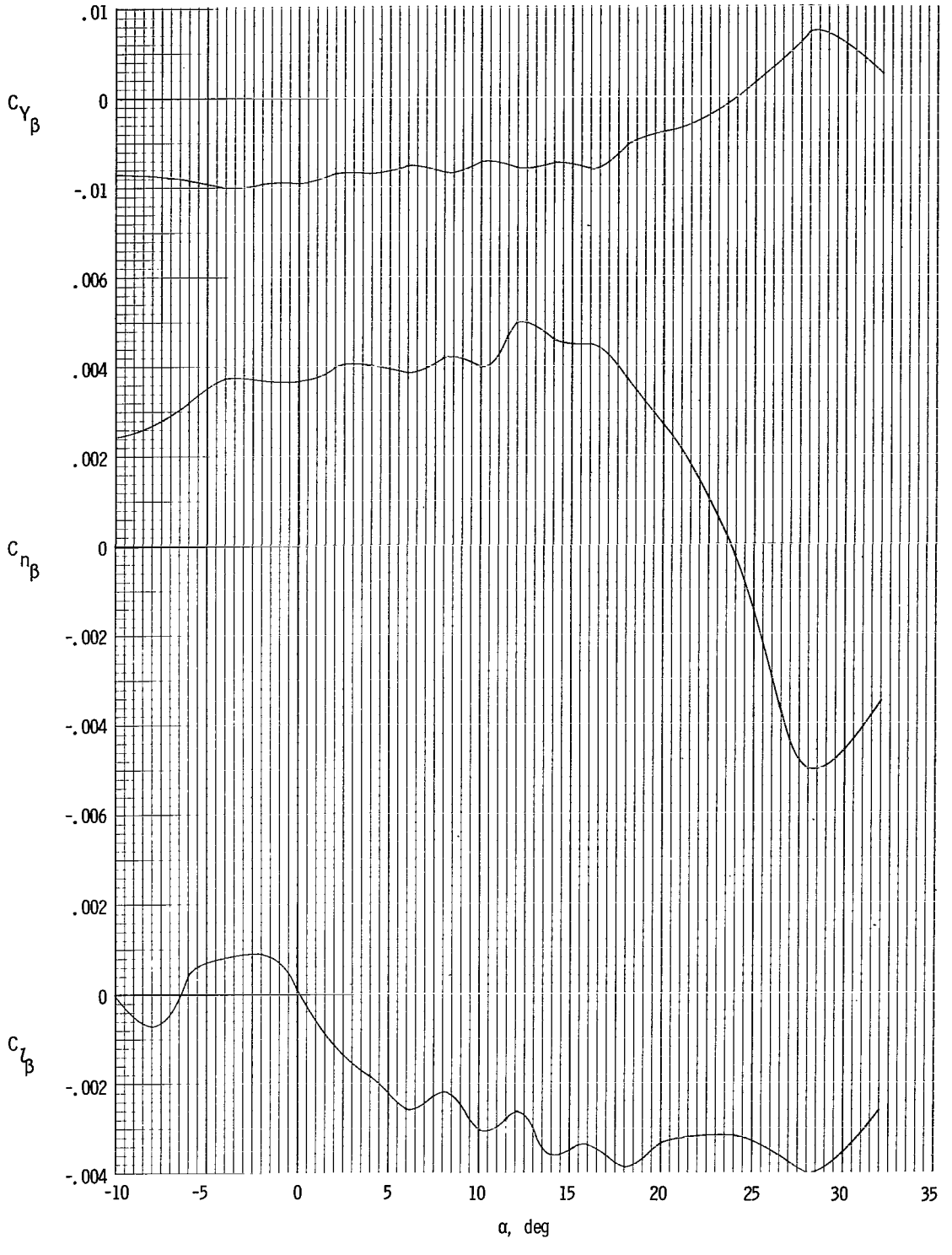

(c) Landing configuration; $\Lambda = 20^{o}$.

Figure 14.- Concluded.

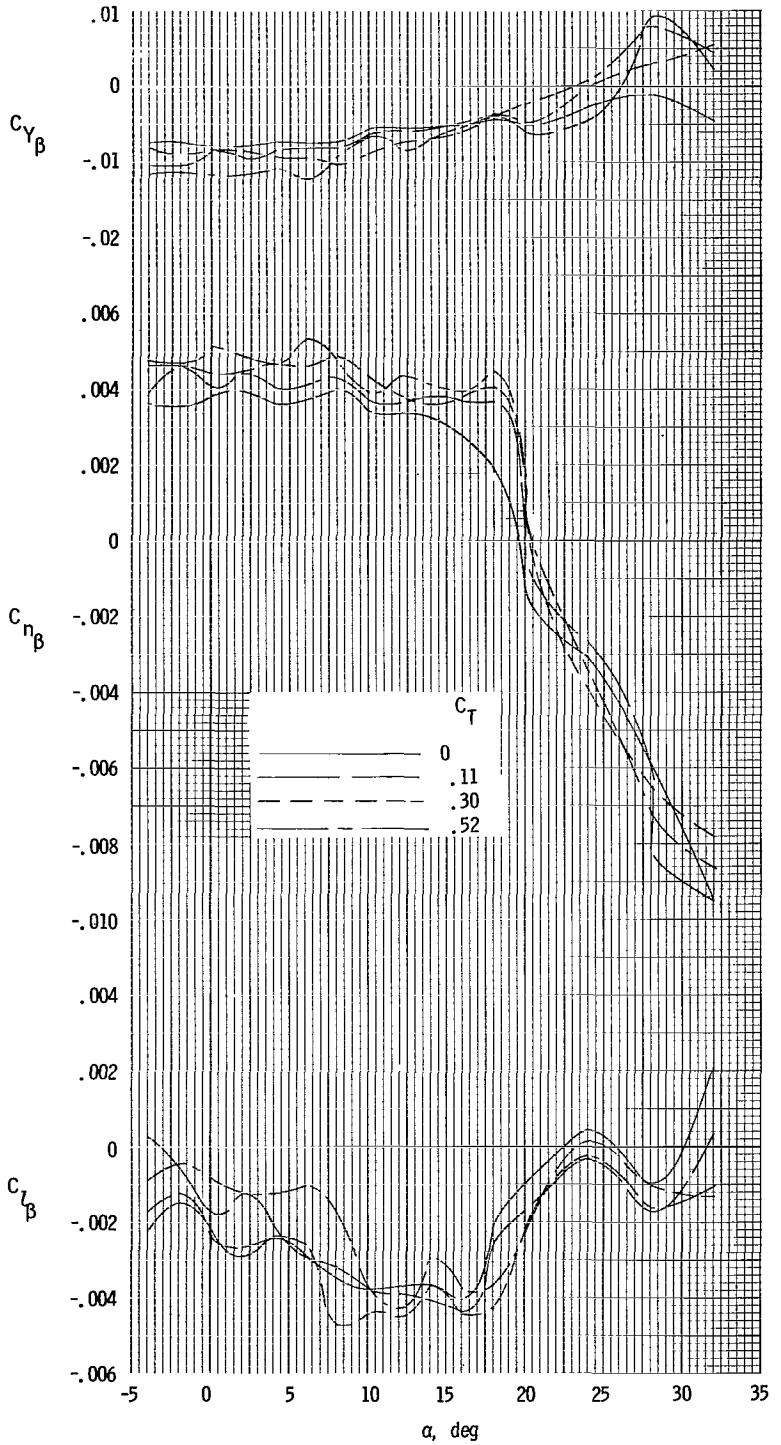

(a) Clean configuration; $\Lambda = 20^0$.

Figure 15.- Effect of power on the static lateral stability characteristics of the model.

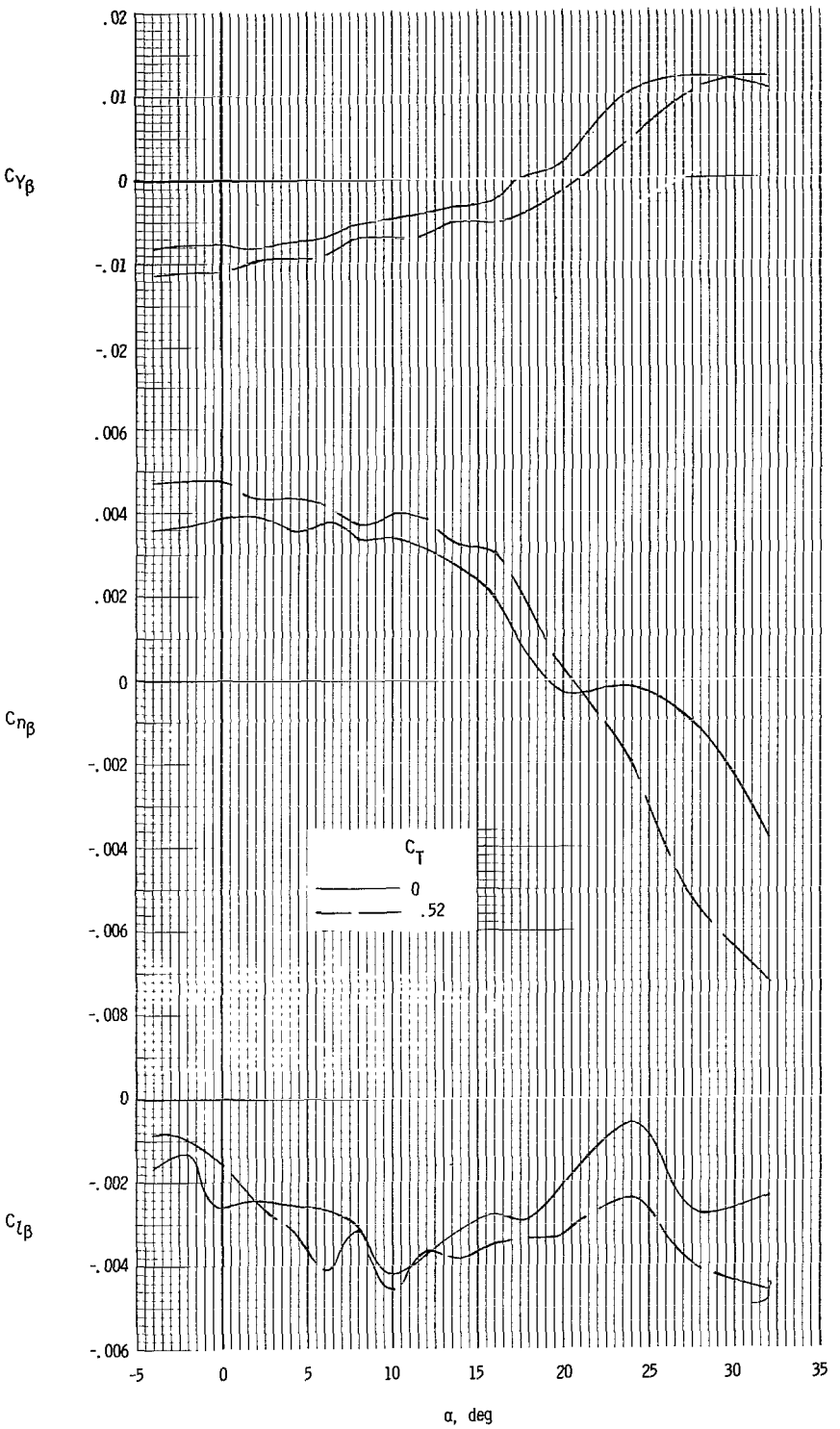

(b) Clean configuration; $\Lambda = 30^0$.

Figure 15.- Continued.

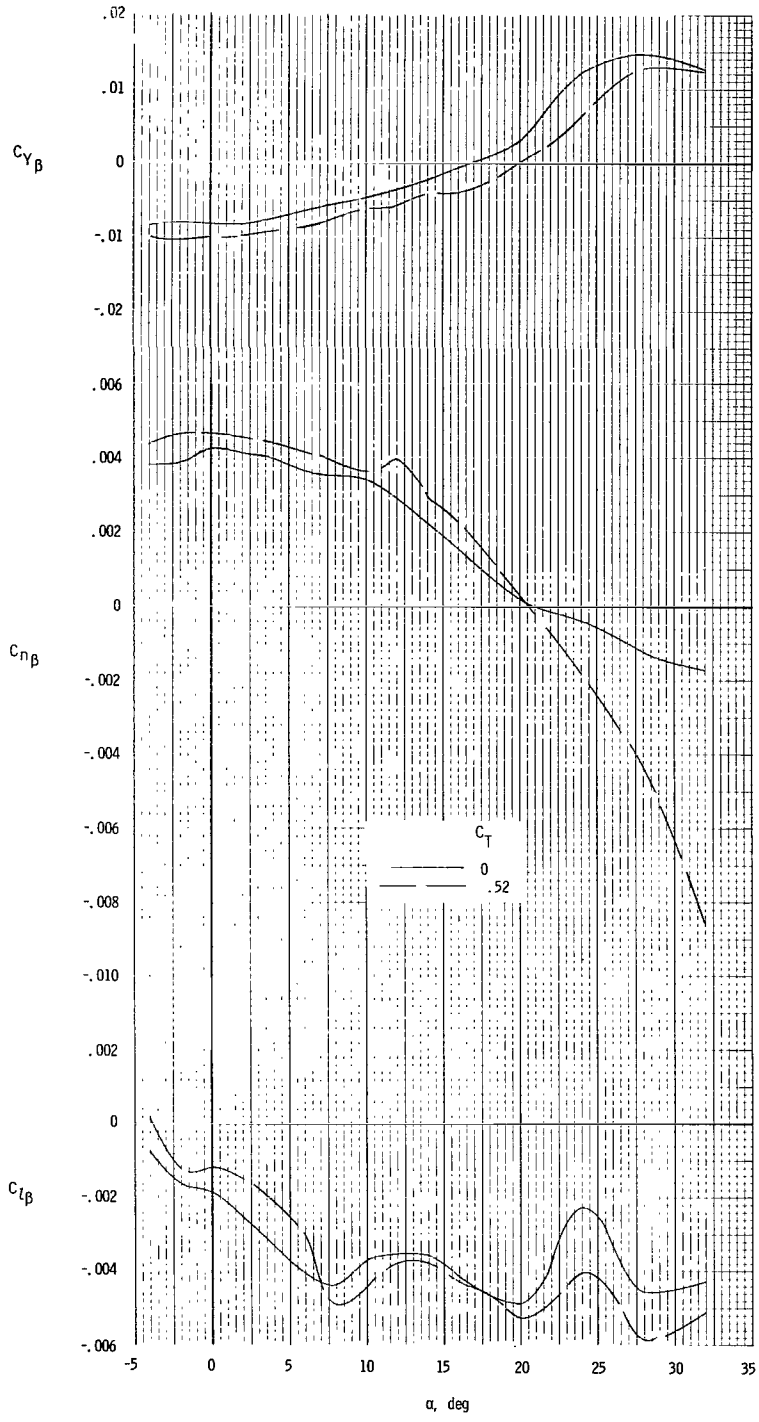

(c) Clean configuration; $\Lambda = 42^0$.

Figure 15.- Continued.

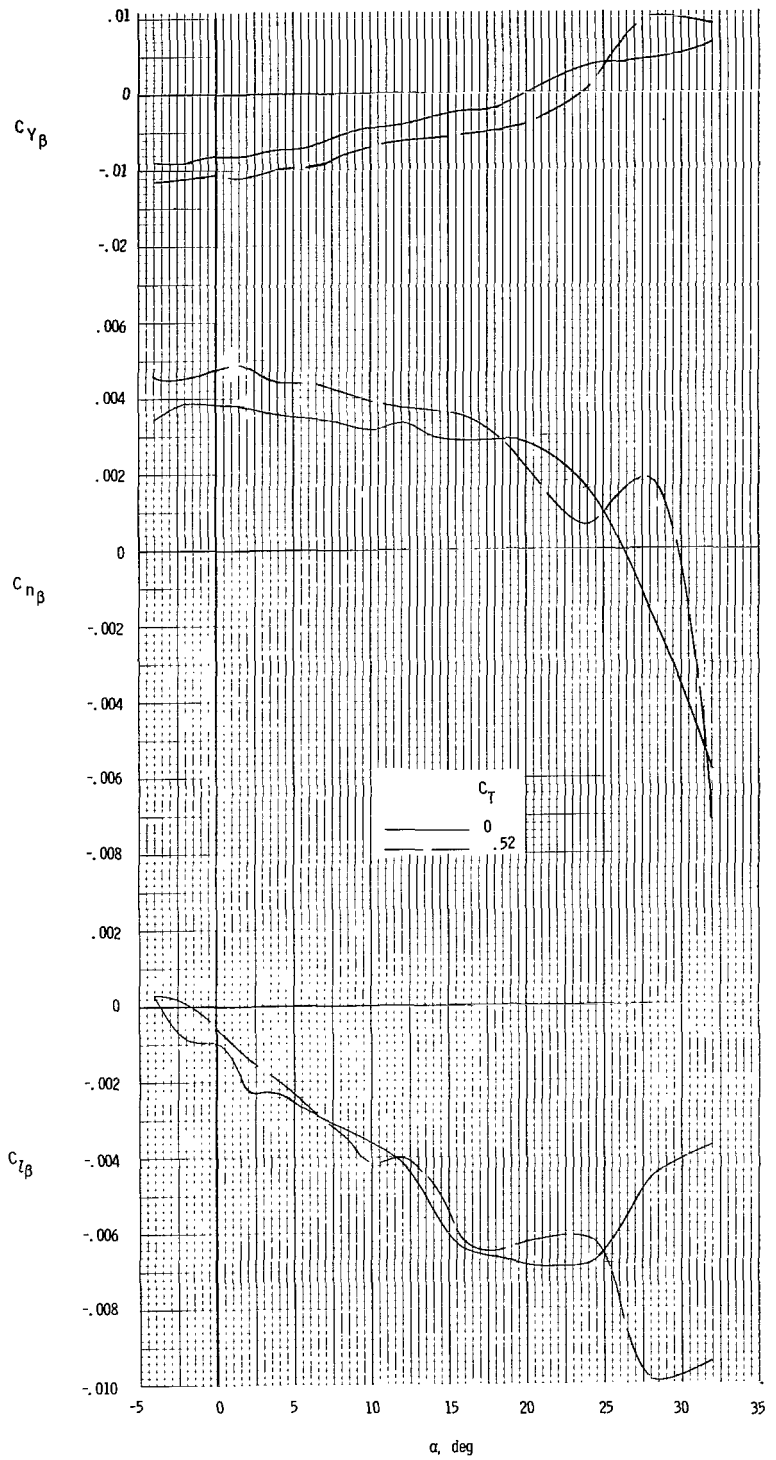

(d) Clean configuration; $\Lambda = 72^0$.

Figure 15.- Concluded.

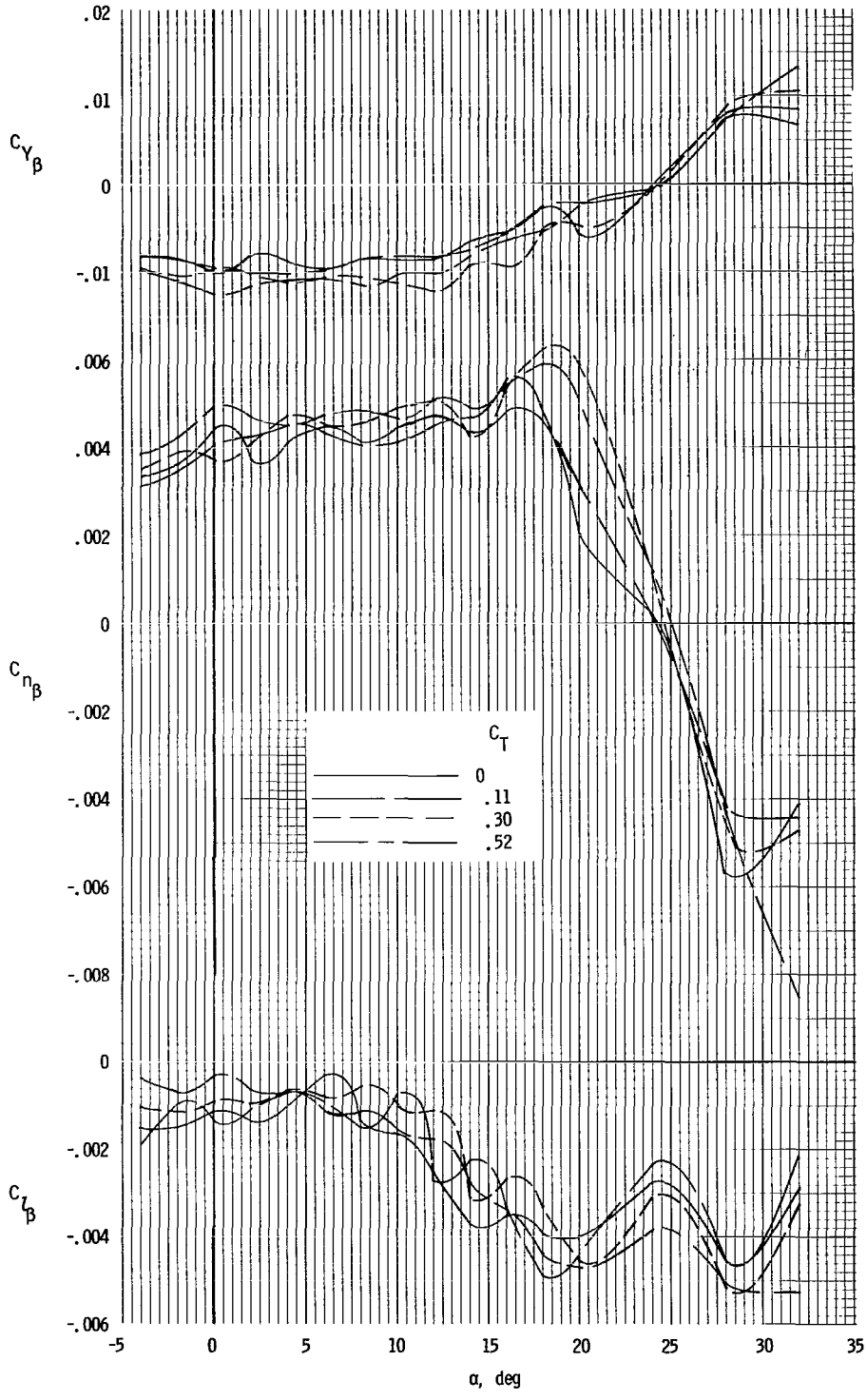

(a) Slats extended; $\Lambda = 20^{\circ}$.

Figure 16.- Effect of power on static lateral stability characteristics of model.

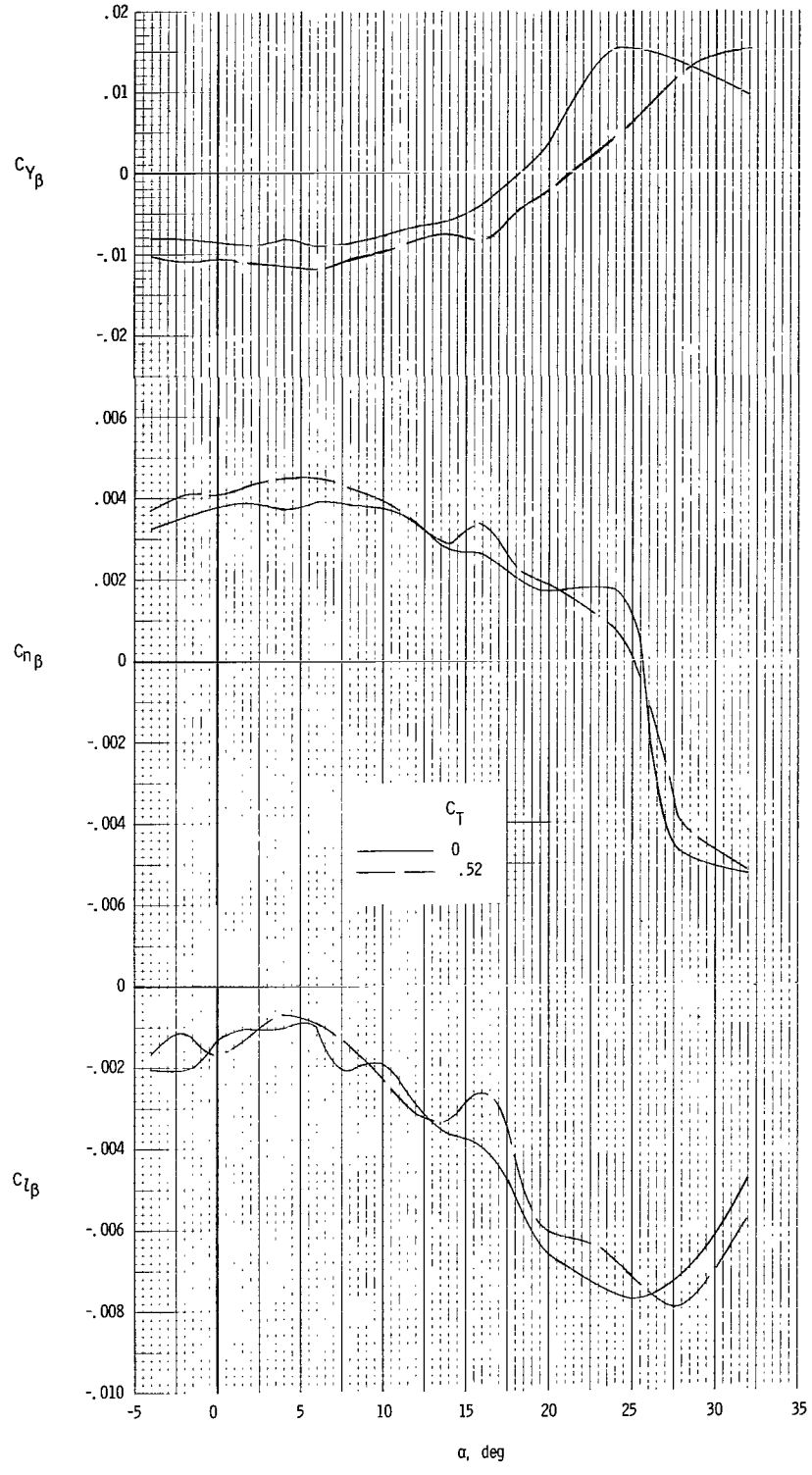

(b) Slats extended; $\Lambda = 30^{o}$.

Figure 16.- Continued.

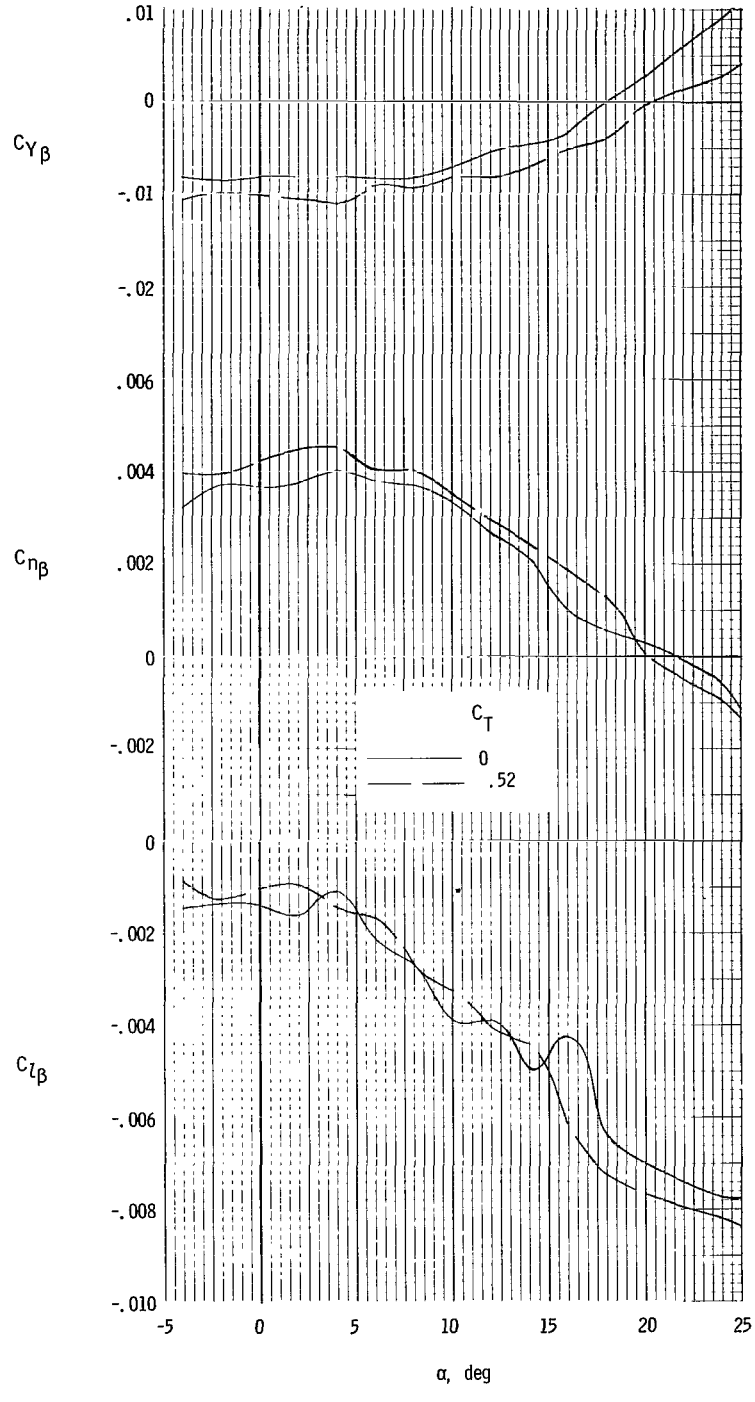

(c) Slats extended; $\Lambda = 42^{o}$.

Figure 16.- Continued.

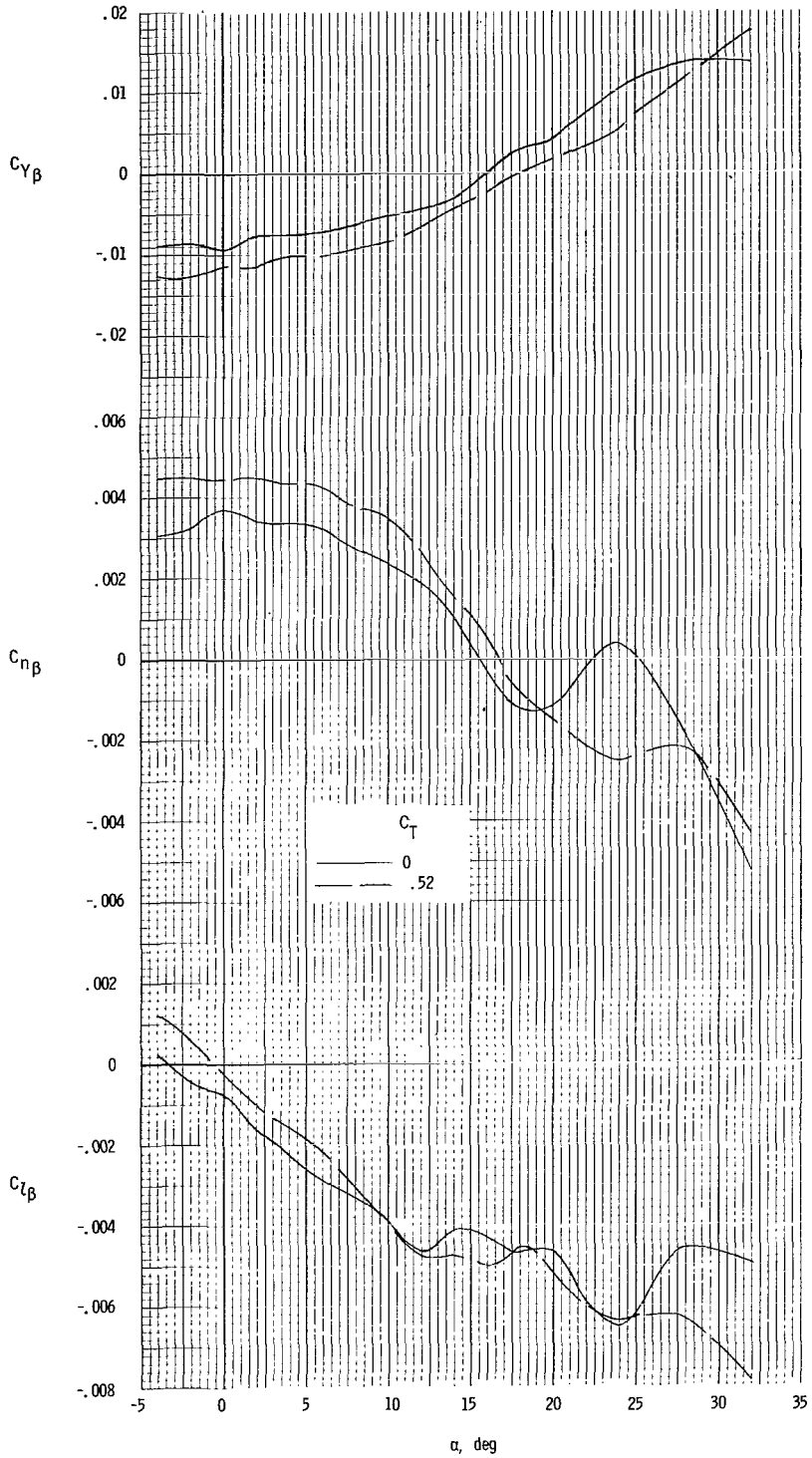

(d) Slats extended; $\Lambda = 72^{o}$.

Figure 16.- Continued.

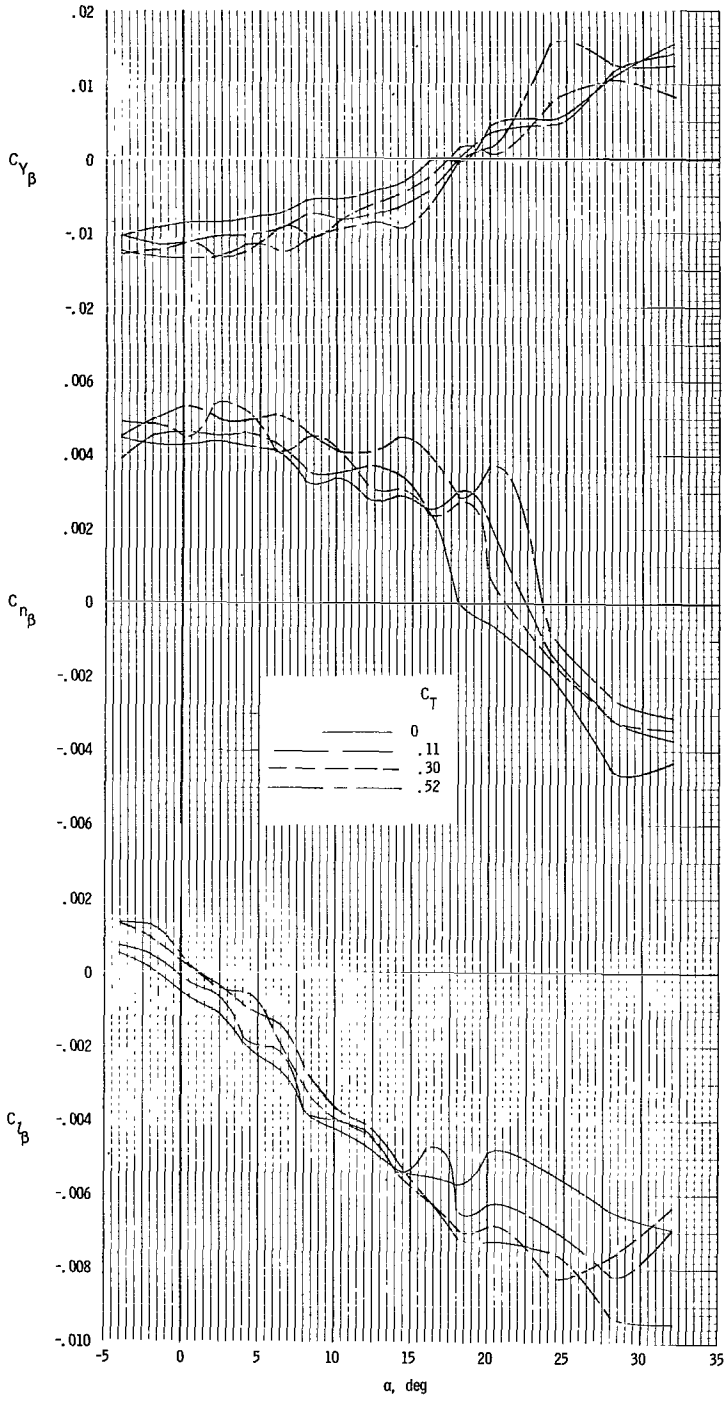

(e) Slats extended, large horizontal tail; $\Lambda = 72^{o}$.

Figure 16.- Concluded.

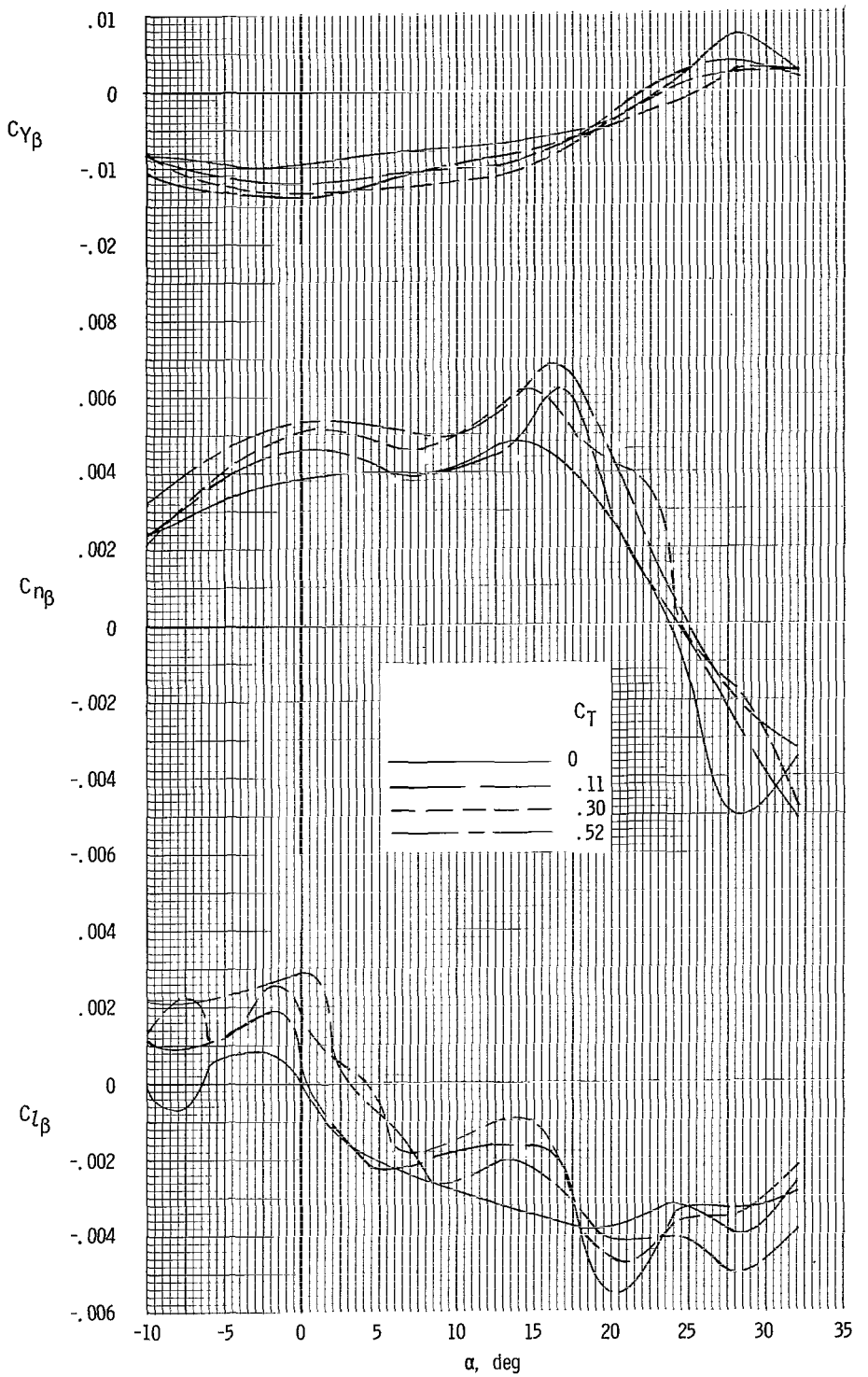

Figure 17.- Effect of power on static lateral stability characteristics of model. Landing configuration; $\Lambda = 20^{o}$.

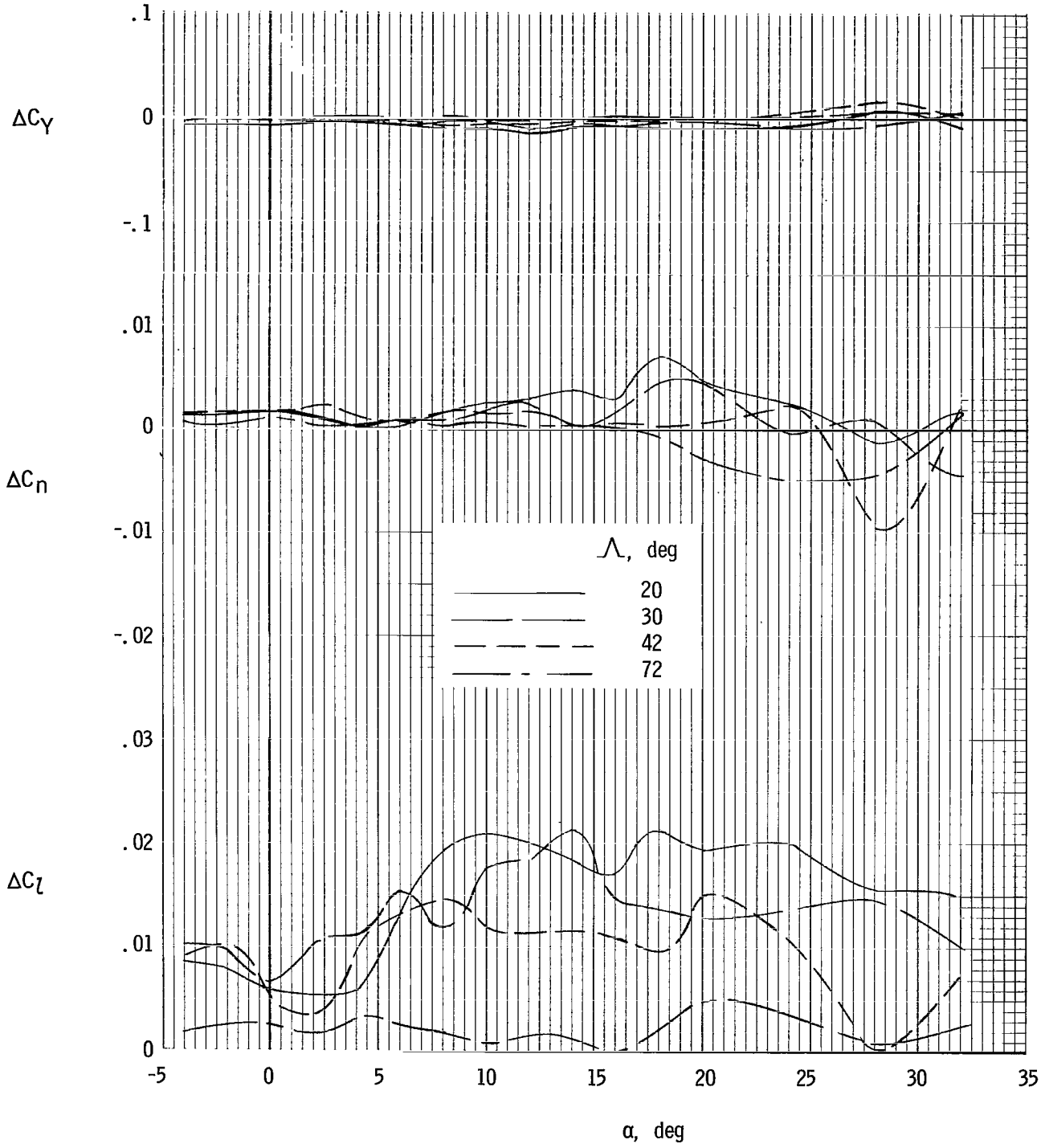

(a) Slats extended.

Figure 18.- Total aileron control effectiveness of the model. $\delta_a = -50^0$.

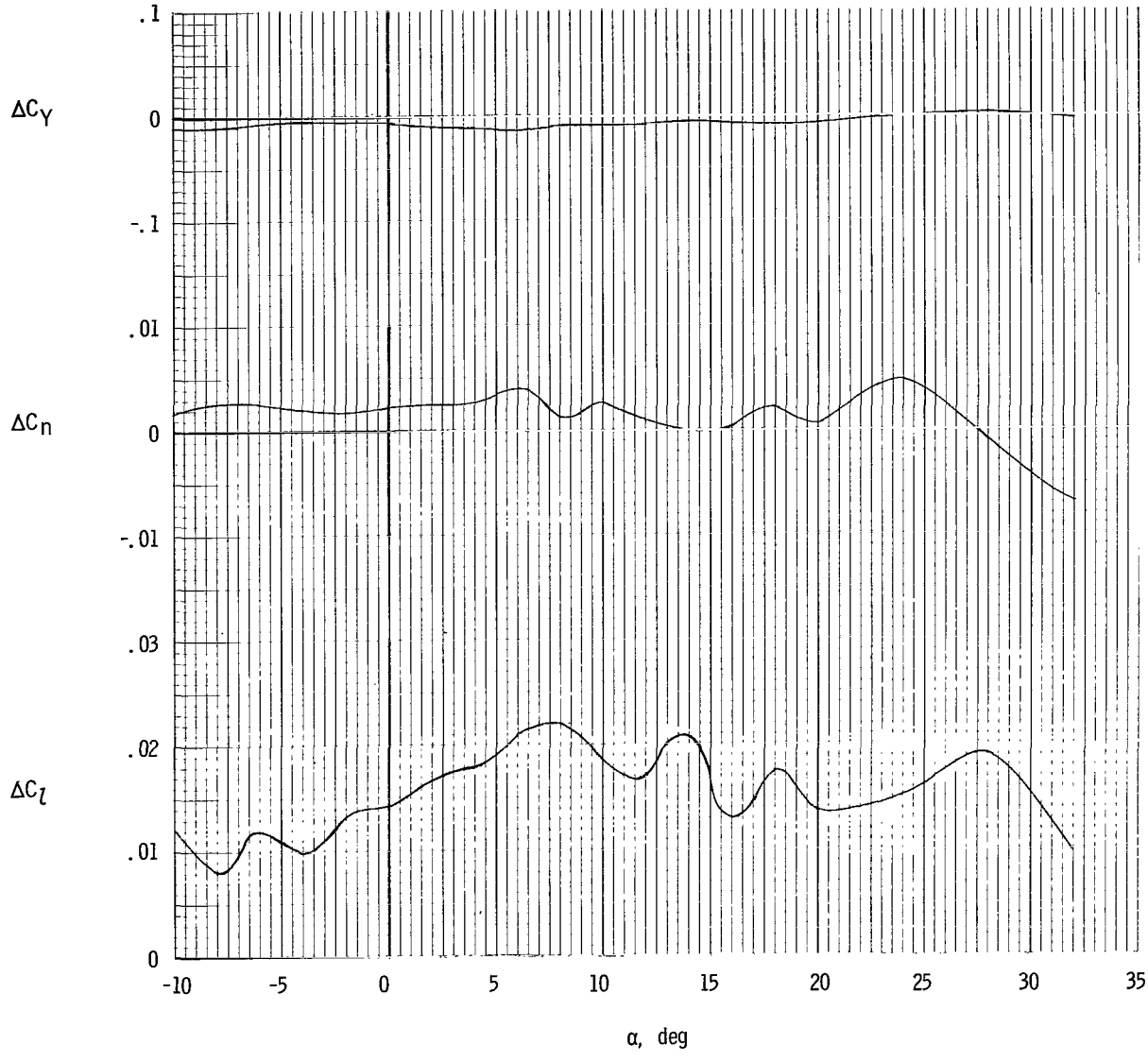

(b) Landing configuration; $\Lambda = 20^0$.

Figure 18.- Concluded.

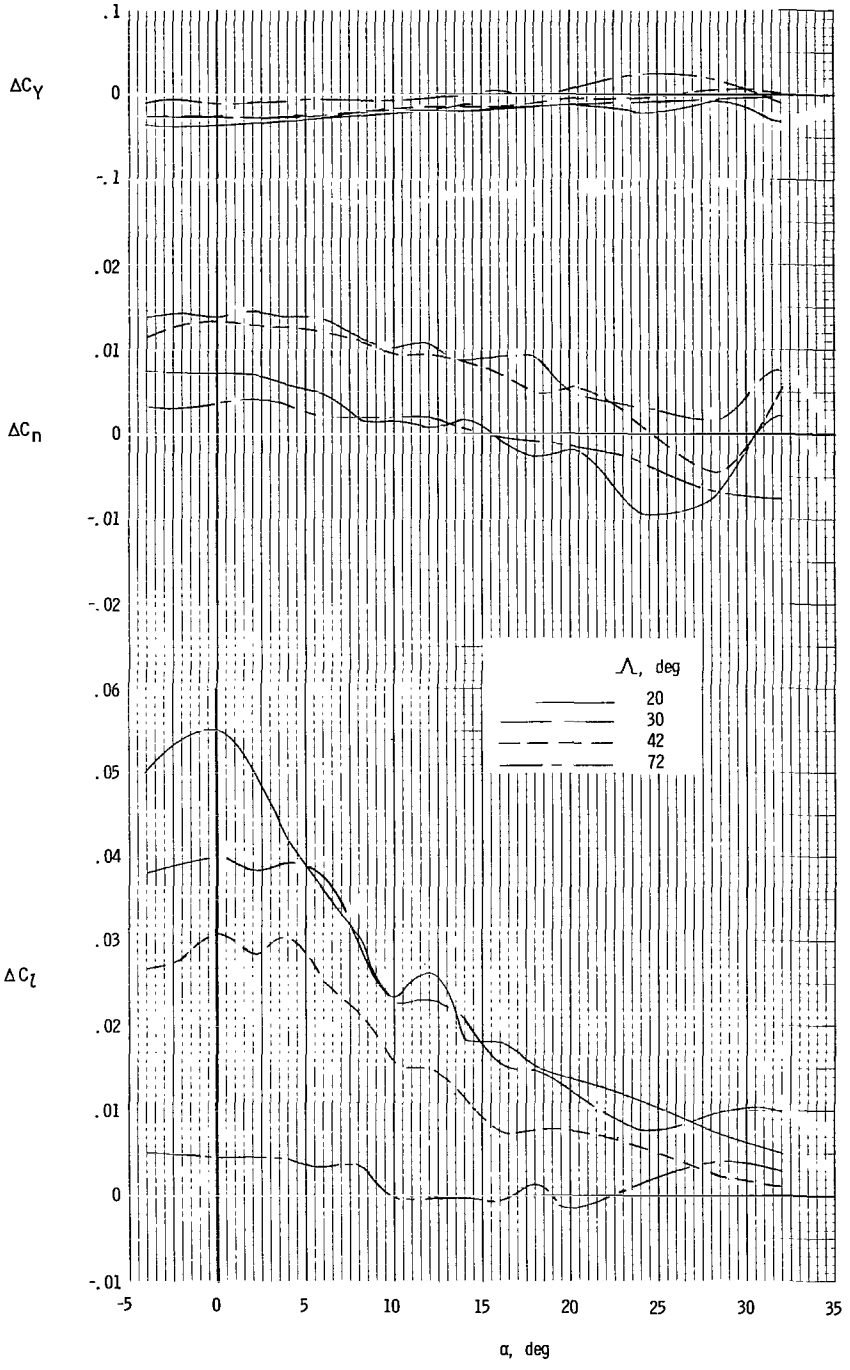

(a) Slats extended.

Figure 19.- Spoiler control effectiveness of the model. $\delta_{sp} = 60^0$.

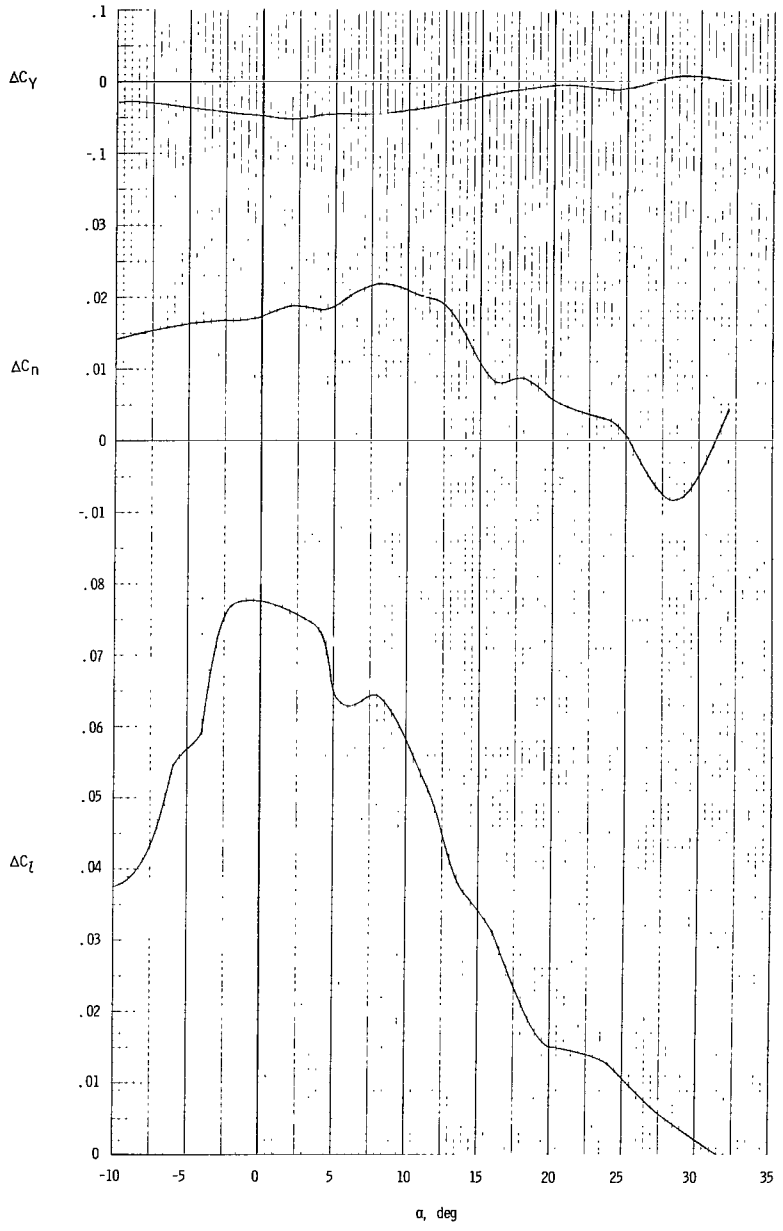

(b) Landing configuration; $\Lambda = 20^{o}$.

Figure 19.- Concluded.

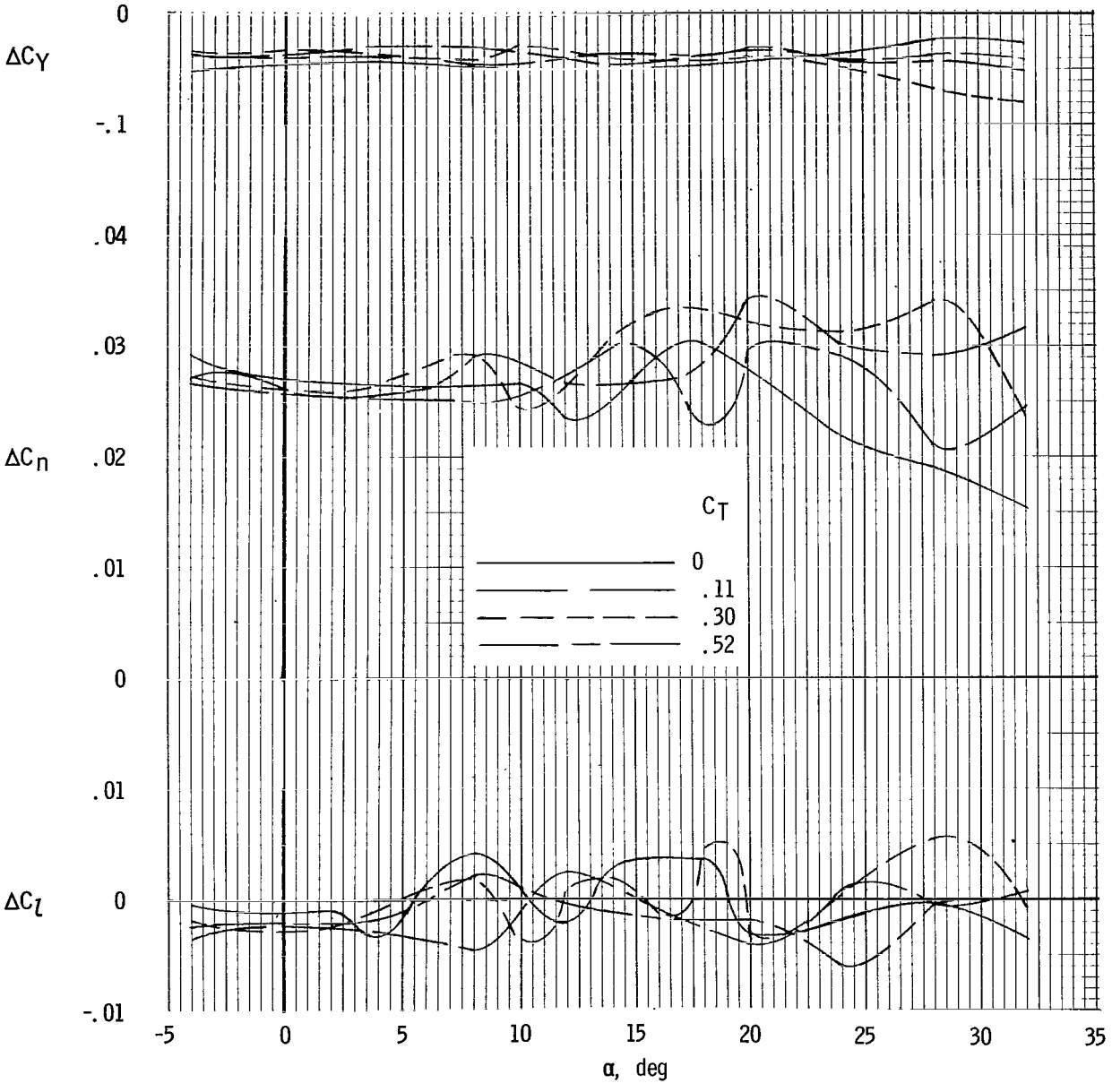

(a) Slats extended; $\Lambda = 20^{o}$.

Figure 20.- Rudder control effectiveness of model. $\delta_r = -18^{o}$.

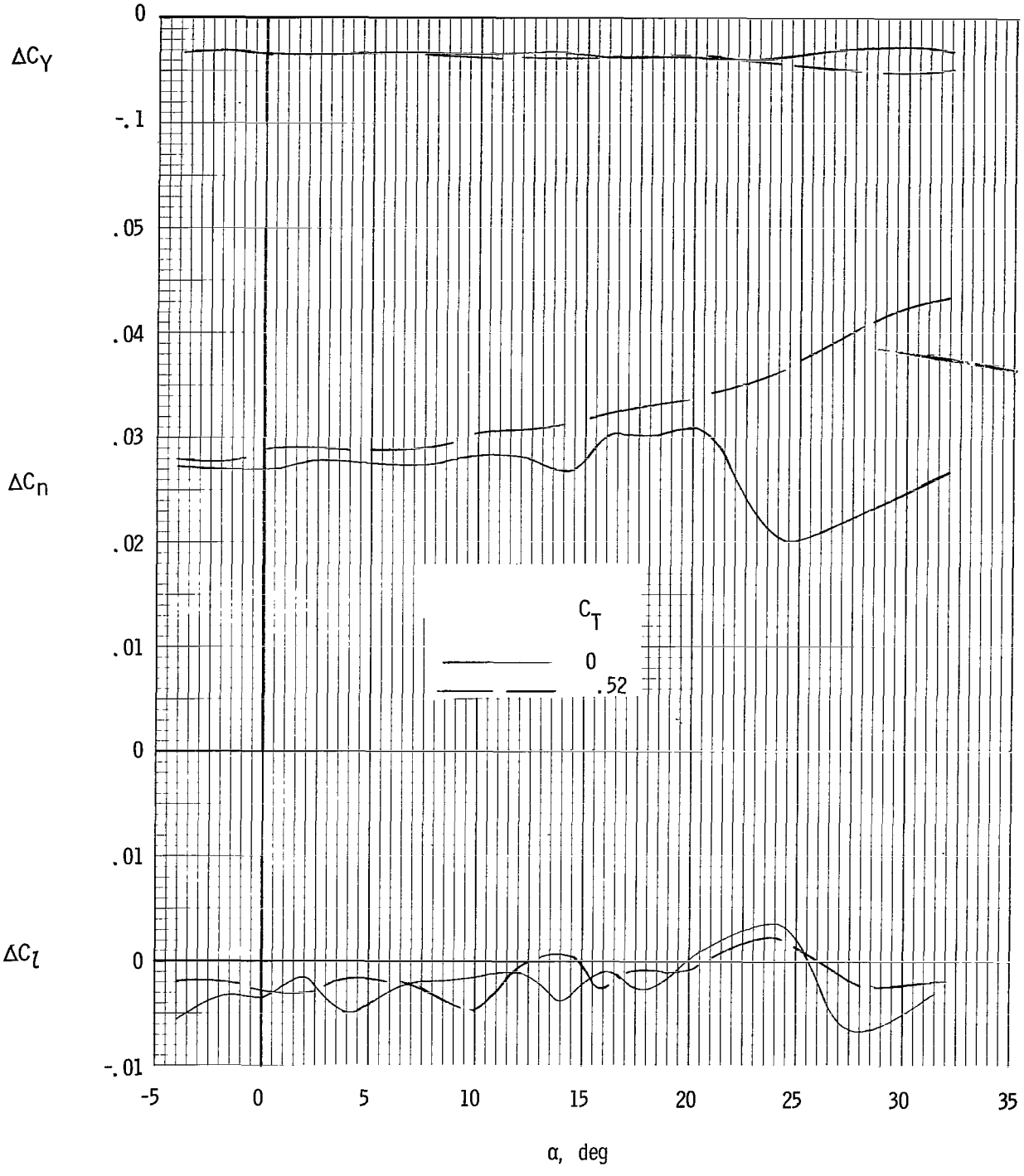

(b) Slats extended; $\Lambda = 30^{o}$.

Figure 20.- Continued.

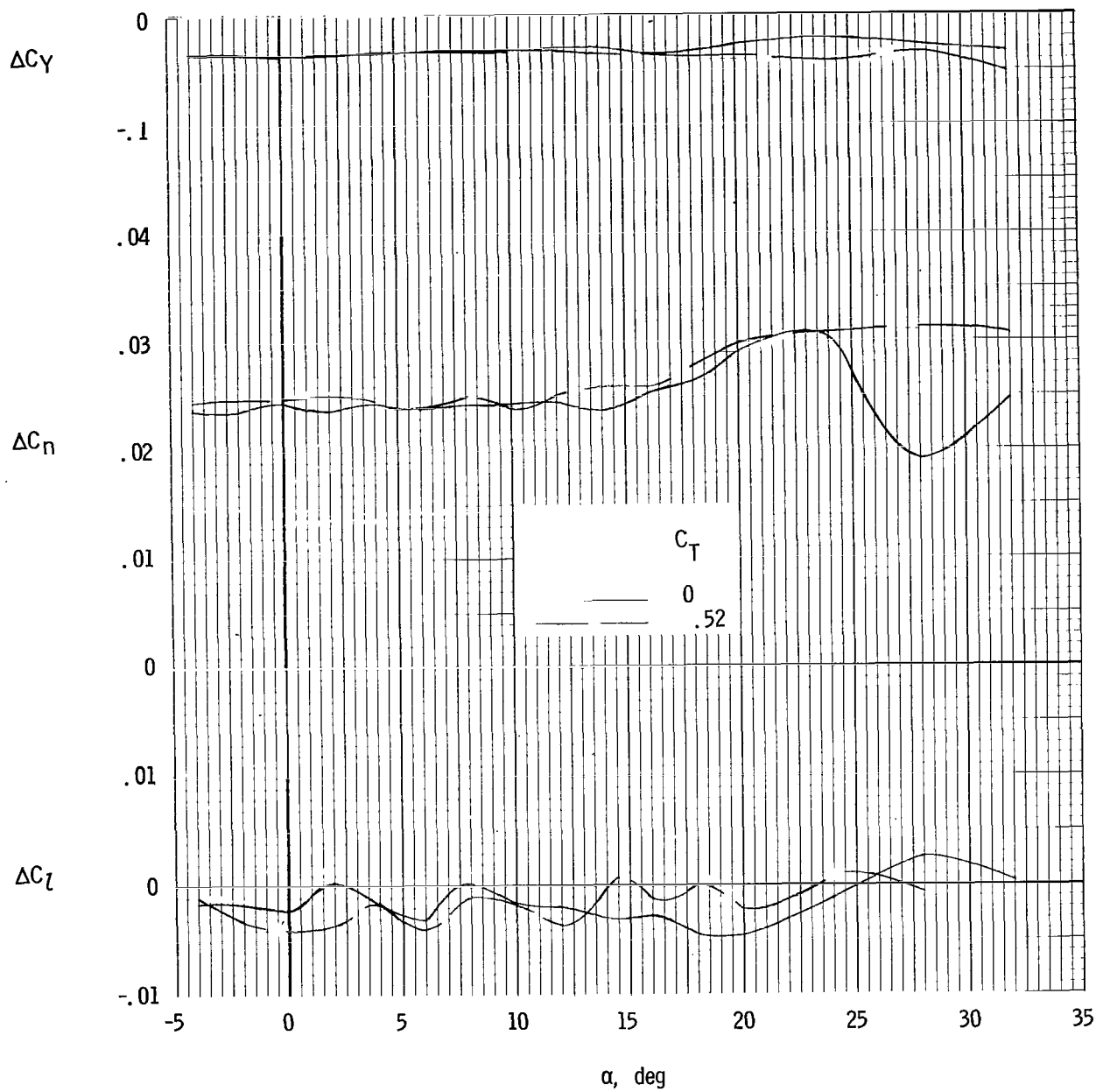

(c) Slats extended; $\Lambda = 42^{o}$.

Figure 20.- Continued.

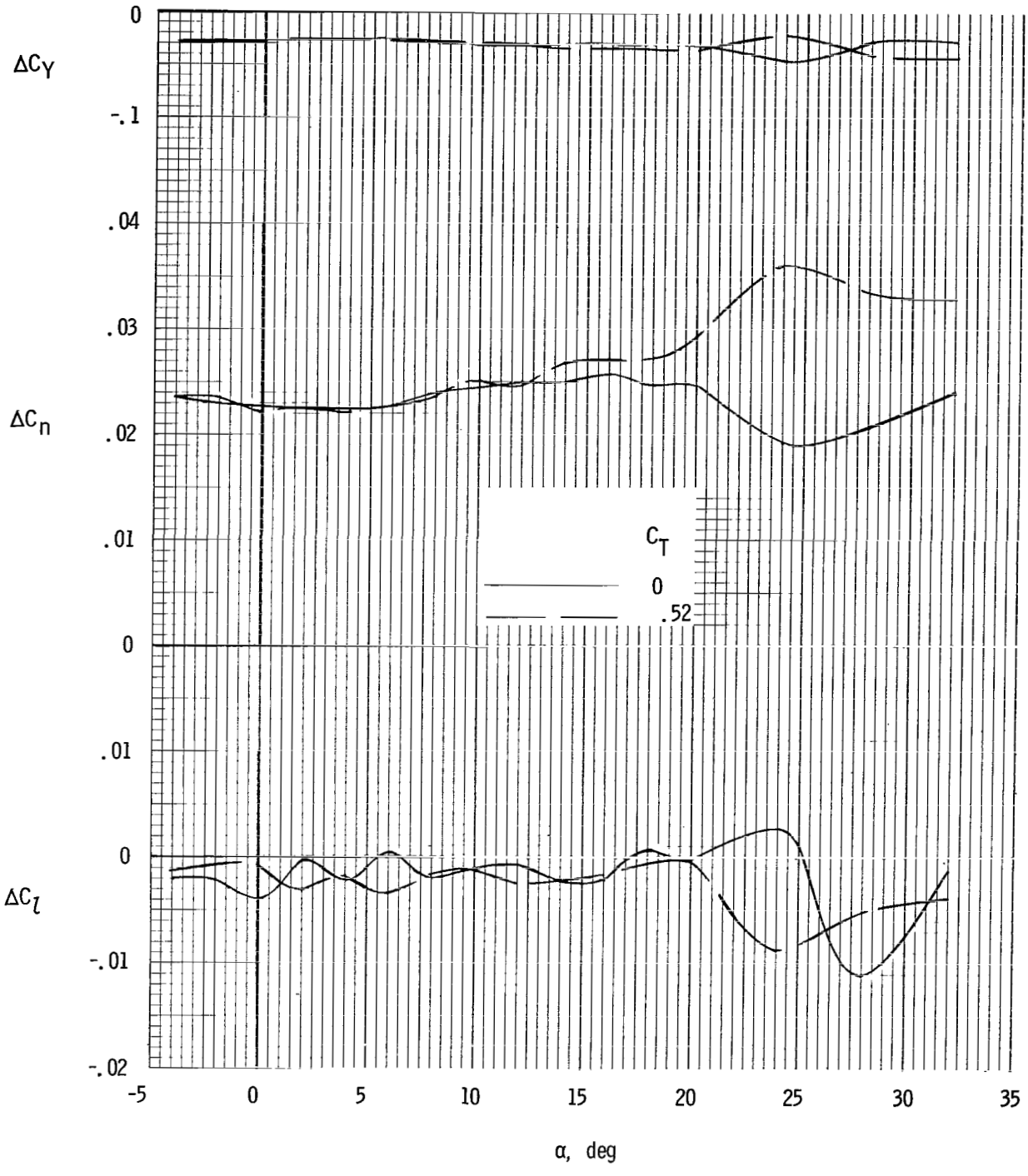

(d) Slats extended; $\Lambda = 72^{o}$.

Figure 20.- Concluded.

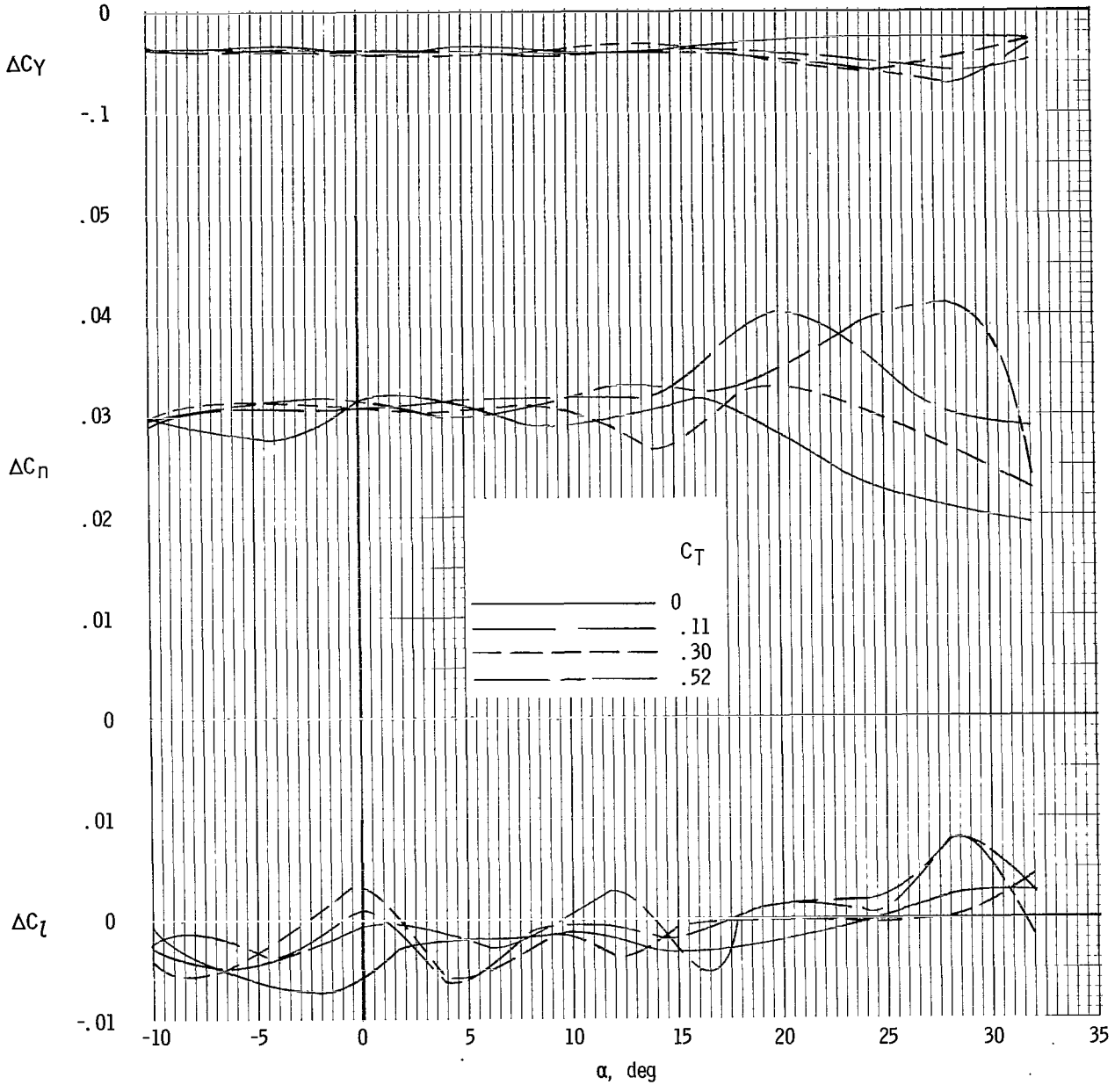

Figure 21.- Rudder control effectiveness of model. $\delta_r = -18^0$; landing configuration; $\Lambda = 20^0$.

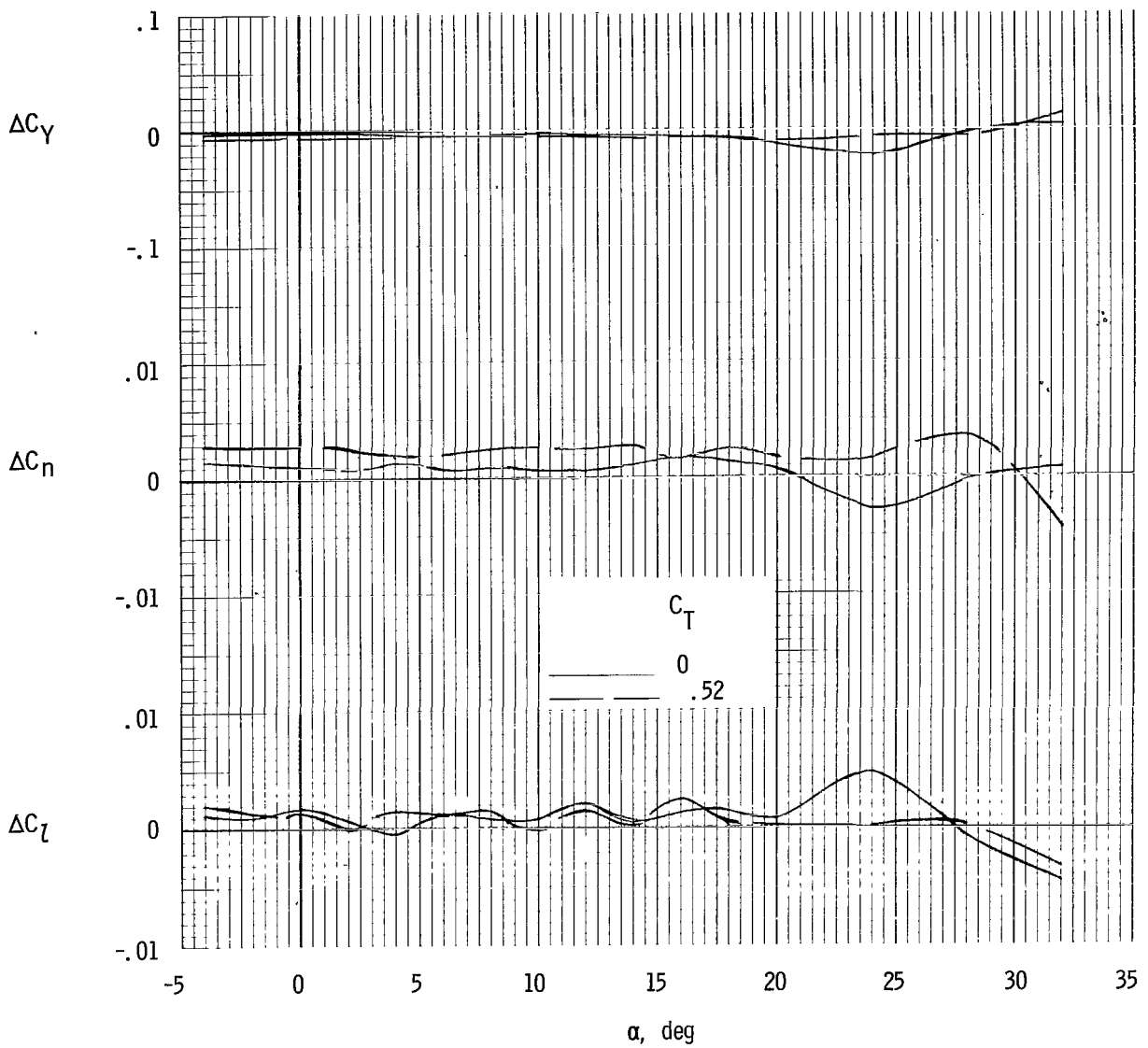

(a) Design horizontal tail.

Figure 22.- Differential deflection of horizontal tail used for roll control $\delta_{i_t} = -10^0$; slats extended; $\Lambda = 72^0$.

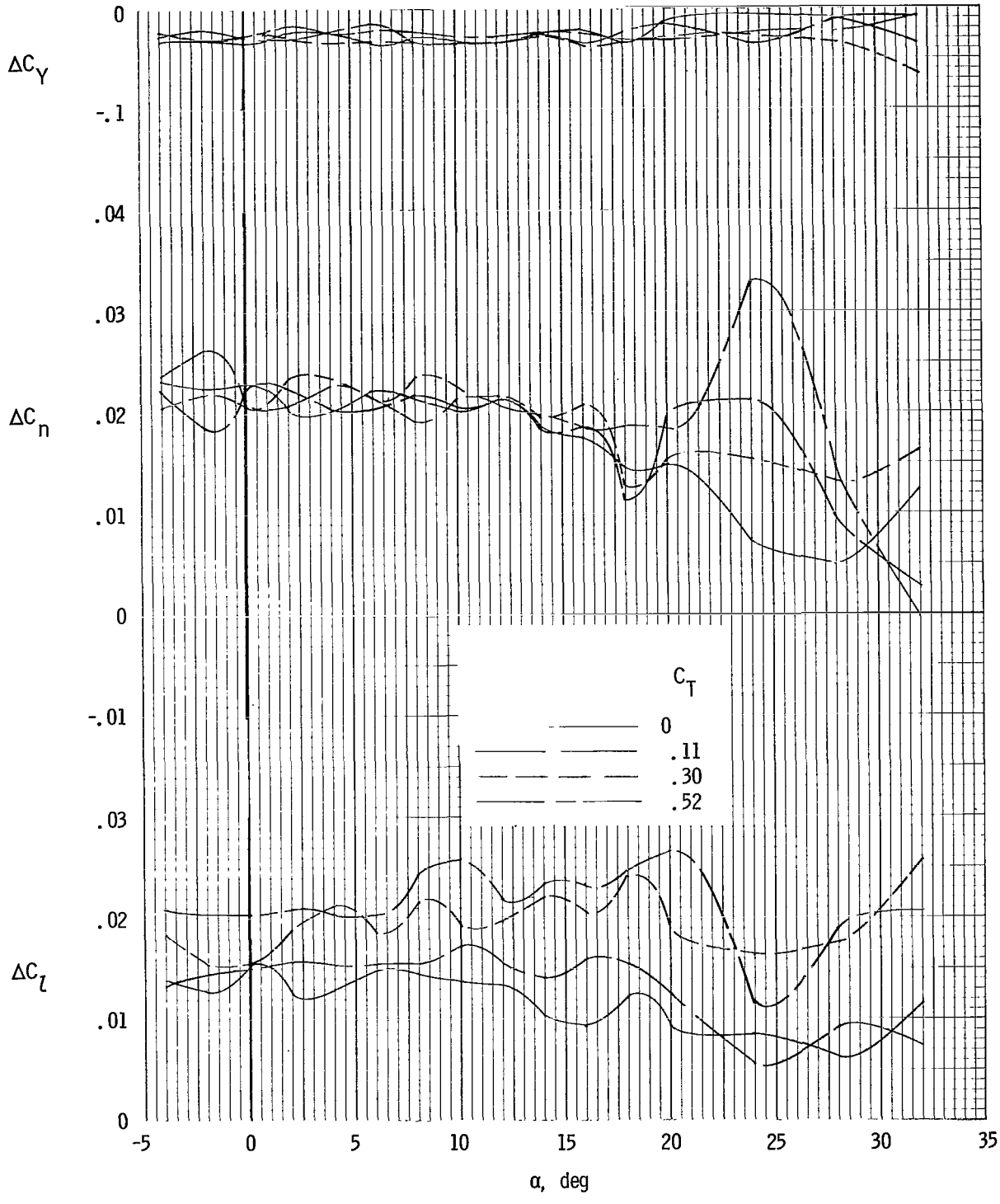

(b) Large horizontal tail; $\Lambda = 72^{o}$.

Figure 22.- Concluded.

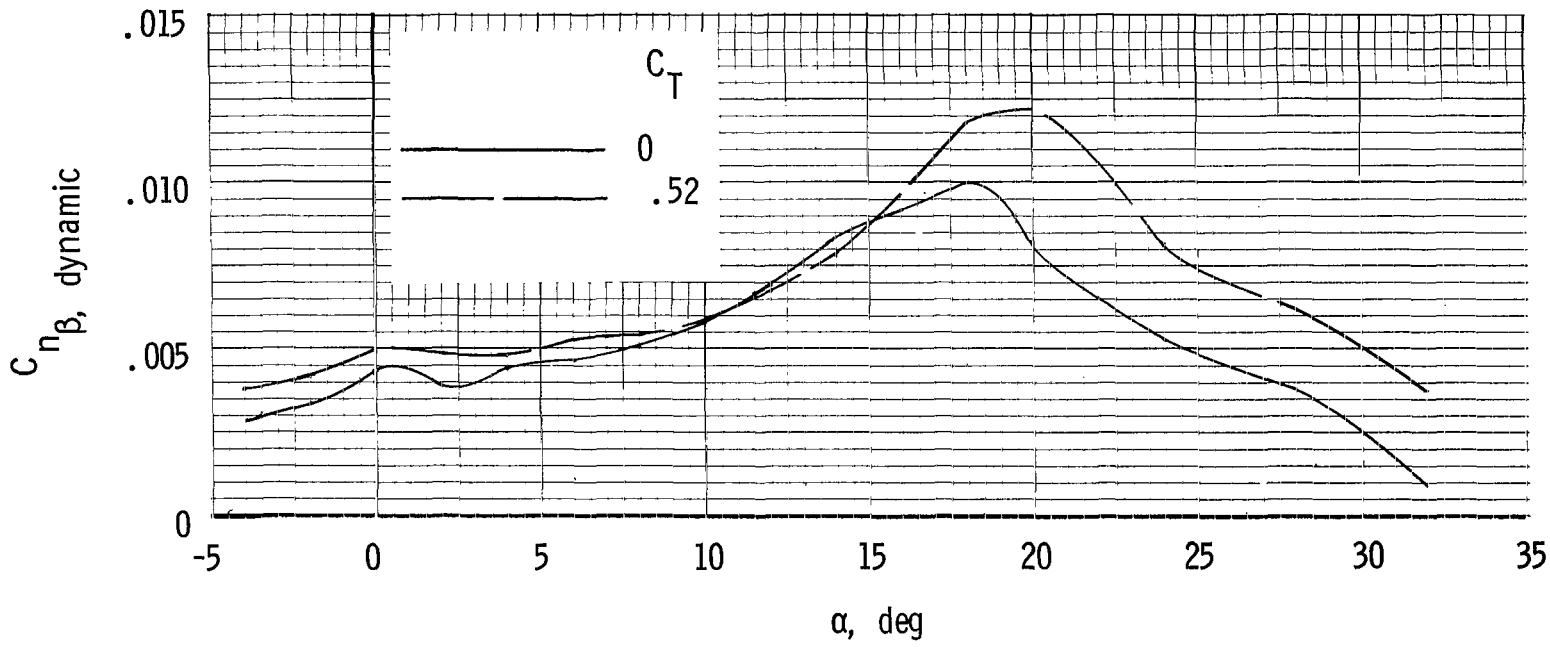

Figure 23.- Calculated values of $C_{n_{\beta,\text{dynamic}}}$. Slats extended; $\Lambda = 20^{\circ}$.

NATIONAL AERONAUTICS AND SPACE ADMINISTRATION
WASHINGTON, D.C. 20546

OFFICIAL BUSINESS

FIRST CLASS MAIL

POSTAGE AND FEES PAID
NATIONAL AERONAUTICS AND
SPACE ADMINISTRATION

"The aeronautical and space activities of the United States shall be conducted so as to contribute . . . to the expansion of human knowledge of phenomena in the atmosphere and space. The Administration shall provide for the widest practicable and appropriate dissemination of information concerning its activities and the results thereof."

—NATIONAL AERONAUTICS AND SPACE ACT OF 1958

NASA SCIENTIFIC AND TECHNICAL PUBLICATIONS

TECHNICAL REPORTS: Scientific and technical information considered important, complete, and a lasting contribution to existing knowledge.

TECHNICAL NOTES: Information less broad in scope but nevertheless of importance as a contribution to existing knowledge.

TECHNICAL MEMORANDUMS: Information receiving limited distribution because of preliminary data, security classification, or other reasons.

CONTRACTOR REPORTS: Scientific and technical information generated under a NASA contract or grant and considered an important contribution to existing knowledge.

TECHNICAL TRANSLATIONS: Information published in a foreign language considered to merit NASA distribution in English.

SPECIAL PUBLICATIONS: Information derived from or of value to NASA activities. Publications include conference proceedings, monographs, data compilations, handbooks, sourcebooks, and special bibliographies.

TECHNOLOGY UTILIZATION PUBLICATIONS: Information on technology used by NASA that may be of particular interest in commercial and other non-aerospace applications. Publications include Tech Briefs, Technology Utilization Reports and Notes, and Technology Surveys.

Details on the availability of these publications may be obtained from:

SCIENTIFIC AND TECHNICAL INFORMATION DIVISION

NATIONAL AERONAUTICS AND SPACE ADMINISTRATION

Washington, D.C. 20546